THE
PHYSICAL REVIEW
A Journal of Experimental and Theoretical Physics Established by E. L. Nichols in 1893
VOL. 59, NO. 4 FEBRUARY 15, 1941 SECOND SERIES

Radiative Transition Probabilities in Heavy Nuclei

Excitation of Nuclei by X-Rays

EUGENE GUTH
University of Notre Dame, Notre Dame, Indiana
(Received October 19, 1940)

From experimental absorption cross sections for excitation of nuclei by x-rays, radiation widths, i.e., emission probabilities are deduced. For the lowest activation levels of In^{115} and Pb widths of the order of a few millivolts are obtained. These widths are of the same order as those of the low levels of the natural radioactive nuclei. The quadrupole radiation widths obtained are within the upper limits set by a sum formula. Formulae for the transition probabilities are given depending both upon energy and spin. A numerical constant entering into the formulae, which is usually calculated from assumed models, is obtained from experiment. A simple expression is given, valid in the neighborhood of the short wave limit, for the intensity of x-rays produced by fast electrons. At the short wave limit the intensity is finite and changes but little both with energy and frequency in the neighborhood of the limit. Therefrom an excitation curve with many flat plateaus follows, each plateau indicating another nuclear level. These flat plateaus reveal directly the shape of isochromats, thus providing a qualitative check on the theory of production of x-rays by fast electrons.

I. INTRODUCTION

UNTIL recently, direct information about the absolute values of nuclear transition probabilities and the level systems of the nuclei involved was obtained only for a few elements. Three groups of experiments have been used for this purpose. (1) The transition probabilities between low levels of natural radioactive nuclei were estimated by comparing the intensity of the long range α-particle groups from the excited levels of these nuclei with that of the γ-rays from the same level. Γ-widths of about a few millivolts were obtained. (2) The transition probabilities between high levels of heavy nuclei were estimated from experiments on the capture of slow neutrons. Γ-widths of about a few tenths of a volt were obtained. (3) The transition probability between a continuous and a discrete state of light nuclei was estimated from experiments on the capture of protons. Γ-widths from a tenth to about a few volts were obtained.

Recently, however, Waldman and Collins excited low metastable states of In^{115} and Pb by x-rays and electrons.[1] This method is capable of extension to higher states and probably to other elements. The present note shows how the experimental excitation curves may be understood quantitatively and how the radiation widths, i.e., the *emission* probability, may be calculated from the experimental *absorption* cross sections. The nuclear levels are given directly by the distances between discontinuities

[1] These data were furnished me prior to their publication by Drs. Waldman and Collins. Cf. also B. Waldman, G. B. Collins, E. M. Stubblefield and M. Goldhaber, Phys. Rev. **55**, 1129 (1939); G. B. Collins and B. Waldman, Phys. Rev. **59**, 109A (1940); B. Waldman and G. B. Collins, Phys. Rev. **57**, 338 (1940).

in the excitation curves. The radiation widths obtained for In^{115} and Pb are of the order of a few millivolts, i.e., of the same order as those of the low states of the natural radioactive nuclei. Incidentally, the excitation curves revealing the shape of the isochromats provide a qualitative check of the theory of the production of x-rays by fast electrons, particularly in the neighborhood of the short wave limit.

For the interpretation of the experimental data, theoretical formulae had to be introduced for: (a) the intensity of the x-rays produced by electrons near the short wave limit; (b) the dependency of the multipole matrix elements involved upon both energy and spin.

The importance of such semi-empirical information about heavy nuclei is borne out by the well-known fact that there are no reliable models for these nuclei. Calculations of the transition probabilities for an α-particle model or the liquid droplet model may and were, in fact, carried out. But the results are not trustworthy.

The excitation of a nucleus by photons may be (1) a line absorption, (2) a Raman effect, and (3) a photo-effect. We consider here the first process only.[2] For In^{115} it may be concluded directly that a line absorption must take place. In the experiments of Goldhaber, Hill, and Szilard, γ-rays from $\frac{1}{2}$ g of Ra irradiated indium without producing any activity.[3] It is now known that the energy of these γ-rays is sufficient to excite In^{115} and the absence of activity is attributed to the fact that none of the known γ-ray energies are equal to the energy of the activation level. The probability of excitation is therefore small. Thus, only irradiation by a continuous x-ray spectrum is likely to lead to a line absorption.

II. Connection Between Absorption Cross Section and Emission Transition Probability

A general formula may be derived, connecting the cross section σ_a for the excitation in line absorption of a level with the emission transition probability.

Let us define $\sigma(h\nu)$ as the absorption cross section for excitation by one photon. Then the dispersion formula holds:

$$\sigma(h\nu)=\pi\lambda^2\cdot\frac{2j_a+1}{2(2j_g+1)}\cdot\frac{\Gamma\Gamma_r}{h^2(\nu-\nu_0)^2+\Gamma^2/4}. \quad (1)$$

Γ is the total gamma-width of a level a with the energy $h\nu_a$ above the ground level g. Γ_r is the partial width for the resonance transition. At the peak of the line, $\sigma(h\nu)$ reduces to the expression

$$4\pi^2\lambda^2\cdot\frac{2j_a+1}{2(2j_g+1)}\cdot\frac{\Gamma_r}{\Gamma};\quad \lambda=\frac{\lambda}{2\pi};$$

j_a and j_g denote the spins of the states a and g, respectively. Formula (1) is valid not only for dipole, but also for electric and magnetic 2^l- and 2^{l-1}-pole radiation, if $\Gamma=\Gamma^{(l)}$ and $\Gamma_r=\Gamma_r^{(l)}$ are taken then as widths for the corresponding multipole radiation.

Let $n(h\nu)d(h\nu)$ designate the number of x-ray quanta produced by one incident electron of the energy E with frequencies between ν and $\nu+d\nu$. $h\nu\cdot n(h\nu, E)d(h\nu)$ is then the intensity. Then the absorption cross section σ_a for production of nuclei in the excited state with energy $h\nu_a$ above the ground state is given by

$$\sigma_a^{(l)}=\int_{\text{over the line}} n(h\nu_a, E)\sigma(h\nu_a)d(h\nu_a)$$

$$=n(h\nu_a, E)\frac{2j_a+1}{2(2j_g+1)}\cdot 2\pi^2\lambda_a^2\Gamma_r^{(l)} \quad (2a)$$

or conversely

$$\Gamma_r^{(l)}=\frac{2(2j_g+1)}{2j_a+1}\cdot\frac{\sigma_a^{(l)}}{2\pi^2\lambda_a^2 n(h\nu_a, E)}. \quad (2b)$$

III. Connection of the Cross Section σ_a with the Experimental Cross Section σ_{exp}

In the actual experiments, the cross section σ_a as defined above cannot be observed. Rather, the internally converted electrons are observed directly because of the decay of a metastable state which lies between the ground state g and the

[2] Estimates show that the cross section for Raman processes on nuclei is rather small and probably not observable. An estimate of widths from photo-effect and photo-fission was carried out by V. F. Weisskopf, to be published soon.

[3] M. Goldhaber, R. D. Hill, and L. Szilard, Phys. Rev. 55, 57 (1939). Also, no effect was observed for the γ-rays of ThC, according to a personal communication of Dr. Goldhaber.

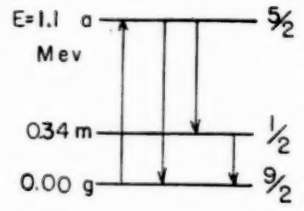

FIG. 1.

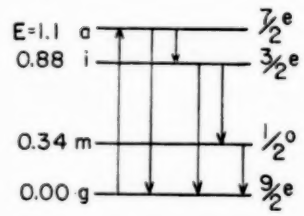

FIG. 2.

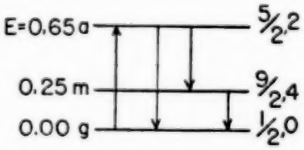

FIG. 3.

activation state a, giving an experimental cross section σ_{exp}. The cross section σ_a refers to the production of this activation level. From σ_{exp} the cross section for production of stable nuclei in the metastable state σ_m may be obtained by division by the coefficient of internal conversion α:

$$\sigma_m = \sigma_{exp} \cdot \alpha^{-1}. \tag{3}$$

The next step is to connect σ_m with σ_a. In order to do that, we must know the relative transition probabilities, activation→ground and activation→metastable. The ratio, f, of the transition probabilities

$$\frac{\text{activation}\rightarrow\text{ground}}{\text{activation}\rightarrow\text{metastable}}$$

consists of the product of two factors: $f = f_S \cdot f_E$. The factor f_S (statistical factor) is simply equal to the ratio of the statistical weights of the ground and metastable levels. The factor f_E (energy factor) arises from the dependency of the transition probabilities upon the energy.

Knowing this ratio, f, one has only to multiply it by σ_m, the cross section for production of nuclei in the metastable state in order to obtain the excitation cross section σ_a:

$$\sigma_a = f \cdot \sigma_m; \quad f = f_S \cdot f_E. \tag{4}$$

This holds if the two transitions to be compared have the same multipole order as is the case for the level scheme of Fig. 1. However, if the transitions have different multipole orders, as is the case for the level scheme of Fig. 2, f will contain a third factor f_l where l denotes the difference in spins of the levels considered. f_l may be taken from formula (10) of Appendix 1. One then has:

$$f = f_S \cdot f_E \cdot f_l. \tag{4a}$$

IV. Dependency of Multipole Transition Probabilities upon the Energy

The factor f_E consists of the ratio of two multipole transition probabilities which depend upon the energy E.

For an electric 2^l-pole or a magnetic 2^{l-1}-pole we have, according to definition

$$\begin{Bmatrix} \Gamma_{el}^{(l)} \\ \Gamma_{magn}^{(l-1)} \end{Bmatrix} \sim \frac{1}{\lambda^{2l+1}} \begin{Bmatrix} |M_{el}^{(l)}|^2 \\ |M_{magn}^{(l-1)}|^2 \end{Bmatrix}, \tag{5}$$

where $|M_{el}^{(l)}|^2$ and $|M_{magn}^{(l-1)}|^2$ designate the square of the absolute values of the coordinate electric 2^l- and magnetic 2^{l-1}-pole matrix elements, respectively. There are good arguments which make it very plausible that the coordinate matrix elements $|M|^2$ are to a good approximation, independent of the energy. Rough estimates and more accurate simple model calculations indicate this, and also a more general argument put forward by Weisskopf and Ewing[4] yields the same conclusion.

We have then:

$$\begin{Bmatrix} \Gamma_{el}^{(l)} \\ \Gamma_{magn}^{(l-1)} \end{Bmatrix} = \begin{Bmatrix} C \\ C' \end{Bmatrix} \cdot E^{2l+1}, \tag{6}$$

where the C and C' depend upon the actual values of the matrix elements involved and are best taken, whenever possible, from experiment. Model calculations are unreliable in this respect and generally give too high values for the constants. For a more complete formula which, however, is based on more special assumptions, cf. Appendix 1.

[4] V. F. Weisskopf and D. H. Ewing, Phys. Rev. **57**, 472 (1940); cf. also Weisskopf, reference 2.

V. Assumptions About the Level Scheme Needed for the Evaluation of the Factors f

The values of the factors f_S and f_E, introduced in formula (4), depend upon the level scheme assumed, namely, upon the values of the spin assigned to the metastable and the activation level and also whether another level between the metastable and the activation level is assumed to exist or not.

For In^{115} the simplest plausible scheme is shown in Fig. 1. On the right side of the scheme we inserted the spins attributed to the levels. All three levels may have the same parity. The height of the activation level corresponds to the threshold of the x-ray excitation and the height of the metastable level is the energy of the electrons arising from internal conversion of the γ-rays emitted by the decay of the metastable state. Both have been observed directly.

This system does not contain the level at approximately 800 kev postulated by Lawson and Cork,[5] since the evidence for it is meager. Contrary to the usual conclusion that the relatively large lifetime of In^{115} necessitates the assumption of a change in parity between the ground and metastable states in addition to a change of the spin by two, no change in parity is postulated.[6] The need for introducing a change in parity may be overcome either by the introduction of a second level between the metastable level and the activation level, or by assuming that the matrix elements involved are much smaller than is generally thought.[7]

It should be pointed out that the transition from the ground to the activation level may turn out eventually to be a magnetic or even an electric dipole transition. In either case, it would be necessary to assume the existence of an intermediate level between the activation level and the metastable level. A probable level scheme is shown in Fig. 2 (cf. ref. 5). The indices e and o designate even and odd. According to well-known selection rules, Fig. 2 means that the transition $g \rightarrow a$ is assumed to be a magnetic dipole transition. For the height of the intermediate level i the value given by Lawson and Cork may be used, better evidence being lacking.

From data on excitation by x-rays alone it is hardly possible to arrive at an unambiguous decision about the multipole character of the activation transition. However, additional data about excitation of nuclear levels by electrons and heavy charged particles may help in this decision, as will be shown at another place (cf. also end of Appendix 1).

In the case of lead, it is not known to which of its four known isotopes, namely, Pb^{204}, Pb^{206}, Pb^{207}, and Pb^{208}, the observed activity should be attributed. For the even isotopes with zero spins a transition having a 0–0 spin change between two states of different parity is also possible,[8] in addition to transitions with changes of the spin. For a spin change 0–0, the internally converted electrons will not be monochromatic. Furthermore, the conversion coefficient will be much smaller than for a transition with change of the spin. Neither of these conclusions has as yet been experimentally tested, because of the short life of the metastable lead level.

Another possibility is a 0–0 transition between states of the same parity by direct interaction between the nucleus the atomic electrons, which penetrate, in this case, into the nucleus. Such a nonradiative transition takes place, according to Fowler,[9] from the metastable level of 1.41 Mev of RaC′ to its ground level. One obtains, however, on all plausible assumptions much too short lifetimes ($\tau < 10^{-8}$ sec.) to account for the observed periods of lead or any other known isomers.[7]

For simplicity, it is assumed here that in the actual transition, a change in the spin takes place just as for In^{115}. A possible level scheme is then shown in Fig. 3. The first column on the

[5] J. L. Lawson and J. M. Cork, Phys. Rev. **57**, 982 (1940), Fig. 12, p. 993.

[6] My attention was called by Drs. Serber and Dancoff to the interesting fact that the assumption of a change of parity between m and g fits the lifetime of m; K/L conversion ratio and K conversion. However, in the estimate of the lifetime model calculations were used. Furthermore, the conversion coefficients for the magnetic 2^4-pole radiation were taken from nonrelativistic calculations of M. H. Hebb and E. Nelson, Phys. Rev. **58**, 486 (1940) which do not hold well for In ($Z=49$) and conversion electrons of 0.34-Mev energy.

[7] Cf. M. H. Hebb and G. E. Uhlenbeck, Physica **5**, 605 (1938).

[8] R. G. Sachs, Phys. Rev. **57**, 194 (1940).

[9] R. H. Fowler, Proc. Roy. Soc. **A129**, 1 (1930). It may be, however, that the observed transition is connected with a spin change of two or more instead of being a 0–0 transition.

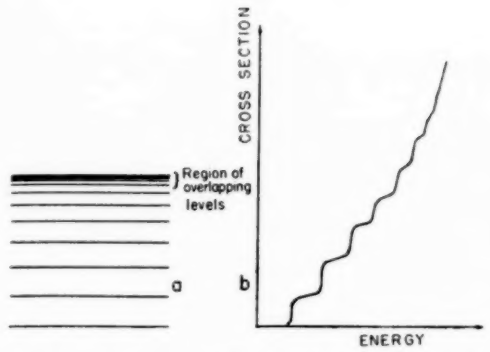

FIG. 4(a). Schematic nuclear level system and (b) the corresponding excitation curve. The theoretically discontinuous corners of the plateaus are rounded off.

right-hand side of the scheme refers to the even active isotope Pb^{204} or Pb^{206} or Pb^{208}, the second to Pb^{207}.

VI. Number of X-Ray Quanta Produced by Fast Electrons Near the Short Wave Limit

In the experiments, excitation curves were taken as a function of the energy of the electrons incident on a gold or lead target. The x-rays produced this way were used to excite In^{115} or Pb. We need, therefore, $n(h\nu, E)$, i.e., the number of quanta produced by one electron at a fixed $h\nu$, namely, $h\nu = h\nu_a$, the value of the threshold (energy of activation level) as a function of energy. $I(h\nu_a \cdot E) = h\nu_a \cdot n(h\nu_a \cdot E)$, as a function of E at fixed ν_a is a so-called isochromat. In checking the theory of the continuous x-ray radiation, it is, from the experimental point of view, best to take isochromats. *It is interesting to point out that the shape of an excitation curve in passing an activation threshold reveals exactly the shape of the corresponding isochromat.* For in formula (2), $n(h\nu_a, E)$ is the only quantity varying with E.

According to the Born approximation the number of quanta at a fixed ν produced by one electron would increase with increasing energy. In fact, the Bethe-Heitler formula gives $n(h\nu_a, h\nu_a) = 0$, i.e., zero number of quanta at the short wave limit. However, Born's approximation does not hold near the short wave limit. The exact theory is known only in the nonrelativistic region. Both Sommerfeld's original approximation and the exact formulae of Sommerfeld and Maue[10] show that the number of quanta is *finite* at the short wave limit and changes but little both with ν and E in the immediate neighborhood of the threshold. As a matter of fact, the isochromats may even decrease with increasing energy. This is true both for the number of quanta integrated over all angles or in a certain specified direction. Quantitatively, one may prove that the exact formulae of Sommerfeld and Maue may be obtained from the Born approximation (which holds rigorously at the long wave end) by multiplication with a factor $f(Z; v, v')$ where v and v' are the velocities of the electron before and after collision and Z is the atomic number.[11]

$$f(Z; v, v') = \frac{1 - e^{-2\pi\alpha Zc/v}}{1 - e^{-2\pi\alpha Zc/v'}} \cdot \frac{v'}{v}. \tag{7a}$$

It is now a plausible assumption that the same factor will convert the Bethe-Heitler formula into a formula valid with good approximation at and around the threshold; i.e.,

$$n(h\nu, E) = n(h\nu, E)_{B-H} \cdot f(Z; v, v'). \tag{7b}$$

Of course, the exact $n(h\nu, E)$ may contain additive terms which go to zero in the nonrelativistic limit. Calculations in which approximate wave functions of Sommerfeld and Maue are used point in this direction. However, comparison of $n(h\nu, E)$, according to formula (7b), and of exact numerical calculations of Jaeger[12] shows that such additive terms are not too important. In fact, formula (7b) gives for $h\nu_a \sim 1$ Mev and $E \sim 1$ Mev an $n(h\nu, E)$ differing by about 15 percent from Jaeger's value. In the immediate neighborhood of the threshold, (7b) may be written in the form:

$$n(h\nu, E) = A \cdot \frac{Z^2 r_0^2}{137} \cdot \frac{1}{h\nu} \cdot N \cdot dx;$$
$$A \leqq 3.44 \text{ for } E \leqq 1.1 \text{ Mev}, \tag{7b'}$$
$$A \leqq 4.89 \text{ for } E \leqq 0.65 \text{ Mev},$$

[10] A. Sommerfeld and A. W. Maue, Ann. d. Physik **23**, 589 (1935).

[11] The factor $\frac{2\pi\alpha Zc/v}{e^{2\pi\alpha Zc/v} - 1} \cdot \frac{2\pi\alpha Zc/v'}{1 - e^{-2\pi\alpha Zc/v'}}$ converts the Born approximation into the old Sommerfeld formula (Sommerfeld, Ann. d. Physik **9**, 257 (1931)) which, however, is itself only an approximation.

[12] J. C. Jaeger, Nature **140**, 108 (1937).

where N is the number of atoms per cm³ and dx is the thickness of the (thin) target. Further away from the threshold, however, the full formula (7b) has to be used. (7b′) does not depend upon E at all.

This behavior of $n(h\nu, E)$ shows that an excitation curve with many flat plateaus is to be expected, each plateau indicating another level; cf. Fig. 4(a) and (b). In fact, for In^{115} and Pb, the first plateau was observed and for In^{115} indication of a second level was also observed. The "flatness" of the first plateau is illustrated by the fact that, according to (7b), $n(h\nu, E)$ increases by less than 2 percent if E is raised from 1.1 to 1.4 Mev. The experimental curves, of course, do not show sharp discontinuities at each level. This is just as for the isochromats, because of the unavoidable slight inhomogeneity of the electron beam.

VII. Calculation of the Widths

The experimental cross sections of Waldman and Collins[13] are:

$$\sigma_{exp}=1\times10^{-34} \text{ for } In^{115}$$

and

$$\sigma_{exp}=2.5\times10^{-34} \text{ for Pb.}$$

The internal conversion coefficients are[14]

$$\alpha=0.5 \text{ for } In^{115}, \quad \alpha\sim1 \text{ for Pb.}$$

Therefore, one has according to formula (2)

$$\sigma_m=2\times10^{-34} \text{ cm}^2 \text{ for } In^{115},$$
$$\sigma_m=2.5\times10^{-34} \text{ cm}^2 \text{ for Pb.}$$

For the simple schemes of Figs. 1 and 3, the statistical factors are:

$$f_S=(2j_0+1)/(2j_m+1)=5 \text{ for } In^{115}$$

and

$$f_S=\tfrac{1}{5} \text{ for Pb (odd isotope).}$$

The energy factors are, according to the energy values indicated in these figures: $f_E=6.4$ for In^{115} and $f_E=11.4$ for Pb. Inserting these factors into formula (4), one has

$$\sigma_a^{(2)}=6.4\times10^{-33} \text{ for } In^{115},$$
$$\sigma_a^{(2)}=5.7\times10^{-34} \text{ for Pb.}$$

Finally, from formula (2b), using formula (7b′) for $n(h\nu, E)$, one obtains

$$\Gamma_r^{(2)}=4.09 \text{ millivolts for } In^{115},$$
$$\Gamma_r^{(2)}=0.28 \text{ millivolt for Pb.}$$

These values for the widths are smaller than an upper limit set by a sum formula for quadrupole transitions. (Cf. Appendix 2.)

Table I gives a comparison of the widths $\Gamma_r^{(2)}$, lifetimes $\tau^{(2)}=h/\Gamma_r^{(2)}$, and $C=\Gamma_r^{(2)}/E^5$ of excited states of natural radioactive nuclei[15] and those of In^{115} and of Pb. In view of the incompleteness of the experimental data and the resulting ambiguity in the assumed level scheme, it is somewhat encouraging to find the same orders of magnitude.

In order to calculate the f-factors for the level scheme of Fig. 2, one has to use formula (10) of Appendix 1. On account of the uncertainty about the intermediate level and about the validity of formula (10) we defer, however, the calculation of the width.

VIII. Doppler Effect and Self-Absorption

In connection with the above evaluation of the widths of excited states, it is important to point out that both for In^{115} and Pb, the Doppler widths are large compared with the radiation widths. The Doppler width of this level of In^{115} is about 0.7 ev. This explains the smallness of self-absorption of the line in question in In^{115} which was observed by Waldman and Collins.

Table I. *Widths of the excited states of* RaC′, ThC′, Pb, In^{115}.

Nucleus	Level	E (Mev)	$\Gamma_r^{(2)}$ (Millivolts)	$\tau_r^{(2)}$ (Sec.)	C (Mev)$^{-4}$
RaC′	1	0.61	2.	3×10^{-13}	2.4×10^{-8}
	3*	1.41	0.01	8×10^{-11}	—
ThC′	1	0.73	1.5	4×10^{-13}	7.3×10^{-9}
	2	1.80	1.0	6×10^{-13}	6.0×10^{-11}
Pb	2	0.65	0.28	2.34×10^{-12}	2.40×10^{-9}
In^{115}	2	1.10	4.09	1.55×10^{-13}	2.59×10^{-9}

* Only conversion electrons observed.

[13] These cross sections are upper limits, taken from thick targets approaching a thin one. The cross sections are taken for electron energies above the threshold. They are sensibly independent of the electron energies.

[14] The value of α for Pb is a plausible assumption, but needs verification by experiment.

[15] Cf. H. A. Bethe, Rev. Mod. Phys. **9**, 229 (1937), Table XXXXIV.

For the Doppler width, one has

$$\Gamma_{\text{Doppler}} = h\nu_a \cdot (2kT/Mc^2)^{\frac{1}{2}};$$
$$M: \text{ mass of nucleus.} \quad (8)$$

At low temperatures, kT in this formula has to be replaced[16] by $k(T+\frac{1}{2}\Theta)$, where Θ designates the Debye temperature of the nucleus. It would be possible to measure the width of the activation level more accurately by direct absorption measurements at low temperatures, were it not for the fact that the value for the Debye temperature for In is still too high for an effective reduction of the Doppler width. All other elements with known metastable levels also have Debye temperatures too high to allow an appreciable reduction of the Doppler width, e.g., lead ($\Theta_D = 88$) Kr, Xe, Ag. The Θ_D-values for In, Kr, Xe were calculated by means of the Lindemann formula:

$$\Theta = 123(T_m/Av^{\frac{1}{3}})^{\frac{1}{2}}, \quad (9)$$

T_m, melting point; A, atomic weight; v, atomic volume. No data on the specific heats at low temperatures are known for these three elements.

It is a pleasure for the author to thank Drs. B. Waldman and G. B. Collins for discussion of their experiments and Drs. H. A. Bethe, W. E. Lamb, Jr., J. A. Wheeler and especially Dr. V. F. Weisskopf for helpful discussions and suggestions.

Appendix 1

More complete formula for multipole matrix elements

A semi-empirical formula for the multipole transition probabilities like (2):

$$\Gamma(E)^{(l)} = c,\ E^{2l+1} \quad (2)$$

gives the dependency upon E but the dependency upon l is not contained completely. Now if one wants to relate the transition probabilities for transitions of different multipole order, one needs a formula giving the dependency upon l more accurately. It may be shown that such a more complete formula will have for electric 2^l- or magnetic 2^{l-1}-pole transitions the general form:

$$\Gamma^{(l)} = B \cdot \frac{2j_i+1}{2j_k+1}\binom{l+1}{l} \cdot [(2l+1)(2l-1)\cdots 3.1]^{-2} E(RE)^{2l}. \quad (10)$$

Here j_i and j_k are the spins of lower and upper state with energies E_i and E_k, respectively; $l = |j_i - j_k|$; $E = E_k - E_i$ measured in units mc^2; R: nuclear radius in units of $\hbar/mc$; B is a constant, to be taken from experiment.[17] This formula, however, is based on less certain assumptions than (2) and may be used only with caution.

Using (10) and the value of the width in Table I for fixing B, one obtains for the lifetime of the metastable state of Pb, assuming again the level scheme of Fig. 3: $\tau^{(4)} \sim 67$ sec. in amazing agreement with the observation (100 sec.). This agreement has, however, to be taken only with great caution, because of the uncertainties in formula (10), in the assumed level scheme, and in the experimental data, inasmuch as for In^{115} the agreement is less good using either the level scheme of Fig. 1 or of Fig. 2. We do not want to discuss this matter further here, but defer it to another paper, where some more applications to isomers will also be treated.

Appendix 2

Sum formula for quadrupole radiation

An upper limit for the dipole matrix element

$$D_{ik} = \sum_{j=1}^{n} \int r_j \psi_i \bar{\psi}_k dr$$

may be derived, as is well-known, from the sum formula:

$$\sum_{i=0}^{k} |D_{ik}|^2 \cdot 2m_p \cdot E_{ik} = n; \text{ namely: } |D_{ik}|^2 < \frac{n}{2mE_{ik}}. \quad (11)$$

n designates the number of radiating particles (protons) with mass m_p.

Similarly, an upper limit for the quadrupole matrix element

$$Q_{ik} = \sum_{j=1}^{n} \int r_j^2 \psi_i \bar{\psi}_k dr$$

may be derived from the sum formula

$$\sum_{i=0}^{k} |Q_{ik}|^2 \cdot \frac{m_p}{2\hbar} = |Q_{kk}|^2;$$

namely:

$$|Q_{ik}|^2 < \frac{2\hbar}{m_p} \cdot \frac{1}{E_{ik}} |Q_{kk}|^2. \quad (12)$$

In contrast to the dipole formula, this last formula contains itself an average value. Assuming, however, $|\varphi_{kk}|^2 \leqq 10^{-48}$ and remembering that

$$\Gamma^{(2)} = \frac{4r}{15}\frac{l^2}{\lambda^5}|Q^2| \quad (13)$$

one sees that the values of Table I satisfy our inequality.

---

[16] Cf. W. E. Lamb, Jr., Phys. Rev. **55**, 190 (1939). The above formula was recommended to the author by Dr. H. A. Bethe. According to Dr. Lamb (personal communication) it is a fair approximation at the two limits $T \gg \Theta$. Lamb replaces T by $\tilde{\epsilon}(T)$ and (Fig. 1, p. 198) gives a plot of $\tilde{\epsilon}(T)$ against T/Θ. For the above-mentioned limits, one obtains (O is the well-known "order of" symbol):

$$\tilde{\epsilon} \sim T + \Theta \cdot O(\Theta/T); \quad T \gg \Theta,$$
$$\epsilon \sim \tfrac{3}{8}\Theta + T \cdot O(T^3/\Theta^3); \quad T \ll \Theta.$$

Therefore, the replacement of T by $(T+\frac{3}{8}\Theta)$ instead of $(T+\frac{1}{2}\Theta)$ is somewhat better.

[17] For an α-particle moving in a potential well, a formula of this type (with $\hbar^{-1}B(2j_i+1)/(2j_k+1) \to 8/137$) was given by Hebb and Uhlenbeck, reference 7.

Experiments with a Slow Neutron Velocity Spectrometer*

C. P. Baker and R. F. Bacher
Cornell University, Ithaca, New York

(Received December 30, 1940)

Neutron bursts were produced by modulation of the arc source of a small cyclotron. Neutrons subsequently slowed down in paraffin were detected by a BF_3 ionization chamber and linear amplifier. Modulation of an additional amplifier allowed the counting of all detected neutrons as well as those arriving in a specified time interval. Time of flight experiments were carried out at 3.0 meters with "on" times of 50 or 100 μsec. (microseconds) out of a period of 2500 μsec. The modulation of the source and detector was accurate to about 5 μsec. The absorption of thin Cd (0.052 g/cm²) shows a resolved resonance absorption with maximum at 0.14 ev. The thick Cd (0.45 g/cm²) absorption was also examined and it was found that the absorption edge was not sharp, the transmission being 0.5 at 0.47 ev. Experiments with thick absorbers of Rh and In showed definite evidence of resonance absorption at 1.0 ev for both elements. Experiments were also carried out to study the delayed emission of thermal neutrons from the paraffin surrounding the source. An effective mean life of 170 μsec. was found. The effect of the resolution of the apparatus was examined and found to be small except for the resonances at 1.0 ev. The effect of the delayed emission of thermal neutrons on the time of flight measurements was also examined. From the thin Cd absorption curve Γ, the total width of the resonance level, was found to be 0.12 ev and from the cross section at resonance

$$[1\pm(1/2i+1)]\Gamma_n,$$

where Γ_n is the neutron width and i is the angular momentum of the absorbing nucleus, it was found to be 5×10^{-4} ev. In this calculation 13 percent abundance of the effective isotope was assumed.

IT is now well known that the absorption of slow neutrons by various nuclei changes rapidly with the kinetic energy of the neutron. All known nuclei show an absorption of slow neutrons which increases with decreasing energy and in addition many show the property of selective absorption for slow neutrons which are believed to lie in a narrow kinetic energy band. These absorption bands are believed to represent states of a compound nucleus and their width is believed to be roughly 10^{-8} of the excitation energy. Through the use of slow neutrons, one is permitted to get a tremendously magnified view of a small section of the energy spectrum in the region of 8×10^6 ev, the binding energy of a neutron. In principle it is possible to get a detailed picture of these absorption bands and thus to obtain useful information for the study of nuclear structure. There are, however, no monoenergetic sources of slow neutrons. Neutrons of the proper energy for study of these resonance effects are produced from the fast neutrons generated in nuclear disintegrations, by subjection of the neutrons to repeated energy losses. In this fashion a continuous neutron energy spectrum is produced and in order to investigate nuclear properties as a function of neutron energy, the energy of neutrons for the particular process under investigation must be determined either by some direct method or by some indirect method.

A number of indirect methods of ascertaining the energy of slow neutrons have been developed, of which the most useful is probably the boron method which is founded on the very reasonable assumption that the absorption by boron is inversely proportional to the neutron velocity. The first direct method was the mechanical velocity selector of Dunning, Pegram, Fink, Mitchell and Segrè.[1] Two sets of cadmium-covered sector disks, separated by a given distance, absorbed neutrons in a given velocity interval which was determined by the speed of rotation of the disks. This selector was used in the neighborhood of thermal energy (0.025 ev) and in order to obtain much higher energy neutrons, excessive rotational speeds would have been necessary. The resolution of the selector depends both upon the geometrical arrangements and upon the available neutron intensity which, with the radon sources used, was not very large.

With the introduction of large artificial sources of neutrons, direct control of the production of

* This work was reported previously in brief. Baker and Bacher, Phys. Rev. **57**, 351 (1940); **57**, 1076 (1940).

[1] Dunning, Pegram, Fink, Mitchell and Segrè, Phys. Rev. **48**, 704 (1935); Phys. Rev. **49**, 103 (1936); Fink, Phys. Rev. **50**, 738 (1936).

neutrons was made possible. With such a modulated source, methods of measuring the neutron time of flight for a given distance were developed by Alvarez[2] and by Fertel, Gibbs, Moon, Thomson, and Wynn-Williams[3] (referred to as FGMTW). Alvarez used the 37″ California cyclotron and produced the desired modulation by control of the plate voltage on the oscillator tubes. Neutrons were detected by a BF_3 ionization chamber located at a distance and the amplifier output was short-circuited except during a certain interval after the burst. Modulation of the oscillator required large amounts of power and the bursts which were produced were of rather long duration and somewhat inaccurately defined, but the experiments which were carried out clearly demonstrated the power of the method. Alvarez found it possible to work with neutrons which had energies up to about 0.025 ev although the resolution was rather low at this energy. FGMTW produced bursts of neutrons by modulating the ion source of a high voltage tube in which deuterons were accelerated and subsequently used to produce neutrons. While Alvarez counted only those neutrons which arrived during a certain interval after the burst, FGMTW obtained a continuous record of neutron arrival by use of an oscillograph. Primarily because of the fact that the modulation of the source was much easier to control, they were able to extend the time of flight measurements to energies of about 0.1 ev.

The present work is based on the use of the arc type ion source[4] in the cyclotron and neutron bursts were produced by modulation of this source. The method of modulation therefore was in principle similar to that used by FGMTW. It seemed difficult, however, to get the desired accuracy in determination of the time of flight from an oscillograph record and hence a modulated amplifier in principle similar to that employed by Alvarez was used. A schematic diagram of the apparatus used in the present work is shown in Fig. 1. Neutrons produced by the cyclotron (1.4-Mev deuterons on Be) were first slowed down in paraffin and then detected by a BF_3 ionization chamber connected to a linear amplifier which operated continuously. The input thyratron of the discriminating amplifier flashed for each neutron detected and the total number of flashes counted through the scale-of-16 counter. The pulses arriving in the desired time interval were selected by the discriminating amplifier which was controlled by the amplifier modulator. The design and operation of the various components of the apparatus will be discussed below.

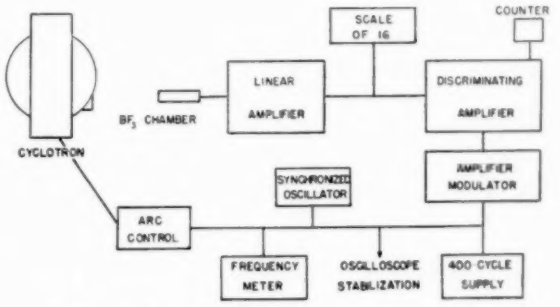

FIG. 1. Schematic diagram of apparatus.

APPARATUS

Source

From previous work on the development of the arc type ion source it was known that this source would operate in the cyclotron from an alternating supply. Preliminary experiments on source modulation were therefore undertaken with the arc operating from a 400-cycle generator. In order to find out how well this operation controlled the deuteron beam, the target was grounded through a resistance of 10^4 or 10^5 ohms and connected to an oscilloscope. With the oscilloscope sweep synchronized to the a.c. supply, square pulses which rose and fell in 10 microseconds or less, were observed and at this stage it was quite possible that the observed width of rise or fall was due to the amplifier which was used with the oscilloscope tube.

It is necessary to be able to regulate the duration of the deuteron burst. This was first done by connecting the arc in series with a thyratron used in a conventional grid-controlled rectifier circuit. The same alternating potential was applied to the grid and plate of this thyratron except that the phase of the potential applied to the former was shifted so that the grid was held negative over part of the operating cycle. The arc was thus

[2] L. W. Alvarez, Phys. Rev. **54**, 609 (1938).
[3] Fertel, Gibbs, Moon, Thomson and Wynn-Williams, Proc. Roy. Soc. **175**, 316 (1940); Nature **142**, 829 (1938).
[4] Livingston, Holloway and Baker, Rev. Sci. Inst. **10**, 63 (1939).

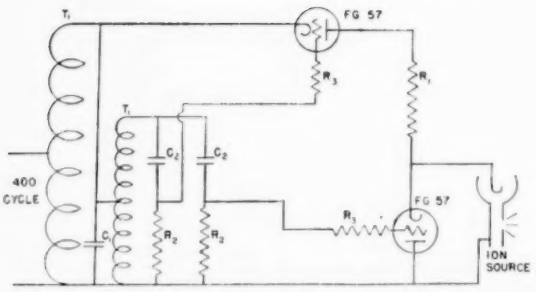

FIG. 2. Arc control circuit. $R_1=50$ adjustable; $R_2=30{,}000$ variable; $R_3=30{,}000$; $C_1=1$; $C_2=0.01$. Resistance in ohms, capacity in μf.

started when the thyratron fired and extinguished when the applied potential became too low. This method has the disadvantage that the critical extinguishing potential and hence the time of extinguishing, depends upon the gas pressure and filament condition in the arc and these are not stable over long periods of time.

It appeared necessary both to start and stop the arc by some thyratron control. The circuit finally adopted is shown in Fig. 2. The upper thyratron starts the arc discharge at some time in the cycle determined by the phase of the applied grid potential and the lower thyratron short-circuits the arc and thereby stops the discharge. The timing of these two events is controlled by the phase-shifting network $T_1R_2C_2$. Both thyratrons are extinguished when the supply voltage changes sign. The resistor R_1 is used to prevent excessive currents when both tubes are conducting. For most stable operation the grid potential should vary rapidly with time in the critical region so that changes in the supply voltage or the firing voltage of the thyratron will have little effect upon the time of firing. The large grid swing (400 volts) used to produce this rapid variation requires the use of the grid resistors R_3 in order to limit the grid current and prevent damage to the tubes. None of the circuit constants was critical except, of course, the phase shifting components which had to be adjusted for the desired duration of the burst. With the 400-cycle modulation used throughout this work, the pulse applied to the arc could be varied from 50 microseconds (μsec.) to somewhat more than 500 μsec. The voltage pulse controlling the arc rose or fell within 5 μsec.

The modulation of the deuteron beam controls the production of fast neutrons but delays may be introduced in the slowing down process. The slowing down took place in a paraffin block in which the Be target was imbedded as shown in Fig. 3. The detecting chamber for the time of flight measurements was placed on a line approximately perpendicular to the face of the paraffin block. Since the average energy of the neutrons is reduced to E/e^n by n collisions with the hydrogen in the paraffin, about 16 collisions are necessary to reduce the energy from 5 Mev to 1 ev. The variation of the mean free path with neutron energy somewhat complicates the calculation of the time of slowing down. Assuming a mean free path of 5 cm for $E>5000$ ev and 1 cm for 5000 ev$>E>$0.1 ev, it takes 0.13 μsec. for a neutron to go from 5 Mev to 5000 ev, 1.5 μsec. to go to 1.4 ev and 4.0 μsec. to go from 5 Mev to 0.19 ev. In general the slowing down time will be of the order of the time for a few mean free paths at the final velocity or a few cm and this distance is small compared to the distance of source to detector.

Somewhere in the region of 0.25 ev, the assumptions made above break down because the energy loss per collision is affected by the presence of the hydrogen chemical bond. In addition, the neutrons at still lower energy are in thermal equilibrium with the paraffin and the delay in emission will depend upon their effective mean life in the paraffin. This latter point was investigated and will be discussed later.

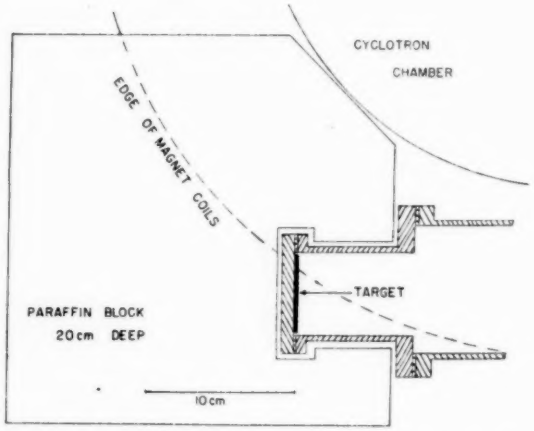

FIG. 3. Target arrangement. Observations were made on a line perpendicular to the face of the paraffin indicated at the bottom of figure.

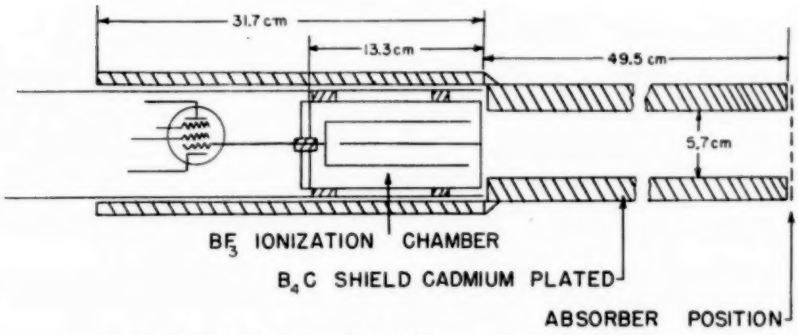

FIG. 4. Ionization chamber and boron carbide collimator.

Detector

The slow neutrons were detected with a BF_3 ionization chamber and linear pulse amplifier. The ionization chamber was cylindrical with inside diameter of 5 cm and 15 cm long and was filled with BF_3 gas at atmospheric pressure. A collecting potential of 800 volts was used to collect negative charges. The chamber was shielded with cadmium and boron carbide and has a collimating tube as shown in Fig. 4. The boron carbide of the collimating tube was about 1 g/cm^2 and about half as much for the chamber shield. Because of the geometrical arrangement and the presence of the first amplifier tube, there was no boron carbide shielding at the back of the ionization chamber although there was a cadmium shield not indicated in Fig. 4. The extension of the boron carbide shield then allowed cadmium penetrating neutrons to come from only a small solid angle. The general position of the ionization chamber with respect to the walls of the room and the cyclotron is shown in Fig. 5. The ionization chamber was placed so that in back it could see only an adjacent room, connection to the amplifier being made by a 1.5-m flexible cable. The collimation in front was such that at 3 m from the source, the view of the ionization chamber was restricted almost entirely to the face of the paraffin block shown in Fig. 3.

Certain special precautions must be observed in the use of the ionization chamber and linear amplifier in time of flight measurements if the time of recording a neutron pulse at the output of the amplifier is to be an accurate measure of the time of arrival of the neutron in the ionization chamber. The collection of negative ions in a BF_3 chamber had been found to give rise to much sharper pulses, as might be expected if the negative ions are electrons. This collection time for positive ions is about 250 μsec. and for electrons about 6 μsec. Since the collection time is dependent on the position of the disintegration in the chamber, it is highly desirable to make this time as short as possible.

Certain modifications were made in the linear amplifier in order to obtain speed of response and avoid excessive smearing of the sharp pulses from the ionization chamber. To do this it is necessary to increase the frequency band passed by the amplifier. The time constants of the interstage coupling elements were reduced by decreasing the size of the coupling condensers to 0.001 μf. This did not give sufficient high frequency response, so it was necessary to reduce the plate and grid resistors to 50,000 ohms. In order not to reduce the gain per stage, tubes with a high amplification factor were substituted for the conventional type 6C6. These tubes were type 1851, with an amplification factor of 6000, and were used in the second and third stages. The shielded wire in the cable between the first and second tubes had a capacity of 3 $\mu\mu$f per cm, and it was found necessary to substitute coaxial cable which had a capacity of a tenth this amount. The wider response of the amplifier made the signal to noise ratio somewhat less than that in conventional amplifiers. This is unavoidable as the noise is roughly proportional to the band width of the amplifier.

Even with these steps taken to increase the amplifier speed a definite time lag was found. A sketch of a neutron pulse as it appears on an oscilloscope screen is shown in Fig. 6. While the pulse seems to start at a time T_1, it is not re-

corded until T_2 when the potential rises to the flash point of the thyratron. The time lag T_2-T_1, was estimated to be about 25 μsec. In the course of the experiments it was found possible to make a measurement of the over-all time lag and this is considered to be more accurate.

The output of the linear amplifier was fed into a separate unit called the discriminating amplifier which is shown in Fig. 7. The input thyratron (type 885) flashed for all neutrons detected. The bias of this tube was adjusted in the usual way to eliminate the noise background and was not changed in the course of an experiment. The thyratron output was fed into two channels. The first of these was connected to a scale-of-16 counter and recorded all neutrons detected. The total number of neutrons detected was used as a measure of the integrated beam intensity and has several advantages over the usual method of beam current integration. Changes in the sensitivity of the detector or efficiency of the target do not, to a first approximation, affect the results if the number of timed neutrons is always referred to the total number. The 56 tube in this channel was used principally as a buffer tube to isolate the output circuit of the thyratron from possible interaction with the scale counter or external disturbances. The second channel was the timing channel, and led to the grid of the type 57 tube. The bias on this tube was adjusted so that the amplification was a critical function of the screen potential. The screen potential was supplied by a square wave generator (amplifier modulator) whose output was adjustable in width and phase so that only those pulses which occurred in a predetermined time interval were amplified. The following 56 was used to amplify and invert the timed pulses and the final 885 operated the mechanical counter which recorded the number of timed neutrons. The circuit components of the output of the first 885 were chosen so that the pulses into the discriminating tube were sharp and of uniform height, which simplified the modulation problem.

The square wave generator or amplifier modulator is shown in Fig. 8. The firing of the first 885 starts the pulse which controls the discrimination and the firing of the second tube stops it by short-circuiting, in a similar manner to the arc control. The time of starting and stopping is determined by the phase-shifting network $T_1C_2R_4$ and since the control of each tube is roughly independent of the other, any desired phase and width of pulse may be obtained. The power supply indicated as a battery must float, but a transformer rectifier system was finally used. The time taken for the pulse to rise from zero to its full value, or to fall, is less than 5 microseconds. The same considerations involving stability that apply to the arc control apply here, so the grid swing used was large (300 to 500 volts).

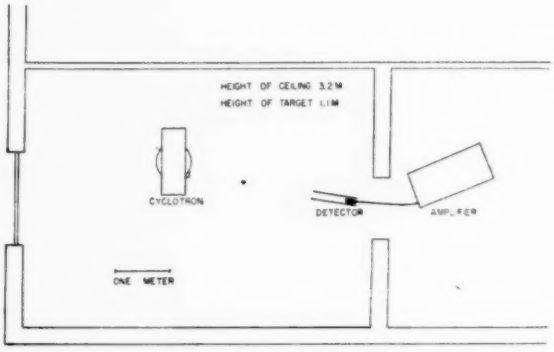

FIG. 5. Room plan.

Calibration

All time measurements were made on the screen of a 5-inch oscilloscope which was synchronized to the 400-cycle supply. For accurate measurements the oscilloscope sweep could be expanded in any region. With a 5-inch sweep the time scale was normally 500 μsec./inch and this was frequently increased to 100 μsec./inch. A central tap switch permitted one to examine the arc control, amplifier modulator, oscillator or various outputs with the oscilloscope. Time settings with the arc control and amplifier modulator could be made to better than 0.05

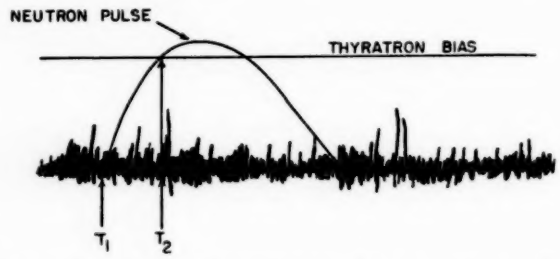

FIG. 6. Sketch of oscilloscope trace showing neutron pulse which starts at T_1 and fires the thyratron at T_2.

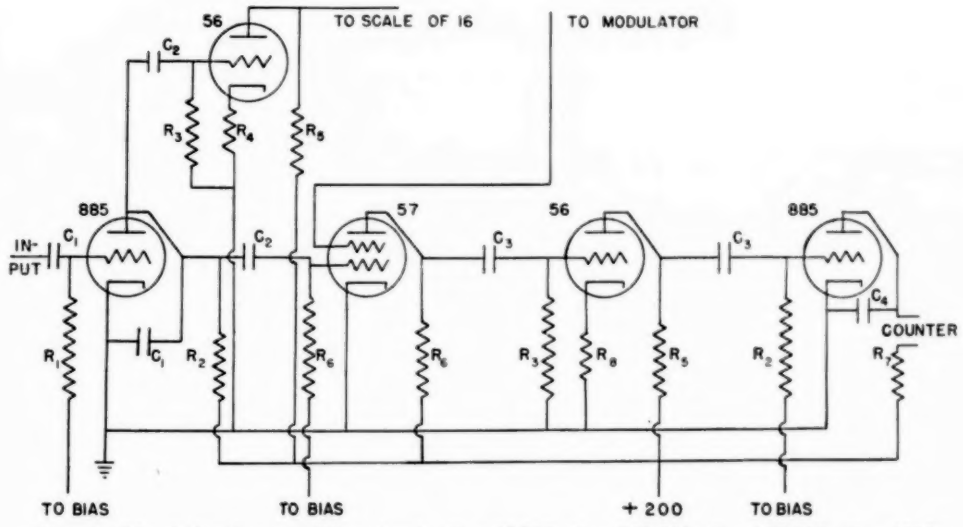

FIG. 7. Discriminating amplifier circuit. $R_1=40{,}000$; $R_2=200{,}000$; $R_3=100{,}000$; $R_4=4000$; $R_5=30{,}000$; $R_6=20{,}000$; $R_7=10{,}000$ adjustable; $C_1=0.00025$; $C_2=0.0001$; $C_3=0.005$; $C_4=1$. Resistance in ohms, capacity in μf.

inch on the oscilloscope screen which corresponded to 5 μsec.

Since a strictly linear sweep is difficult to obtain and the sweep frequently used in an expanded, nonlinear condition, all time measurements were referred to a 10-kilocycle oscillator synchronized to the 400-cycle supply. This was used to calibrate the oscilloscope trace. For greater accuracy, time measurements were made in 50-μsec. units, corresponding to one loop on the oscillator wave; i.e., the source time, detector time and interval between were set to be a certain number of 50-μsec. loops. The oscillator used was the so-called "transitron"[5] and the synchronization was introduced on the control grid of the 57 tube normally connected to the cathode.

The frequency of the 400-cycle motor generator set was checked against a separate stable oscillator of known frequency. It was found that the generator frequency was constant to about 1 percent.

It is important to know the time lag of the entire time measuring apparatus. In addition to the time lag in the amplifier, there is a lag of the order of 10 μsec. due to the acceleration of the deuterons. This lag depends on the cyclotron "D" potential, the 10-μsec. estimate being based on the assumption of 100 revolutions of ions at a frequency of 10 megacycles. The sum of all the time lags was measured directly by finding the time interval between production of the arc pulse and the detection of the first neutrons at the detector. With no time lags, this interval should be approximately zero for the very fast neutrons which first reach the detector in the same position used for time of flight measurements. In order to increase the number of fast neutrons the paraffin was removed from around the Be target. The detector time was then adjusted to be just before the source time and the detector time changed until it overlapped the source time. Counts were taken as a function of the detector time and the results are shown in Fig. 9. With 30 μsec. overlap of the source and detector the observed count was apparently just background, but for greater overlap the number

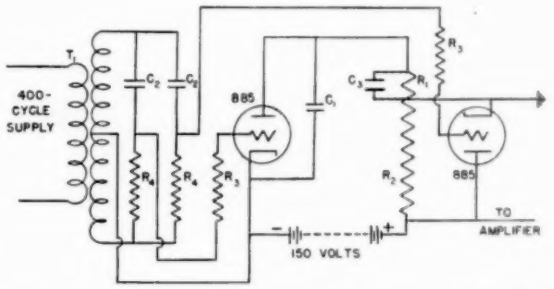

FIG. 8. Amplifier modulator circuit. $R_1=10{,}000$; $R_2=50{,}000$; $R_3=500{,}000$; $R_4=20{,}000$; $C_1=0.1$; $C_2=0.02$; $C_3=0.005$. Resistance in ohms, capacity in μf.

[5] C. Brunetti, Rev. Sci. Inst. **10**, 85 (1939).

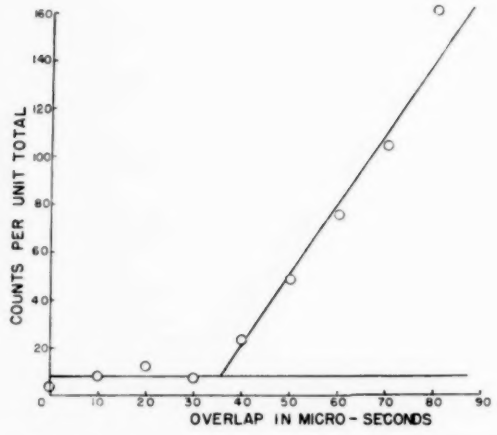

FIG. 9. Determination of over-all time lag. Neutrons counted *vs.* overlap of "on" times of source and detector.

of counts increased approximately linearly. The linear increase was extrapolated to the background and an effective time lag of 35 μsec. obtained. This time lag must be subtracted from all time measurements. It is gratifying but possibly fortuitous that this figure agrees with the sum of the amplifier lag and estimated lag in the cyclotron.

EXPERIMENTAL PROCEDURE

The apparatus was put into operation at first with the cyclotron ion source unmodulated and the amplifier was then adjusted for the best ratio of counting rate of neutrons to background. The ion source was next operated from the arc control which was adjusted for the length of burst desired. When the ionization chamber was placed at the proper distance and the amplifier connected to the oscilloscope the neutron velocity spectrum could be seen, the group at thermal energies being particularly striking. The square topped wave which modulated the amplifier was then adjusted for the desired time of flight. Counting was started with a three-pole switch which simultaneously started the scale-of-16 counter, the timed counter, and an electric clock. The observations were timed in order to be able to correct for noise and contamination background. Counts were taken until the desired number of timed neutrons were recorded, the number being determined by the statistical accuracy desired and convenient to obtain, usually 10 percent. For convenience in recording, observations were made for an integral number of revolutions of the mechanical counter dial at the output of the scale-of-16 counter, or in units of 960 recorded neutrons. The number of timed neutrons was referred to the total number of neutrons recorded in the same time interval. The time settings were made by switching the controlling pulse and the synchronized oscillator alternately onto the oscilloscope screen so that a direct comparison was made. At the end of an observation the time settings were checked before a new adjustment was made, although it seldom happened that any unexpected shift occurred. For absorption experiments observations were made with and without the absorber in place, with no change in the timing so that if the settings were stable any error in the initial adjustment of the width of the setting had little effect on the measured absorption.

For absolute absorption measurements it was necessary to compare the untimed neutrons with and without the absorber. This was necessary because the timed neutrons were referred to the untimed and the latter represented different numbers of incident neutrons for the runs with and without absorber. In order to avoid errors due to change in intensity of the source, this comparison was made by a succession of 30-second runs with and without absorber over a period of 10 minutes with the cyclotron operating under steady conditions.

It was found that with a thick boron carbide absorber (2 g/cm^2) in front of the ionization chamber, there was an appreciable background which decreased rapidly (Fig. 10), being approximately 5 percent at 300 μsec. after the end of the burst. This background is probably due to neutrons which are scattered around the room and which might penetrate the shielding and possibly be absorbed in the chamber. Such neutrons would, of course, take much longer to lose energy because of the long distance between collisions. The data were always corrected for this background.

Since it is known that the neutrons have a considerable life in the paraffin as thermal neutrons it is to be expected that thermal neutrons will be emitted after the neutron burst. This delayed emission has a considerable effect in these experiments and was therefore measured

directly with the ionization chamber in contact with the paraffin. The results and their effect upon the resolution of the apparatus will be discussed. With the ionization chamber in the same position, the neutrons from the block were also investigated with a thick Cd absorber (0.45 g/cm²) interposed. It was found that very few neutrons were detected after the production had stopped. If the gas pressure in the cyclotron was deliberately raised some neutrons were detected after the arc had stopped. With increasing gas pressure the number of these neutrons increased and the time after the extinguishing of the arc during which they were seen, increased until finally little effect of the arc modulation could be detected. When the gas pressure was too high a bright glow could be seen between the "*D*'s" indicating that the unmodulated neutrons came from ions originating outside the arc. In these experiments, care was taken to operate the cyclotron chamber at sufficiently low pressure to avoid this difficulty.

Results

The data were first corrected for the noise and contamination background taking into account the fact that for the timed neutrons the amplifier was sensitive for only a small fraction of the time. The timed neutron counts were then corrected for the fast neutron background as shown in Fig. 10. In the experiments carried out at 3 meters, this introduced an appreciable correction only for those neutrons with energy above 0.5 ev. For the data without the absorber the number of fast neutrons per unit total was subtracted from the number of counts per unit total to obtain the final result. The data with absorber, after being corrected for noise, were multiplied by the ratio of the untimed totals so that the numbers correspond to the same number of incident neutrons from the cyclotron. The number of fast neutrons per unit total already computed was then subtracted directly to obtain the corrected number with absorber. The ratio of the corrected numbers with and without absorber then gives the transmission directly and with the known number of atoms per cm² in the absorber, the cross section is obtained. The above procedure for the fast neutron background assumes that this background is the same with and without the absorber. Since it was rather laborious to do, this was not checked experimentally, but it seems very reasonable.

The time of flight associated with each point is the interval between the middle of the "on" time of the arc and the "on" time of the amplifier. These times were measured from the position of the controlling pulses on the oscilloscope screen and the 35-μsec. time lag was subtracted.

The results for a thin Cd absorber (0.052 g/cm) are shown in Fig. 11. The points indicated as circles were taken with a source-detector distance of 3.0 meters and an "on" time of source and detector of 100 μsec. The points indicated by crosses were taken with a source-detector distance of 1.5 meters and a source and detector "on" time of 50 μsec. so the resolution is the same for both sets. The times of flight have in each case been divided by the distance of flight so the axis represents the time of flight for one meter. The absorption maximum has been clearly resolved, the maximum cross section appearing for a one-meter time of flight of 190 μsec. or an energy of 0.14 ev. There is a definite indication of an ill-defined minimum in the neighborhood of 0.03 ev and below this energy the cross section seems to rise slowly. The statistical accuracy of each point is about 10 percent in the measurement of the transmission. No correction has been applied for the possible effect of the resolution of the apparatus or the effect of delayed emission of thermal neutrons, both of which are discussed later.

The absorption of thick cadmium (0.45 g/cm²) was initially undertaken in order to get some experience at higher energy (see Fig. 12). Knowledge of the absorption is also useful because such a thickness of cadmium is often used

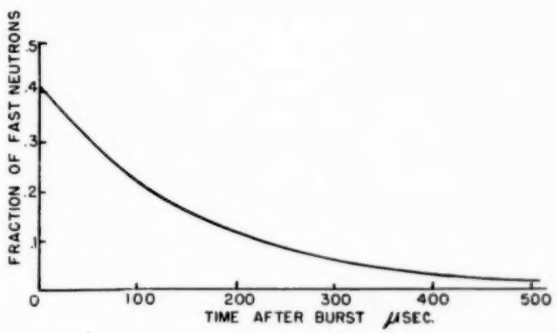

Fig. 10. Fast neutron background.

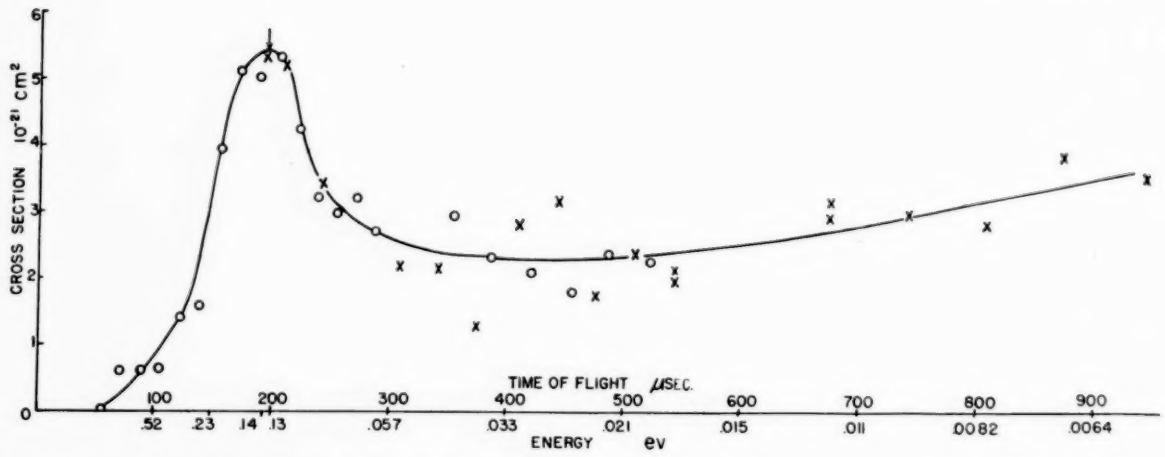

FIG. 11. Absorption of thin cadmium (0.052 g/cm²). Cross section for all cadmium isotopes *vs.* time of flight for 1 meter with corresponding energy points shown below. ○ : 3 meters source detector distance; × : 1.5 meters.

as a screen in slow neutron experiments. These data were taken at a distance of 3.0 meters between source and detector and the "on" times were 100 μsec. The absorption at low energy is practically complete and extends to much higher energy than the thin cadmium absorption, being 0.5 at 0.47 ev. The absorption edge is not sharply defined and the effect of the resolution of the apparatus on this edge is not large as will be shown later. The statistical accuracy above 0.4 ev is 10 percent but at lower energy it was decreased because of the long time involved in taking accurate data where the transmission is low. At 0.21 ev the error is 15 percent and the lowest energy point has a statistical error of 25 percent. No correction for delayed emission of thermal neutrons need be considered for these data as the energy range is above that where the thermal distribution plays an important role.

The results of the measurements of the transmission of indium and rhodium are shown in Figs. 13 and 14. These data were taken at a distance of 3 meters between source and detector and with source and detector "on" times of 50 μsec. which gave the highest resolution used in this work. Since these measurements were of an exploratory nature, thick absorbers (0.39 g/cm² for In and 0.60 g/cm² for Rh) were used. The transmission curves clearly show the resolution of the resonances which are at approximately 1.0 ev for each absorber. The probable errors of about 10 percent for In and from 10 to 20 percent for Rh, were governed largely by the long time it took to get data at high energy. For a single point on the Rh curve at 1.0 ev, counts were taken for about 40 minutes without interruption. It will appear that for high energy, a considerable correction for the resolution of the apparatus is necessary if a reasonable determination of the cross section as a function of energy is wanted. The present data are not sufficiently accurate to warrant these corrections and no attempt was made to make the measurements absolute.

The effective mean life or the delayed emission of thermal neutrons from the paraffin block was measured by placing the face of the ionization directly against the paraffin block. A burst of deuterons was produced for 50 μsec. and neutrons were counted in 50-μsec. intervals starting 15 μsec. after production had stopped. The results of this experiment are shown in Fig. 15 where the timed neutrons per unit total are plotted on a logarithmic scale against the time after the end of the burst. Except for the first two points, they seem to lie on a straight line indicating an exponential decay and an effective mean life of 170 μsec. The statistical accuracy of the data is better than 5 percent but in this measurement any error in adjusting the width of the detector "on" time enters linearly into the results. This error was not greater than 5 μsec. or 10 percent but it is the largest source of error in the results.

Resolution of Apparatus

It is quite clear that experiments with higher resolving power would have given greater detail in the results, but this was not feasible with the present equipment largely because of intensity. In the absence of such information, it is desirable to examine in some detail how the results are affected by the resolving power of the apparatus. No entirely satisfactory method of correcting for the resolving power of the apparatus has been found, although several methods have been used to attack the problem which give interesting results and are of help in the evaluation of the data.

If there is a uniform production of neutrons for a time δ and recording of neutrons for the same interval at a time s after the production of neutrons has stopped, neutrons having times of flight between s and $s+2\delta$ will be recorded and the most favored time of flight will be $s+\delta$. The function $f(s, t)$ expressing the distribution in time of flight to which the apparatus is sensitive starts from zero at $t=s$ and increases linearly until $t=s+\delta$ and decreases linearly until $t=s+2\delta$. With the proportionality constant C, $f(s, t)$ is expressed by the following relations.

$$f(s,t)=\begin{cases}0, & t<s,\\ (t-s), & s<t<(s+\delta),\\ 2\delta-(t-s), & (s+\delta)<t<(s+2\delta),\\ 0, & (s+2\delta)<t.\end{cases}$$

The distribution function $f(s, t)$ and its relation to the "on" times is shown in Fig. 16.

Fundamentally the problem of finding the actual number of neutrons, as a function of time of flight, from the observed data $D(s)$ amounts to finding a solution to the integral equation

$$D(s)=C\int_{s}^{s+2\delta} N(t)f(s,t)K(t)dt, \qquad (1)$$

where f is the function just described, $N(t)$ is the neutron distribution from the source which is the function that is to be found, and $K(t)$ represents the variation in the efficiency of the detector with neutron energy. If $K(t)$ is known (for instance, it would be a constant times t if the $1/v$ law holds for boron) the analysis can be simplified by considering the product $K(t)N(t)$ as a single function $M(t)$. $f(s, t)$ can be considered as a function of $s-t$ which is zero outside the limits s to $s+2\delta$ so the integral equation can be written

$$D(s)=C\int_{-\infty}^{\infty} M(t)f(s-t)dt. \qquad (2)$$

With the introduction of the Fourier transforms this equation can be solved for $M(t)$. This form of the solution is not, however, easily adapted to the practical problem since a function cannot easily be found to fit the data and in any case the labor involved is considerable and the data do not warrant such treatment.

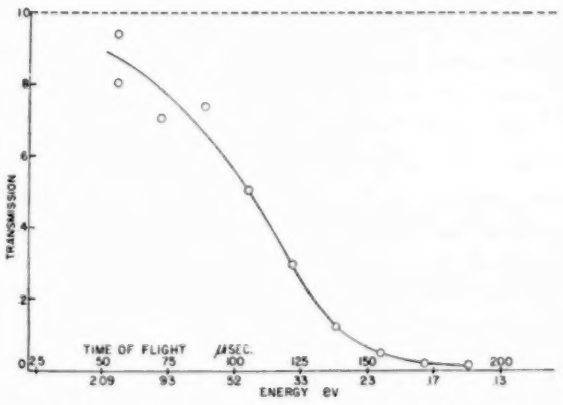

Fig. 12. Transmission of thick cadmium (0.45 g/cm²) *vs.* time of flight for 1 meter. Data were taken at 3 meters.

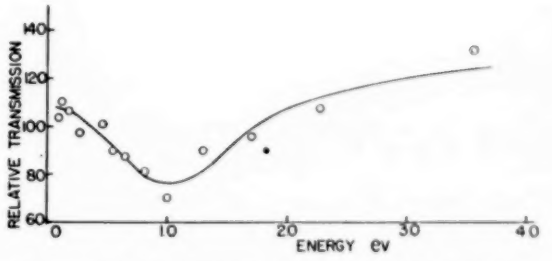

Fig. 13. Relative transmission of indium (0.39 g/cm²) *vs.* energy showing effect of the resonance at 1.0 ev. Data were taken at 3 meters.

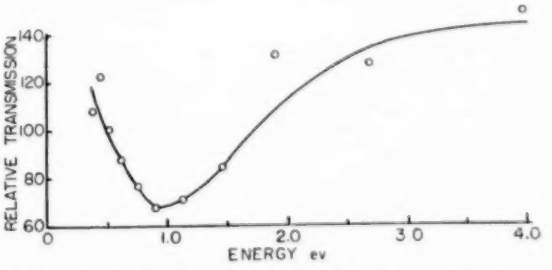

Fig. 14. Relative transmission of rhodium (0.60 g/cm²) *vs.* energy showing effect of resonance at 1.0 ev. Data were taken at 3.2 meters.

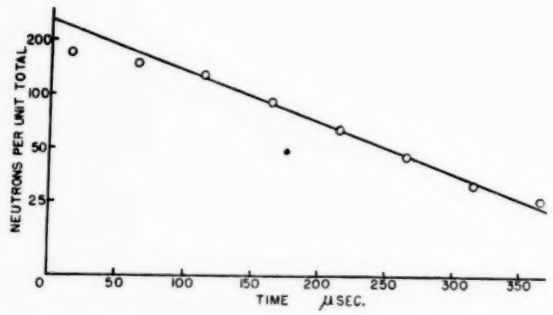

FIG. 15. Neutron decay in paraffin. Effective mean life 170 μsec.

The problem can be simplified by introducing an approximation for the function $M(t)$ in the form of the first three terms of the Taylor's expansion of $M(t)$ about t_0. Making a change of variable $t'=t-(s+\delta)$, one has for the distribution function,

$$\begin{aligned} f&=0 \quad \text{for} \quad |t'|>\delta, \\ f&=t'+\delta \quad \text{for} \quad -\delta<t'<0, \\ f&=\delta-t' \quad \text{for} \quad 0<t'<\delta. \end{aligned}$$

Without the primes, D becomes

$$D(t_0)=C\int_{-\delta}^{\delta} f(t)\Big[M(t_0)+tM'(t_0)+\frac{t^2}{2}M''(t_0)+\cdots\Big]dt. \quad (3)$$

The value of the constant C is not important as it is fixed for any f, and the transmission which is the interesting datum is the ratio of two observations of D. C can be evaluated by considering $K(t)$ and $N(t)$ to be constant and unity, the observation then representing a unit number of neutrons.

$$1=C\int_{s}^{s+2\delta} f(s,t)dt=C\delta^2 \quad \text{or} \quad C=1/\delta^2.$$

The integration gives

$$D=M\delta^2+M''\delta^4/12+\cdots. \quad (4)$$

The absence of a term in M' in this expression is due directly to the symmetry of $f(s,t)$ about $t=t_0$. In obtaining a transmission curve the ratios of the numbers with and without the absorber are considered, so the interesting information is $T=D_2/D_1$. The analysis is the same for the two cases except that for D_2 the corresponding function M_2 is not the number of neutrons from the source but is the number transmitted by the absorber or $M_2=A(t)M_1$ where A is the transmission of the absorber. The measured transmission is then expressed by

$$T=\frac{A(t)M(t)\delta^2+(\delta^4/12)[A''(t)+2M'(t)A'(t)+A(t)M''(t)]}{M(t)\delta^2+(\delta^4/12)M''(t)}. \quad (5)$$

In powers of δ, this may be written

$$T=A+[(A''+2A'M')/M](\delta^2/12)+\text{higher powers}. \quad (6)$$

If the resolution width is small the true transmission is given directly by the data as might be expected. To a second approximation the data are unaffected by the slope of the curve A, if the function M is large and slowly varying with energy. M is the product of the number of neutrons from the source and the efficiency of the detector and is therefore the effective number of neutrons or the number seen by the detector. Under these conditions only the curvature of the transmission curve will alter the data. In the vicinity of a resonance line the curvature may possibly be so great that the data do not give a good picture of the true transmission unless the resolution of the experiment is sufficiently increased.

In order to get a clearer picture of the effect of resolution on the data, the problem was approached from the opposite direction. Instead of attempting a solution of Eq. (1) for $N(t)$ in terms of the data, hypothetical curves for $N(t)$ were plotted and the corresponding functions $D(s)$ were computed for several values of δ which determines the resolving power. The Breit-Wigner theory predicts that the cross section in

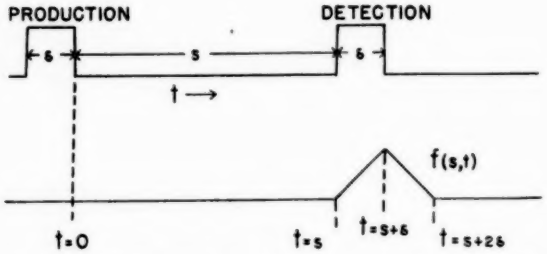

FIG. 16. Distribution function $f(s,t)$ showing relation to "on" times of source and detector.

the neighborhood of a resonance absorption is given in terms of the resonance energy E_R and the total width Γ by the following expression[6]

$$\sigma(E)=\sigma_0(E_R/E)^{\frac{1}{2}}\Gamma^2/[\Gamma^2+4(E-E_R)^2], \quad (7)$$

where σ_0 is the cross section at $E=E_R$.

$$\sigma_0=\frac{\pi}{2}\left(1\pm\frac{1}{2i+1}\right)\frac{\hbar^2}{2ME_R}\frac{4\Gamma_N}{\Gamma}. \quad (8)$$

Γ_N is the neutron width and i the angular momentum of the absorbing nucleus. The transmission of an absorber which has such a cross section will be

$$T(E)=e^{-\sigma n},$$

where n is the number of atoms per cm². $T(E)$ was then plotted on an axis representing time of flight for 1 meter. The value of σn was chosen such that there was almost complete absorption at resonance, since thick absorbers were actually used for indium and rhodium. The energy $E_R=1.0$ ev was also picked to correspond to this case. Curve 0 in Figs. 17 and 18 is for $T(E)$ under these circumstances with $\Gamma=0.2$ and $\Gamma=0.4$ ev, respectively. Curves 1 and 2 represent the transmission which would be observed for the resolution indicated by the distribution functions shown at the bottom of each plot. They were computed by approximate numerical evaluation of the integral in Eq. (1) for a number of values of s and a smooth curve drawn through the points. These curves correspond to "on" times

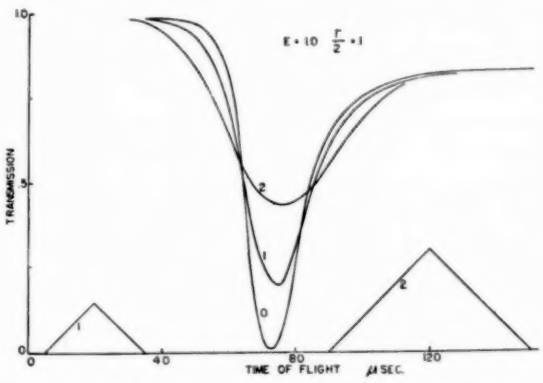

FIG. 17. Dispersion curve for $\Gamma=0.2$ and minimum transmission at 1.0 ev (curve 0). Effect of resolution by distribution functions indicated, is shown in curves 1 and 2.

[6] H. A. Bethe, Rev. Mod. Phys. 9, 69 (1937). See Eq. (428).

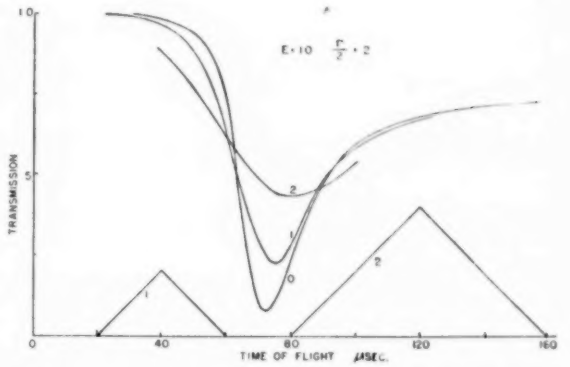

FIG. 18. Dispersion curve for $\Gamma=0.4$ and minimum transmission at 1.0 ev (curve 0). Effect of resolution by distribution functions indicated, is shown in curves 1 and 2.

for 3 meters of 45 and 90 μsec. for Fig. 17 and of 60 and 120 μsec. for Fig. 18. Curve 1 in each case corresponds approximately to the resolution which was actually used for indium and rhodium. The effect of the apparatus is to make the minimum of the transmission curve broader and less deep in both cases, although curve 1 follows the original curve reasonably well except for the depth of the minimum.

The resolution width on a time of flight axis is constant as this is the directly measured quantity. The resolution at a particular energy, however, increases with decreasing energy so that for thin cadmium, although the resolution corresponded to an "on" time of 100 μsec. at 3 meters, the transmission minimum was much more clearly resolved.

The effect of the resolution on an absorption edge was also studied in essentially the same way, in order to examine the effect of resolution on the thick cadmium measurements. The original curve in this case was obtained by fitting two exponential functions (see curve 0, Fig. 19). These two functions, $A(2-e^{-xt})$, Be^{-xt}, were joined at $T=0.5$ and the coefficients so adjusted that the curve corresponded to the observed transmission for thick cadmium. The derived curves are numbered to correspond to the resolution functions indicated below. Curve 1 which is indistinguishable from the original curve, was obtained for an "on" time equal to the inverse of the decay constant of the exponentials. Curves 2 and 3 were obtained for "on" times of twice and three times this amount. All the curves intersect

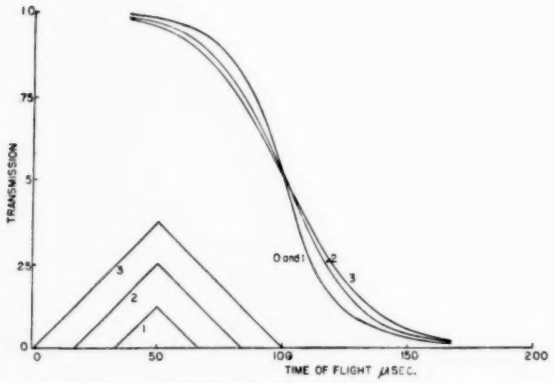

FIG. 19. Resolution of double exponential function simulating an "absorption edge." Curves 1, 2 and 3 give the effect of the resolution of the apparatus for the distribution functions indicated.

for a transmission value of one-half so that this point is given correctly regardless of the resolution used. This will, in general, be true only if the original transmission curve is symmetrical about this point. The general shape of the transmission curve is not greatly altered with any of the resolving powers illustrated. The thick cadmium measurement was made with the resolution illustrated by curve 2. The effect of the resolution on a sharp edge was also investigated. This, of course, shows considerable effect of the resolution but the result was a much sharper break than that observed for thick cadmium.

It was also found that the resolution of the apparatus had no effect on the shape of a single exponential function, i.e., if $M(t)$ is an exponential, the derived function is also an exponential function with the same decay constant. Consequently the delayed emission results do not need to be corrected for resolution.

When the time of flight is such that there is an appreciable contribution to the beam from the thermal distribution the effect of delayed emission must be considered. The resolving power will be decreased since the neutron pulse will be broader, and the simple resolution function $f(s, t)$ will no longer apply. Furthermore, the energy to be associated with a given time of flight setting will be changed if the delayed neutrons make an important contribution. The actual importance of the delayed neutrons depends on two considerations: (1) the relative number of cascading neutrons to thermal neutrons in the energy or time of flight interval to which the apparatus is sensitive, and (2) the amount of distortion of the delayed emission tail of the pulse due to the variation in the number—energy distribution of thermal neutrons, i.e., neutrons emitted long after the pulse must have a shorter time of flight or higher energy to arrive at the detector at the same time as neutrons emitted soon after the pulse. Above an energy $E=kT=0.025$ ev, this will decrease the effect of the tail as the number of neutrons decreases with increasing energy. The amount of this decrease depends on the particular energy setting.

The variation in the number-energy relationship also causes a distortion of the pulse itself, giving more weight (in a region above $E=kT$) to the neutrons emitted in the early part of the pulse because of the greater number of neutrons of lower energy or longer time of flight in the distribution. This distortion also affects the energy to be associated with a given setting of the apparatus. The amount of the distortion correction depends on the source-detector distance since this distance determines the spread in energy which corresponds to a given spread in time or resolution width.

The amount of distortion of the pulse and its tail can be computed with the aid of the number-energy relationships as given by Bethe.[7] These are expressed as $N(E)dE$, but to apply to this problem they must be expressed not in terms of the number as a function of energy in an energy interval, but in terms of time of flight in a time of flight interval. When they are so expressed, Q, the rate of neutron production taken as unity, and the values of the constants introduced, Bethe's Eq. (440) for the number of cascading neutrons becomes

$$N(t)dt=1.8\times10^{-8}/d^{-1}dt, \qquad (9)$$

and Eq. (461) for the thermal neutrons becomes

$$N'(t)dt=4.05\times10^{4}d^{3}t^{-4} \times\exp\left(-2.01\times10^{5}d^{2}/t^{-2}\right)dt, \qquad (10)$$

where t is the time of flight in μsec. from source to detector and d is the source detector distance in meters. It is not correct to use these expressions

[7] H. A. Bethe, Rev. Mod. Phys. **9**, 69 (1937). See Eqs. (440) and (461).

as they stand, in order to compare the number of thermal and cascading neutrons since equilibrium of thermal neutrons with the source was assumed in the derivation of $N'(t)$ above, and this condition is not satisfied in the problem under consideration. The cascading neutrons probably come into equilibrium with the source in a very short time (order of 10 μsec.) but because of the long mean life (approximately 200 μsec.) it takes much longer for the equilibrium number of thermal neutrons to be established. For any time of the order of the mean life the number of thermal neutrons in the paraffin increases during the burst. As the duration of the burst used in the experiments was always short compared to the time necessary to establish this equilibrium, this effect was important. If the time of slowing down to thermal energies may be neglected (10) should be multiplied by a time factor $(1-e^{-t'/\tau})$ where t' is measured from the start of the burst and τ is the mean life of thermal neutrons in the paraffin. This time factor also causes an additional distortion of the pulse giving more weight to the end of the pulse and therefore higher energy neutrons. At energies greater than kT it is in the opposite direction to the distribution distortion.

To illustrate the effect of these corrections on the data a sample calculation was made of the effect of distortion of the pulse shape and of delayed emission. Simplified conditions of source-detector distance of 3 meters, source "on" time of 100 μsec., and an infinitesimal detector "on" time were assumed. The relative number of neutrons from various parts of the pulse and its tail which would be recorded at the detector are given in the last five columns of Table I for time of flight settings from the center of the pulse corresponding to 0.2, 0.15, and 0.10 ev. In the second column the ratio of the number of thermal neutrons at the pulse center to the number of cascading neutrons is given. It may be seen on the basis of these assumptions that the thermal distribution is not important at an energy of 0.2 ev and while there will be some distortion of the pulse shape at this energy the effect of the delayed emission will be in the opposite direction and can essentially be neglected. At 0.15 ev the effect of pulse distortion is not great but the effect of the tail of the pulse begins to be appreciable and the resolution is not as good. The thermal neutrons, however, still make only about half the contribution to the number of recorded neutrons so the effect on the data is not large. At 0.10 ev the time distortion begins to be more important than the distribution distortion and the effect of the tail is more important. Furthermore, the beam is now predominantly thermal neutrons so the energy to associate with the time setting computed from the time of flight from the center of the pulse is too low by 10 percent or more. The decrease in resolving power at this and all lower energies, begins to have an appreciable effect on the data. In this region, however, the time of flight is longer (686 μsec. for 3 meters) and as the energy decreases the effect of the increasing spread in the effective "on" time becomes less important because of the increasing time of flight. For energies less than kT the distortions will be markedly different, but as the data do not indicate any rapid variation in the transmission curves in this region the resolution and distortion corrections were neglected as small in magnitude and importance.

The effect of the chemical bond on the slowing down process has been neglected in the above calculations. If the effect is appreciable it will probably result in a slower loss of neutron energy which makes the thermal neutrons less important in comparison to the cascading neutrons, both because of the increased number of cascading neutrons and because of the increased delay in the production of thermal neutrons. These calculations might therefore be considered as showing the maximum expected effect, but can only be considered as indicating the order of magnitude because of the lack of detailed knowledge of the slowing down process.

TABLE I. *Relative numbers of neutrons from various parts of a 100-μsec. pulse and its tail with short detector time. N'/N gives the ratio of thermal to cascading neutrons.*

		Time in μsec. from the Start of the Burst				
Energy ev	N'/N	25	50 Pulse Center	100 Pulse End	125 Tail	150 Tail
0.20	0.33	0.91	1.0	0.38	0.13	0.027
0.15	1.2	0.71	1.0	0.81	0.52	0.18
0.10	3.9	0.60	1.0	1.26	0.98	0.60

Discussion of Results

The plot of the thin cadmium data (Fig. 11) clearly shows the resolution of the resonance and gives a maximum value of the cross section of 5.4×10^{-21} cm^2 at 0.14 ev. Below this energy the cross section decreases to about 2.3×10^{-21} cm^2 and then rises slowly with decreasing energy. The minimum appears to be in the neighborhood of 0.03 ev but since the minimum is not well defined and the points are scattered, the energy of this minimum cross section cannot be stated accurately. The cadmium resonance unfortunately comes at an energy where the corrections involving the thermal group of neutrons are most uncertain. As previously indicated, the effect of delayed emission becomes noticeable somewhere below 0.15 ev and is an appreciable effect at 0.10 ev. The shape of the low energy side of the resonance is therefore under suspicion. At still lower energy the time of flight is long enough that the effect of delayed emission and distortion of the pulse shape have a less important effect. The relative error in the energy may still be considerable. A corrected plot of the data was made which included an approximate correction for the delayed emission but not the distortion of the pulse, thus making a considerable over-correction for the effect of the thermals. The energy of the maximum was shifted only 0.02 ev to 0.16 ev. This seems to be sufficiently small so that for the present it is best to omit corrections for the delayed emission in the thin cadmium data. Also the ratio of cascading to thermal neutrons is not well known as a function of energy in this range because of the uncertain effect of the hydrogen chemical bond. With more complete information about the slowing down process and with more accurate data such corrections will be important.

The cross section in the region of the maximum agrees surprisingly well for the data taken at 3 meters and at 1.5 meters. These data also agree well with the data taken at still shorter distances in preliminary work. This seems to preclude the possibility of gross accidental or systematic errors in the measurement since timing errors would be expected to be constant and not to vary linearly with the distance from source to detector. Also uncorrected errors due to delayed emission or pulse distortion would affect the data taken at various distances differently.

A measurement of the cadmium cross section by the time of flight method was made by FGMTW.[3] They show a high point in the cross section plot at 0.10 ev. This rough agreement is fortuitous, since the position of the high point is not sufficiently well established because of the small number of observations and the low resolution in their results. At energies below the high point they find a cross section which decreases continuously with energy, in disagreement with the present results which show a minimum and then an increasing cross section. The increasing cross section has better theoretical justification, for at sufficiently low energy the $E^{-\frac{1}{2}}$ factor in the Breit-Wigner formula will predominate and predicts a $1/v$ cross section.

A determination of the cadmium resonance was also made by Hoffman and Livingston[8] who arrived at their results by measuring the cross section in boron of those neutrons which were not absorbed in cadmium. This essentially amounts to an inference of the constants of the cadmium resonance without resolving the line. They found $E_R=0.18$ ev and $\Gamma=0.15$ ev and in view of this very indirect method, their results are in sufficient agreement with the present results.

In order to determine the width of the resonance, an attempt was made to fit the data with a dispersion curve.[7] A point-by-point fit of the data to a dispersion curve was not feasible because of the complexity of the effect of resolution on the shape in the intermediate and thermal energy region, and because of the statistical inaccuracy of the data. A simple criterion, however, is to compare the ratio of the cross section at resonance with the cross section at some other energy, i.e., to solve Eq. (7) for Γ^2 and evaluate it by introducing the measured values of the cross sections.

$$\Gamma^2=\frac{4(E-E_R)^2}{(\sigma_0/\sigma)(E_R/E)^{\frac{1}{2}}-1}. \qquad (11)$$

The ratio of the cross section at resonance to the cross section at the low energy minimum gives $\Gamma(\mathrm{Cd})=0.12$ ev. Insufficient resolution would make the measured cross section at resonance lower than it actually is, but would have less effect on the minimum as it is much broader on a

[8] J. G. Hoffman and M. S. Livingston, Phys. Rev. **52**, 1228 (1937).

time of flight axis. The observed ratio is therefore equal to or smaller than the true value and the value of Γ computed from it is an upper limit.

A check on this value of the width can be made by considering the ratios of the cross section at resonance to the cross sections at higher energies. With the thick cadmium measurements, the ratio of the cross section at resonance to the cross sections at 0.26, 0.36, 0.52 and 0.80 ev gives values of Γ of 0.12, 0.17, 0.23 and 0.31 ev, respectively. Whether this variation of Γ computed on the basis of a single resonance is real or whether it is entirely due to an effect of resolution has not been determined. Since the resolution correction to the thick cadmium data is about equal to the probable error in the measurements, these data could not give a conclusive answer. The resolving power of the apparatus could give rise to a discrepancy in this direction, so that the smaller value of Γ which agrees with the result from thin cadmium is probably the best.

From a knowledge of the absolute cross section at resonance and the effective width, one can obtain the neutron width Γ_N from Eq. (8). It seems likely that the absorption in cadmium is by one of the odd isotopes whose abundances are 12.3 and 13 percent. If one assumes 13 percent abundance of the effective isotope, the cross section at resonance becomes $\sigma_R' = 4.2 \times 10^{-20}$ cm^2. Since $i = \frac{1}{2}$ for the odd isotopes, $\Gamma_N' = 3 \times 10^{-4}$, or 10^{-3} ev, depending upon the angular momentum of the resulting nucleus.

The data for thick cadmium are not subject to the uncertain corrections which must be considered for thin cadmium, since the data are taken at a higher energy where the effect of the thermal neutrons can be largely neglected. Certainly, the effect of delayed emission does not require any appreciable correction above 0.15 ev. These data fit the sample resolution curve given in the previous section very well, hence a good idea of the amount of the resolution correction can be obtained (compare curves 0 and 2, Fig. 19). The shape of the curve is not seriously altered by this effect, and probably at no point is the transmission value altered by more than 0.08. In general, the resolution correction is of the order of magnitude of the probable error in the measurement of the transmission value.

What has been referred to as an absorption edge in cadmium is seen to be poorly defined since there is no energy where one can say that the transmission decreases rapidly. It is probably best merely to say that for the thickness used 0.45 g/cm^2), the energy for a transmission of one-half is 0.47 ev, and that below 0.2 ev the transmission is negligible (3 percent or less).

The data for indium and rhodium are also free from the uncertainties introduced by the thermal distribution since the interesting parts of the curves are in the region of higher energy. On the other hand, the shapes of the curves are definitely affected by the resolution of the apparatus. Although the smallest "on" times were used for these measurements, the energy resolution is much poorer in this region than in the region of the cadmium resonance. When one compares the data with the curves shown in Fig. 17 it is evident that the absorption line is more poorly resolved than in the hypothetical case. Although the "on" times, actually used, correspond to case 1 the resolution realized corresponds more nearly to case 2. The thickness of the absorbers used was such that the transmission at resonance was almost certainly negligible, while the data show a transmission at resonance probably over one-half. This indicates that the width of the line is somewhat less than was chosen for sample plots to illustrate the resolution where the smallest value of Γ considered was 0.2 ev. Since the corrections due to the low resolution were rather large and the data of an exploratory nature, it did not seem reasonable to try to make any resolution corrections. It appears that the width is probably less than 0.2 ev, and that the energy of the minimum in the transmission is about 1.0 ev. The observed shape of the resonance, however, is not entirely due to the resolving power of the apparatus since the resolution used was such that a very sharp resonance could at most affect four adjacent points. The breadth of the absorption lines observed for rhodium and indium is, therefore, not negligible in comparison with the resolution width, even though the correction for resolution is large. No information about the cross section can be inferred from the data since absolute calibration of the transmission was not made.

The energies of the indium and rhodium resonances have been determined by the boron

method. Goldsmith and Rasetti[9] found values of 1.16 ev and 1.38 ev for rhodium and indium, respectively. Later measurements by Hornbostel, Goldsmith, and Manley[10] on the self- and mutual absorption of the resonance neutrons in rhodium and indium give values for Γ of 0.13 and 0.07 ev for rhodium and indium, respectively, and the difference in the energies of the resonances as 0.15 ev. While it is difficult to see how the time of flight measurements could be in error by more than 0.2 ev, in view of the uncertainties in both methods the results are in good agreement. The widths from absorption measurements are well within the upper limit set by these results, and the difference in energy of 0.15 ev is within the experimental error of this work.

The time of flight measurements give a direct determination of the resonance energy and the approximate agreement with the results of the boron method constitute a check on the $1/v$ absorption in boron. A direct measurement of the boron absorption was made by Fertel *et al.* with results inconsistent with the $1/v$ law. The most serious disagreement is at low energy where they found much too low a cross section. This disagreement is in the same energy region and in the same direction as their disagreement with the results of this work on cadmium, so that one is tempted to suspect some systematic error in their results at low energy. There were some experimental difficulties, and the authors state their regret that they were unable to pursue their investigations further. In view of the many good reasons for expecting the $1/v$ law to hold, in addition to the check in this work, their results cannot be considered as a basis for serious doubt of the $1/v$ absorption in boron, although it would be desirable to repeat the boron absorption experiment.

The study of the delayed emission was undertaken primarily to ascertain the effect upon the time of flight measurements and the experimental conditions were the same except for the detector position. It also provides some direct evidence of the existence of thermal neutrons for some considerable period after the burst although the geometry of the experiment was not well suited to an accurate determination of the mean life. It was found that the effective mean life of thermal neutrons coming out of the block is 170 μsec. This, however, is somewhat shorter than the true mean life because of diffusion of neutrons from the inside of the block to the surface where they escape.

The effect of the diffusion can be estimated,* if one assumes as initial conditions the stationary neutron distribution due to a uniform production of thermal neutrons in an infinite slab of paraffin of thickness $2a$. Under these conditions the neutron current at the surface of the slab is

$$j=\frac{2q}{a}\sum_{n\ \mathrm{odd}}\frac{\exp\left[-(1+n^2\gamma^2)t/\tau\right]}{1+n^2\gamma^2}.$$

q is the number of thermal neutrons produced per cm per sec., τ is the true mean life of neutrons in the paraffin and $\gamma=\pi\lambda/2a$ where λ is the diffusion length, approximately 2 cm. For the source used a is 10 cm. The current j was plotted logarithmically against t/τ and the best straight line approximation to this function was plotted in the time interval in which observations were taken. The slope of this line indicated that the observed decay or effective mean life, if the above conditions had been fulfilled, would have been 20 percent less than the true mean life in the paraffin. This gives a mean life of 210 μsec., but the geometrical correction in the actual conditions used (Fig. 3) is probably larger than this, thus indicating a still longer true mean life. The effect of the lack of homogeneous sources would be in the opposite direction. These results therefore cannot be used accurately to determine the true mean life. A determination of the mean life of neutrons in water was made by Frisch, v. Halban and Koch[11] who arrived at the result 270 μsec. from a measurement of the capture cross section. Reduced to paraffin this would be 230 μsec. in agreement with the corrected value above.

The writers are grateful to H. A. Bethe and G. Placzek for numerous stimulating discussions during the course of these experiments.

[9] H. Goldsmith and F. Rasetti, Phys. Rev. **50**, 328 (1936).

[10] Hornbostel, Goldsmith and Manley, Phys. Rev. **58**, 18 (1940).

* The writers are indebted to G. Placzek for this calculation.

[11] Frisch, v. Halban and Koch, Kgl. Danske Videns. Selskab. Math.-fys. Medd. **15**, 10 (1937).

Long-Lived Radioactive Carbon: C^{14}

S. RUBEN AND M. D. KAMEN
Radiation Laboratory and the Department of Chemistry, University of California, Berkeley, California

(Received December 2, 1940)

A long-lived activity has been obtained by deuteron bombardment of graphite. This activity has been shown by chemical methods to be isotopic with carbon. The same activity has been obtained by slow neutron irradiation of nitrogenous compounds (NH_4NO_3, NH_4NO_2, etc.). The radiations consist of low energy negative electrons with a range of 19 ± 2 mg/cm² aluminum (145 ± 15 kev upper energy limit). No soft or hard gamma-rays could be detected. The nuclear reactions must be C^{13} (d, p) C^{14} and N^{14} (n, p) C^{14}. A sample has been followed in a screen wall Geiger counter for 9 months and has shown no decay. From cross section and yield estimates the half-life of C^{14} is probably 10^3–10^5 years. The production, isolation, and detection of C^{14} for tracer work is described.

THERE are 5 known isotopes of carbon, stable C^{12} (~99 percent abundance), stable C^{13} (~1 percent abundance), C^{10} (8.8-second half-life),[1] C^{11} (21-minute half-life),[2] and C^{14} (half-life 10^3–10^5 years).[3] The production and properties of C^{14} will be described in this paper. In view of the possible application of C^{14} as a tracer,[4] a discussion of relative yields and specific activities obtainable is included together with a brief description of detection methods.

It is of interest to review briefly the history of C^{14}. In 1934 Kurie, using a Wilson cloud chamber, studied the fast neutron disintegration of nitrogen and observed in addition to the known[5] alpha-particle emission, another type of transmutation,[6] less frequent, in which singly charged heavy particles were emitted. Kurie suggested these were protons due to

$$n_0^1+N_7^{14}\rightarrow C_6^{14}+H_1^1+Q_1. \qquad (1)$$

Later Bonner and Brubaker,[7] irradiating nitrogen with slow neutrons, observed a few heavy tracks (~1.06-cm range) which they attributed to alpha-particles. Burcham and Goldhaber[8] demonstrated these tracks were protons and suggested they originated from reaction (1). Bonner and Brubaker[9] agreed with Burcham and Goldhaber and moreover estimated $Q_1=0.58\pm0.03$ Mev. From the known mass difference between neutron and proton, C^{14} was estimated to be unstable with respect to N^{14} by ~0.17 Mev so that it could be expected that C^{14} would be a beta-emitter of relatively long half-life. McMillan[10] found a long-lived soft radiation from metal scraped from inside the cyclotron vacuum chamber and suggested it might be due to C^{11} formed by the reaction

$$D_1^2+C_6^{13}\rightarrow C_6^{14}+H_1^1+Q_2. \qquad (2)$$

Unfortunately, the sample was accidentally lost before any chemistry was performed. However, the upper energy limit of the beta-radiation was measured by Libby and Lee[11] using a screen wall Geiger counter and found to be ~10 kev. (It seems quite likely this activity was due to H^3 which was discovered by Alvarez and Cornog.[12]) Shortly after, the writers had occasion to prepare N^{13} (by deuteron bombardment of graphite) for use as a tracer in nitrogen fixation experiments. The same graphite target was used in all bombardments and after ~1000 μ amp. hr. of 8-Mev

[1] Barkas, Creutz, Delsasso, Fox and White, Phys. Rev. **57**, 562 (1940).
[2] Cockcroft, Gilbert and Walton, Proc. Roy. Soc. (London) **A148**, 225 (1935).
[3] S. Ruben and M. D. Kamen, Phys. Rev. **57**, 549 (1940); **58**, 194 (1940).
[4] C^{11}, despite its short half-life has already been used rather extensively as a tracer, cf. G. T. Seaborg, Chem. Rev. **27**, 199 (1940).
[5] N. Feather, Proc. Roy. Soc. (London) **A136**, 709 (1932).
[6] F. N. D. Kurie, Phys. Rev. **45**, 904 (1934); **46**, 330 (1934).
[7] T. W. Bonner and W. M. Brubaker, Phys. Rev. **48**, 469 (1935).
[8] W. E. Burcham and M. Goldhaber, Proc. Camb. Phil. Soc. **32**, 632 (1936).
[9] T. W. Bonner and W. M. Brubaker, Phys. Rev. **49**, 223 (1936); **49**, 778 (1936).
[10] E. M. McMillan, Phys. Rev. **49**, 875A (1936).
[11] W. F. Libby and D. D. Lee, Phys. Rev. **55**, 245 (1939).
[12] L. W. Alvarez and R. Cornog, Phys. Rev. **56**, 613 (1939).

deuterons it was burned to CO_2 which was precipitated as $CaCO_3$. A fraction of this material, when mounted on the inner surface of a cylinder and counted in a screen wall counter of the type developed by Libby,[13] gave an effect of 16 ± 2 counts/min. It was possible to show this effect was not due to natural contamination of the chemical reagents used. It seemed desirable, however, to obtain stronger samples before drawing any positive conclusions. It was apparent that a prolonged bombardment was necessary and, due to the heavy schedule under which the cyclotron was operating, this was not possible until recently. In the meantime B_2O_3 was bombarded in a gas-tight target chamber with 32-Mev alpha-particles accelerated in the 60″ cyclotron in a search for C^{14} produced by

$$_5B^{11}+{}_2He^4\rightarrow{}_6C^{14}+{}_1H^1+Q_3. \qquad (3)$$

It had been observed that when B_2O_3 is bombarded with deuterons the major fraction of the newly formed C^{11} is expelled from the target as CO.[14,15] After $\sim10\,\mu$ amp. hr. of alpha-particle bombardment, the gas from the target chamber was introduced into an ionization chamber connected to an FP-54 electrometer tube and amplifier circuit.[16] No evidence for any long-lived activity was found.

At this time Pollard[17] and Bower and Burcham[18] presented additional evidence for the production and instability of C^{14}. Pollard investigated the protons from reactions (2) and (3). Using 3-Mev deuterons, the longest proton range was 81.1 ± 2 cm yielding $Q_2=8.21$ Mev. Bombardment of boron with ThC alphas produced protons with a 97.6-cm range; Po alpha-particles gave a proton group of 42.1-cm range. These experiments yielded an average $Q_3=0.66$ Mev and using these values he proposed the mass of C^{14} to be 14.00780 ± 0.00020 and thus unstable with respect to N^{14} by ~300 kev. His attempts to detect an activity ascribable to C^{14} after $\sim6\mu$ amp. hr. bombardment of graphite with 3-Mev deuterons were unsuccessful. Bower and Burcham, using 0.8-Mev deuterons, found a 48-cm group of protons which they attributed to reaction (2) with $Q_2=6.1$ Mev. Recently Bennett, Bonner, Hudspeth and Watt[19] have confirmed this observation, using targets enriched in C^{13}.

Isolation of C^{14} After Prolonged Deuteron Bombardment

By resorting to the method of internal targets[20] it was finally found possible to produce appreciable amounts of an activity which was proven chemically to be isotopic with carbon. A probe target, covered with a small quantity of Aquadag, was inserted into the vacuum chamber and subjected to a 40-μ amp. beam of 7–8 Mev deuterons for ~120 hr. The probe was frequently removed and examined and the Aquadag renewed whenever necessary. The target prepared in this way proved unsatisfactory for prolonged bombardment and was finally removed and examined for activity. For a second bombardment, the graphite was electroplated with copper and hard soldered to the probe surface. The graphite was of a type prepared for use as an anode in a high power rectifier tube. This target proved more satisfactory and was able to withstand 500–600 μ amperes of ion current without appreciable deterioration. This probe was placed far into the vacuum chamber to intercept high currents ($\sim500\,\mu$ amperes) of 3–4-Mev deuterons until 13,000 μ amp. hr. had been accumulated.

Since high specific activities are necessary for many tracer experiments it is apparent that the bombardment of carbon enriched in C^{13} is desirable. Professor H. C. Urey and Dr. D. W. Stewart very kindly sent us 0.63 gram of ~23 percent C^{13} as amorphous carbon prepared by the reduction of enriched NaCN with magnesium at ~400°C. A portion of this carbon was placed

[13] W. F. Libby, Phys. Rev. **46**, 196 (1934).
[14] Yost, Shinohara and Ridenour, J. Chem. Phys. **3**, 133 (1935).
[15] Ruben, Kamen and Hassid, J. Am. Chem. Soc. **61**, 661 (1939); **62**, 3443 (1940).
[16] We are indebted to Dr. E. Segrè for the loan of the electrometer and for aid in many of the measurements made with it.
[17] E. Pollard, Phys. Rev. **56**, 1168 (1939).
[18] J. C. Bower and W. E. Burcham, Proc. Roy. Soc. (London) **A173**, 391 (1939).
[19] Bennett, Bonner, Hudspeth and Watt, Phys. Rev. **58**, 478 (1940). Holloway and Moore (Phys. Rev. **57**, 1086A (1940)) were unable to detect the protons from $C^{13}(d,p)C^{14}$. They placed a lower limit of 1.2×10^{-28} cm² on the value for the cross section of this reaction at 1 Mev.
[20] R. R. Wilson and M. D. Kamen, Phys. Rev. **54**, 1031 (1938).

in a steel mold and subjected to high pressure[21] (40 tons/in.^{2}). The material failed to cohere and examination under a microscope revealed a granular structure quite different from graphite found to press well. Since no equipment for very high temperature work was available, the carbon was sent to the Edgewater Works of the National Carbon and Carbide Corporation, at the suggestion of Dr. H. C. McPherson. In these laboratories, after considerable effort, Dr. McPherson succeeded in preparing several satisfactory targets. The procedure employed by Dr. McPherson involved dilution of the amorphous carbon with a suitable amount of pitch binder. The mixture was pressed into a mold to make a slab 2 mm thick and 1 cm square. The slab was baked at 1200°C and then "graphitized" (heated in vacuum) at 2800°C to drive off all volatile matter. The resultant material contained 9.3 percent C^{13}, a reduction by a factor of more than two from the starting material. (Such loss is unavoidable with small quantities of carbon). The slab was sprayed with molten copper (Schoop process) to provide a tenacious metallic backing for soldering the material to the water-cooled probe surface. It was necessary in some instances to repeat the spraying since the slabs showed a tendency to embrittle and disintegrate when reheated. The slabs which survived this treatment possessed about $\frac{1}{5}$ the heat conductivity of the best graphite obtainable and proved to be adequate as target material. One slab mounted with phos-copper solder on a probe withstood 10 hours' bombardment with 300 μ amperes of 3–4-Mev deuterons and showed no visible deterioration.

Chemical Identification

The graphite was burned in a stream of oxygen and the resultant gases passed over hot cupric oxide and finally absorbed in $Ca(OH)_2$. The precipitated $CaCO_3$ was filtered and carefully washed. The filter paper containing the precipitate, when placed over a thin-walled aluminum Geiger counter (0.1 mm wall thickness), failed to show any activity. A portion ($\frac{1}{3}$) of this sample, spread out in a thin film inside a cylinder which was introduced into a screen wall counter, was active (~400 counts/min.). In the counting arrangement used, the cylinder containing the sample could be slid to and fro over the counting region, thus enabling alternate readings of sample activity and background to be taken. The procedure was repeated using ordinary $CaCO_3$ prepared in the same way to test for activity in the reagents. The $CaCO_3$ precipitate obtained in this way showed no activity.

The active $CaCO_3$ was treated with acid and the CO_2 collected. After drying, this was introduced into a Geiger counter and gave an effect of ~2000 counts/min. The 5-fold increase in activity was due to increased solid angle and elimination of self-absorption. The active gas was absorbed in $Ca(OH)_2$ and reconverted into CO_2 several times with no loss in specific activity. However a preliminary measurement indicated the range of the radiations in aluminum to be approximately 12 mg/cm^2; which is close to the known value for S^{35}. The procedure used to this point did not exclude the possibility that part or all of the activity was due to $S^{35}O_2$. Carrier (inactive) SO_2 was mixed with the active gas and the mixture treated with $KMnO_4$ in sulfuric acid solution to oxidize the SO_2 to SO_4^{--}. There was no loss in gaseous activity. In another experiment the mixture of the gaseous activity and inactive SO_2 was absorbed in alkali and the SO_3^{--} oxidized to SO_4^{--} with I_3^-. The CO_2 was liberated by acidifying the solution and absorbed in $Ca(OH)_2$. The $CaCO_3$ was active, there being no loss in specific activity.

Production of C^{14} by Neutron Transmutation of Nitrogen

It was realized from the very beginning that deuteron bombardment of carbon was not the best method for preparing C^{14} in high specific activity suitable for tracer work. The transmutation of N^{14} by slow neutrons (reaction 1) offered many attractive features: (1) Possibility of obtaining very high specific activity since the target material is not carbon but nitrogen. (2) Production of C^{14} is achieved as a by-product of cyclotron operation and thus does not interfere with other research. (3) Any strong neutron source will suffice. It is not necessary to go to high bombarding voltages (3–4 Mev as is the case for

[21] We are indebted to the Department of Civil Engineering for cooperation in these experiments.

deuteron bombardment). (4) The nitrogenous material, also containing some hydrogen, can profitably replace water or paraffin as a shielding material.[22]

While the slow neutron experiments are by no means complete, the results obtained thus far conclusively indicate this to be the most practical method for C^{14} production.

Two five-gallon carboys filled with saturated solutions of ammonium nitrate were placed in the region opposite the deflector of the Berkeley medical cyclotron. The solutions were irradiated with neutrons during a period of ~6 months. Approximately 40,000 μ amp. hr. of deuteron bombardment at 16 Mev of various targets (principally beryllium and phosphorus) took place in this time. A chemical analysis was performed in which carbon monoxide, carbon dioxide, methane, carbon, methanol, cyanide and formaldehyde were added as carriers and then separated and analyzed for radioactivity. After vigorous and prolonged shaking the gaseous compounds were pumped off. The gases were oxidized to carbon dioxide and absorbed in $Ca(OH)_2$. The $CaCO_3$ was very active, containing 10^5 counts/min. By the chemical methods described above the activity was shown to be isotopic with carbon.

Charcoal and other sediment was separated from the NH_4NO_3 solution by filtration. This proved to be completely inactive. Cyanide was precipitated as AgCN which also was inactive. Methanol and formaldehyde were distilled from an aliquot (~10 percent) of the NH_4NO_3 and the distillate divided into 2 portions. From one portion the insoluble hydrazone of formaldehyde prepared by the addition of excess 2,4 dinitrophenyl hydrazine was found to be inactive. The methanol from the other portion was volatilized and passed over hot cupric oxide. The resulting CO_2 was not active. For future experiments a more complete and elaborate chemical analysis has been devised.

In addition to NH_4NO_3 solutions, several samples of solid NH_4NO_3 (~1 lb.) as well as concentrated NH_4NO_2 solutions have been irradiated with neutrons. C^{14} was found only in the gaseous fraction. The solid NH_4NO_3 was irradiated in sealed soft glass containers. No volatile activity could be pumped off the solid even after addition of carrier gases. However, when the solid was dissolved in water the gaseous fraction contained 1000 counts/min. Evidently the gases are firmly trapped and are released only when the crystals are completely dissolved.

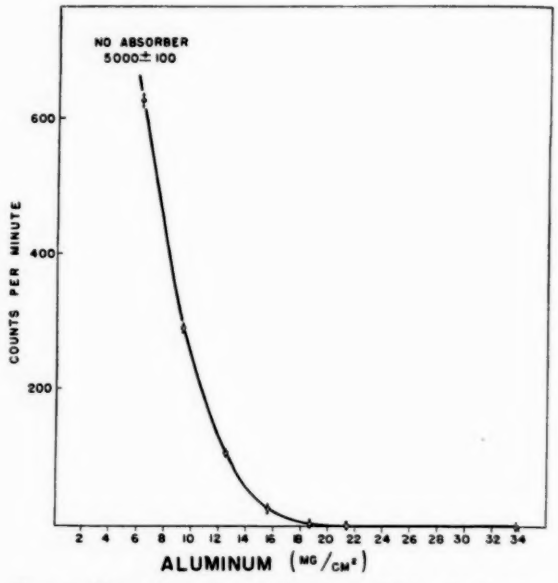

FIG. 1. Absorption of radiation from C^{14} in aluminum.

A large number of other nitrogen compounds are being irradiated not only to determine the best conditions for large scale[23] C^{14} production but also to investigate the chemistry of the recoiling carbon as a function of the chemical environment. Experiments are now in progress with urea, melamine, dicyandiamide, etc.[24]

PROPERTIES OF THE LONG-LIVED RADIATION

The absorption of the radiation in Al was measured by wrapping the screen wall of the Geiger counter with thin Al foils. With the first CaC^*O_3 sample (prepared by deuterons on carbon) which had an activity of only 400 counts/min. (background was 120/min.), the activity coming through 12 mg/cm² Al was 0±6

[22] C. Lapointe and F. Rasetti, Phys. Rev. **58**, 554 (1940), have found the total capture cross section of nitrogen for thermal neutrons to be 1.2×10^{-24} cm². Hydrogen has a cross section of 0.2×10^{-24} cm².

[23] It is a matter of common knowledge that NH_4NO_3 is thermodynamically unstable. However, it seems certain that its solution at room temperature offers no explosion hazard.

[24] We are indebted to the American Cyanamid Corporation for the gift of large quantities of these materials.

counts/min. However with a very thin layer ($\sim$0.1 mg/cm^2) of CaC^*O_3 (produced from NH_4NO_3) which had an activity of 5000 counts/min., 0.5 percent$\pm$0.1 percent of this effect was still observable at 13 mg/cm^2. The first estimate of the range was too low and it seems a more accurate value is 19$\pm$2 mg/cm^2. The absorption curve is shown in Fig. 1. Since the activity coming through 19 mg/cm^2 is $<$0.1 percent of the initial effect it is safe to conclude that γ-rays of $\sim$100 kev or more are absent. If the radiation consisted wholly of positrons the annihilation γ-rays should have given an effect of 100 counts/min. coming through the Al.[25] A comparison of the absorption in Cellophane and Al indicates the absence of soft γ-rays. 3.26 mg/cm^2 of Cellophane absorbed 69$\pm$4 percent while the same amount of Al absorbed 71$\pm$4 percent of the radiation.[26] Therefore it seems safe to conclude negative electrons are being emitted and the unstable isotope is C^{14}. If the upper energy limit of the beta-ray spectrum is taken to be 145,000$\pm$15,000 ev and the mass of N^{14} to be 14.007526,[27] the mass of C^{14} is calculated to be 14.00768. It is also possible, with the neutron-proton mass difference,[27] to determine $Q_1 = 0.64$ Mev. The estimate of Bonner and Brubaker[9] of 0.58$\pm$0.03 Mev is in agreement with this value.

The activity of a sample has been followed for 9 months and no decay observed. From this fact alone the half-life must be longer than 30 years. It is possible to make rough estimates of the half-life from the yields and cross sections. The $C^{13}(d, p)C^{14}$ experiments indicate 10^3–10^4 years while the $N^{14}(n, p)C^{14}$ data suggest 10^4–10^5 years. A lower limit of 1000 years is not unreasonable. Using the same technique employed in the H^3 work,[28] ($n_0^1 + {}_3Li^6 \rightarrow {}_2He^4 + {}_1H^3$), Goldhaber concludes[29] the half-life to be longer than 300 years.

The upper energy limit of $\sim$150 kev coupled with the long half-life ($\sim 10^3$ years) is quite unexpected. It would have been supposed that the decay of C^{14} to N^{14} would be an allowed transition analogous to the He^6–Li^6 case. Dr. P. Morrison has calculated that on this basis, a maximum half-life value of the order of a day is to be expected. Since the actual half-life is quite certainly a factor of 10^5–10^6 greater it follows that C^{14}–N^{14} decay involves a forbidden transition. In consequence,[30] it must be supposed that configurations with high angular momentum make appreciable contributions to the ground state of C^{14}. A similar[31] situation has been found in the case of Be^{10}, a nucleus which might be expected to behave like He^6, i.e., decay with a short half-life. Actually, despite the high upper energy limit of the emitted electrons ($\sim$580 kev), Be^{10} seems to have a very long half-life (about 10^3–10^5 years).

It is of interest to note that because of their long half-lives the production of macroscopic amounts of C^{14} and Be^{10} is at hand and in the near future it may be possible to determine their nuclear spins, etc. If the half-life of C^{14} is assumed to be 10^4 years, then 0.1 microgram is present in the sample prepared from the transmutation of nitrogen.

In conclusion, a few remarks may be made regarding the measurement of C^{14}. For small samples (up to $\sim$50 mg), counting as gaseous CO_2 seems to be the simplest and most sensitive method. Carbon dioxide, with a trace of foreign gas (H_2O, C_2H_5OH, O_2, etc.) has been found[32] in this laboratory to be a quite satisfactory counter gas. However, since CO_2 requires relatively high counting voltages, the source of very steady high potential may be a limiting factor. For the measurement of large samples of low specific activity the use of thin carbonate (Li_2CO_3, etc.) layers inside a screen wall counter is the most efficient technique.

In many respects it is unfortunate that the half-life of C^{14} is so long, since, for the production of strong samples, long time exposures are required. On the other hand, it is possible to concentrate C^{14} by various isotope separation methods (chemical exchange, thermal diffusion, ultracentrifugation, etc.) and thus material of low

[25] This estimate is based on measurements with a positron emitter (Na^{22}) under the same conditions.
[26] A more detailed investigation of the spectrum by Dr. J. Halpern and Mr. R. C. Raymond, using a Wilson cloud chamber, is now in progress.
[27] Hahn, Flügge and Mattauch, Ber. **73**, 1 (1940).
[28] R. D. O'Neal and M. Goldhaber, Phys. Rev. **57**, 1086 (1940).
[29] Conference on Applied Nuclear Physics, Massachusetts Institute of Technology, 1940.
[30] We are indebted to Professor J. R. Oppenheimer and Dr. L. I. Schiff for valuable discussions on this point.
[31] E. M. McMillan and S. Ruben, unpublished.
[32] T. H. Norris, private communication.

specific activity (including the end products of tracer experiments), can be reconcentrated. A given sample of C^{14} (and C^{13}) may, therefore, be used repeatedly. When the use of C^{14} and C^{13} becomes widespread enough, it should be feasible for a commercial company to perform this task at a nominal cost.[33]

[33] The Eastman Corporation, at the suggestion, and with the cooperation, of Professor H. C. Urey, has begun the concentration of N^{15} on a small scale. It is reasonable to believe that the interest and demand for carbon tracers will far exceed the supply of the radioactive isotopes and, therefore, the large scale concentration of C^{13} is of considerable importance.

Note added in proof.—The estimate for the C^{14} half-life was made by three different methods (1) the yield of C^{14} coupled with an extrapolation of Amaldi's curve (cf. Bethe's review) for the $C^{12}(d, p)C^{13}$ reaction and Pollard's value for the yield ratio $C^{13}(d, p)C^{14}/C^{12}(d, p)C^{13}$, (2) the $C^{13}(d, p)C^{14}$ cross section was estimated by comparison with the $B^{10}(d, n)C^{11}$ yield at bombarding energies of 7–8 Mev, (3) the C^{14} yield from the slow neutron irradiation of NH_4NO_3. Method (1) gave $2 \cdot 10^4$ years while (2) yielded $2 \cdot 10^3$ years. Schultz and Watson, Phys. Rev. **58**, 1047 (1940), have found Pollard's $C^{13}(d, p)C^{14}/C^{12}(d-p)C^{13}$ yield ratio was high by a factor of 5–10. This seems to bring the first two C^{14} half-life estimates into agreement at 10^3 years. The $N^{14}(n, p)C^{14}$ experiments suggest a still longer half-life for C^{14}. Hence it seems reasonable to regard 10^3 years as a lower limit.

We cannot adequately express our gratitude to the members of the Chemistry and Physics Departments, as well as many others, for their help and encouragement. It is a pleasure to thank Professor E. O. Lawrence and the staff of the Radiation Laboratory for their assistance and cooperation. Financial assistance from the Research Corporation and the Rockefeller Foundation to the Radiation Laboratory is gratefully acknowledged.

FEBRUARY 15, 1941 PHYSICAL REVIEW VOLUME 59

Ionization and Dissociation of Diatomic Molecules by Electron Impact

HOMER D. HAGSTRUM* AND JOHN T. TATE
University of Minnesota, Minneapolis, Minnesota

(Received August 15, 1940)

An extension of the mass spectrometric method of study of ionization and dissociation processes occurring in diatomic molecules under electron impact and the results of further investigation of the molecules H_2, CO, NO, N_2, and O_2 are discussed. The shapes of the peaks which appear in the graph of resolved ion current as a function of ion accelerating potential are analyzed and accounted for in terms of the wave-mechanical theory of the diatomic molecule and the characteristics of the mass spectrometer. It is indicated how the study of the peak shape coupled with appearance potential measurements has made possible conclusions concerning the nature of the dissociation process and the structure of the molecule. Differences between previous mass spectrometric data and those from other sources have been clarified either by obtaining better data with the mass spectrometer or by formulation of a satisfactory interpretation of the difference based on conclusions of an analysis of the ion peak shape. Values of dissociation energies, ionization potentials and interpretations of the processes that occur are given.

INTRODUCTION

COLLISIONS of electrons of low velocity with diatomic molecules may produce charged fragments of the molecule. The data on the minimum electron energy necessary to produce these fragments, the identification of them and of the processes involved may permit one to determine the heat of dissociation of the molecule. The relative abundance of the ion products and the probability of a process as a function of the electron energy are also of interest.

In the usual mass spectrometer the ions of a given m/e value are segregated and the dependence of the ion current on the energy of the bombarding electrons and on the gas pressure in the collision chamber is determined.[1–4] In the

* Now at the Bell Telephone Laboratories, New York.

[1] For a review of all work previous to 1931 see H. D. Smyth, Rev. Mod. Phys. **3**, 347 (1931). Reviews have also been given by H. Kallmann and B. Rosen, Physik. Zeits. **32**, 521 (1931); W. de Groot and F. M. Penning, *Handbuch*

dissociation of diatomic molecules some fragments are given kinetic energy. This initial kinetic energy cannot be determined easily by the mass spectrometer. By means of a modified apparatus Lozier[5] studied the minimum electron energy at which an ion with a definite kinetic energy would appear. He was able to verify theoretical predictions on the dissociation of hydrogen. The retarding potential method of Lozier has been improved[6–10] and a number of diatomic molecules studied. The method is limited in that the m/e value of the ion cannot be determined.

It is the purpose of this paper to show how an analysis of the peaks in the curves of ion current observed with a mass spectrometer yields information on the ionization and dissociation of diatomic molecules which previously could be obtained in part from the retarding potential methods and in part from the mass spectrometer. Information on the potential energy curve involved in the dissociation process, a method of distinguishing between dissociation and ionization processes which yield ions with the same m/e values and new interpretations of measurements on the appearance potentials and relative abundance of ions have been obtained.

Data on H_2, O_2, CO, N_2, and NO are given. Earlier discrepancies are cleared up and some known dissociation processes are studied quantitatively for the first time.

Experimental Arrangement

The mass spectrometer is similar to that described by Tate, Smith and Vaughan[3] and by Nier.[11] The dimensions are shown in Fig. 1. The ions are formed in the electron beam of ribbon form and are accelerated to the slit S_1. Additional acceleration is given to them between the plates S_1 and S_2. The ion current passing through S_3 is plotted as a function of the accelerating field between the electron beam and S_2.

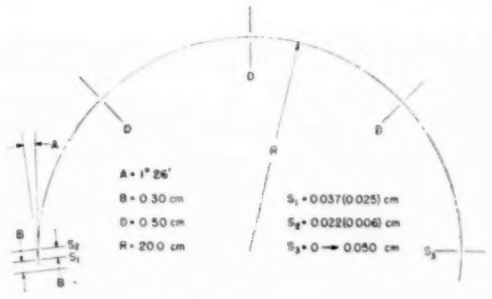

FIG. 1. Geometrical details of the mass spectrometer. Slits S_1 and S_2 were widened during the course of the work and both values of slit width are given. The width of slit S_3 is adjustable between the limits given but was usually kept about half open. The lengths of the slits are S_1 0.8 cm, S_2 0.8 cm, S_3 1.0 cm. A drawing-out field between the back plate and S_1 of about 30 volts per cm was used. The dimensions of the defining slit of the electron beam are 0.01×0.5 cm. The plane of the beam is half-way between the back plate and the first ion slit.

For a particular curve or peak it is essential that the field of the electromagnet be maintained constant and that there be no drift in the accelerating electric fields. The electromagnet is operated by storage batteries and the electric potentials are obtained from batteries or a 1000-volt stabilized rectifier.[12] No difficulty has been encountered in obtaining very steady operating conditions. The ion current is measured by a direct-current amplifier with a Western Electric electrometer tube D96475 in a modified Barth circuit described by Penick.[13]

A porcelain leak[14] admits gas to the system in which a pressure of 10^{-4} mm Hg is ordinarily maintained. A tungsten filament was used with H_2, N_2 and CO_2, and an oxide-coated filament with NO and O_2. Hydrogen, oxygen and nitrogen were obtained from commercial tanks and were admitted to the apparatus through a liquid-air trap. The carbon monoxide was prepared[15] by treating oxalic acid with concentrated sulphuric acid and washing of the resultant gases with concentrated potassium hydroxide and alkaline

der Physik (J. Springer, Berlin, 1933), Vol. 23/1; H. Sponer, *Molekülspektren* (J. Springer, Berlin, 1936).
[2] A. L. Vaughan, Phys. Rev. **38**, 1687 (1931).
[3] J. T. Tate, P. T. Smith and A. L. Vaughan, Phys. Rev. **48**, 525 (1935).
[4] A. O. Nier and E. E. Hanson, Phys. Rev. **50**, 722 (1936).
[5] W. W. Lozier, Phys. Rev. **36**, 1285 (1930).
[6] J. T. Tate and W. W. Lozier, Phys. Rev. **39**, 254 (1932).
[7] W. W. Lozier, Phys. Rev. **44**, 575 (1933); **45**, 840 (L) (1934).
[8] W. W. Lozier, Phys. Rev. **46**, 268 (1934).
[9] E. E. Hanson, Phys. Rev. **51**, 86 (1937).
[10] R. Buchdahl, Phys. Rev. **57**, 1071A (1940).
[11] A. O. Nier, Phys. Rev. **52**, 933 (1937).
[12] F. V. Hunt and R. W. Hickman, Rev. Sci. Inst. **10**, 6 (1939).
[13] D. B. Penick, Rev. Sci. Inst. **6**, 115 (1935).
[14] W. R. Smythe, Rev. Sci. Inst. **7**, 435 (1936).
[15] E. H. Archibald, *The Preparation of Pure Inorganic Substances* (Wiley and Sons, New York, 1932).

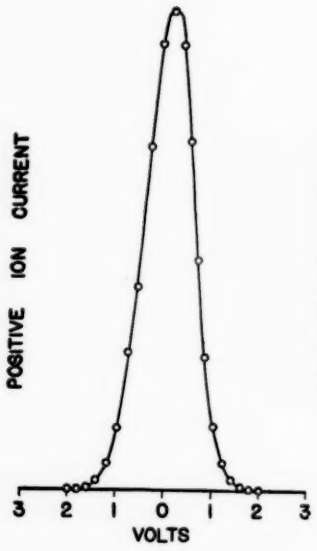

FIG. 2. Peak shape for an ion which is formed with no initial velocity. (type 0). This particular peak is for N_2^+ from N_2. The abscissas give ion accelerating potential measured from the center of the peak which corresponds to a total acceleration through approximately 500 volts.

pyrogallol solutions. The gas was dried by passing it through phosphorus pentoxide and a liquid-air trap. The NO was prepared[15] by the action of sulphuric acid on a solution of potassium nitrite and potassium iodide. The gases formed were passed through a dry-ice trap to remove water and the higher oxides of nitrogen and the NO collected in a liquid-air trap and fractionally distilled a number of times.

For each gas a study was made of the abundances and appearance potentials of ions from impurities which have the same m/e as ions from the molecule under investigation. It was always possible to regulate the amounts of impurities present by baking out or further purification of the gas sample so that their effects were entirely negligible.

The minimum energy of the bombarding electron for the observation of an ion is called its appearance potential. In comparing appearance potentials, the amplifier is adjusted to give the same rate of increase of ion current above the break for each ion. The ionization potential of argon was used to obtain absolute values of electron energies. In studying the shape of ion peaks, the bombarding electrons were accelerated through a potential drop of 100 volts.

ANALYSIS OF PEAK SHAPES

Certain features of the shapes of the curves of ion current observed with a mass spectrometer have been noted by previous investigators.[3, 4] The peaks for certain ions "trail out" on the high mass side. This characteristic was attributed to ions which possess some initial kinetic energy. Hustrulid, Kusch and Tate[16] reported observation of a number of satellite peaks for ions from benzene vapor. The separate peaks were assumed to be formed by ions with relatively high kinetic energy in a narrow range.

The shape of an ion peak depends mainly upon two factors: (1) the characteristics of the instrument, (2) the distribution in initial kinetic energy of the ion. The ions with different initial velocities are not focused by our instrument at the same point. This characteristic permitted a study of these initial velocities from which some information on the structure of the diatomic molecule may be obtained.

Instrumental factors affecting the width of an ion peak are the finite width of slits and diaphragms, space charge effects, shape of electron beam and the fact that ions are formed at different points in the accelerating field below S_1 (Fig. 1). If the ion products have no initial energy other than that of thermal agitation and if ions with the small range of kinetic energy for this case are collected equally efficiently, the curve of ion current has the symmetrical form shown in Fig. 2. A curve of this form we shall designate as type 0. It is obtained when ions with essentially zero kinetic energy are formed as for example in a process involving only ionization.

An ion which is the result of dissociation may have initial energy of several electron volts. Since ions of the same m/e value must have the same velocity at the entrance slit to be focused on the exit slit, ions with different initial velocities will require different accelerating potentials to be brought to a focus. Thus a curve of ion current *vs.* accelerating potential will have a form different from that of Fig. 2 and will yield information on the initial velocities of the ions. From this information data on the structure of the molecule may be obtained.

The effect of the initial ionic velocity apart from instrumental factors on the collection of ions will now be considered. A complete solution which takes all factors into account becomes

[16] A. Hustrulid, P. Kusch and J. T. Tate, Phys. Rev. **54**, 1037 (1938).

exceedingly involved. But one may rather easily carry through a simplified calculation to determine the percent of ions formed with different kinetic energies which pass through the *first slit* from a given point in the electron beam. The results are shown in Fig. 3. The method of obtaining the results is described in the figure caption. The final over-all curve showing the dependence of collection on the initial kinetic energy is curve 3 in Fig. 3. It is evident that ions of very low or zero kinetic energy are much more efficiently collected than those of higher energy.

Distribution in kinetic energy of ion products

Condon[17] has shown that the wave-mechanical formulation of the Franck-Condon principle predicts the dependence of the probability of transition between two molecular vibrational states in which a photon is emitted or absorbed upon the value of the so-called overlap integral:

$$[\int \psi_U \psi_L dr]^2. \qquad (1)$$

In this expression ψ_U is the wave function of the upper state, ψ_L is the wave function of the lower state and r is the nuclear separation. The case of absorption for which ψ_U is the eigenfunction of a state above the asymptote in the continuum corresponds to a transition induced by electron impact resulting in dissociation of the molecule. The success of the application of the Franck-Condon principle to the prediction of possible electron impact processes in hydrogen[18–20] suggests the use of expression (1) in a more detailed discussion of electron impact processes in diatomic molecules.

The probability of transition produced by electron impact is a function of the energy of the transition (E_t), the energy of the bombarding electron (E_e) and of the overlap integral. For values of E_e well above that of E_t it appears that the probability depends mainly on the overlap integral. The value of E_e was 100 electron volts which is well above the usual value of 20 to 35 electron volts for E_t. The form of the function does not alter radically with E_t. This is evidenced by measuring as a function of E_e the efficiency of formation of ions collected at different points on an ion peak which involve different values of E_t.

The value of the probability of transition is found by methods suggested first by studies of the continuous absorption spectra.[21–23] The probability of finding the molecule with a given separation of the atoms is proportional to ψ_L^2. The probability of electronic transition with a given nuclear separation maintained is then taken as proportional to ψ_L^2 for that separation. If the upper potential energy curve representing the state to which the molecule is taken is known and the F-C principle is assumed to be valid, then the curve representing the distribution in

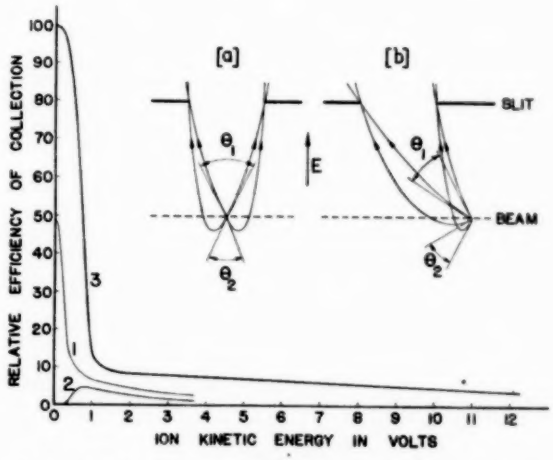

FIG. 3. Efficiency of collection of ions by the mass spectrometer as a function of initial kinetic energy. Investigation of the motion of ions in the collision chamber has been simplified by neglecting space charge and the magnetic field and by assuming that the ions are formed with velocity vectors pointing uniformly in all directions with zero components along the electron beam. (a) and (b) show the limiting paths of ions which pass through the first ion slit from two lines in the electron beam. Ions initially directed inside the angles θ_1 and θ_2 pass through the slit. Curve 1 gives qualitatively the relative efficiency for case (a), curve 2 for case (b). The second ion slit and analyzer diaphragms (see Fig. 1) perform a further selection by limiting the spread in angle at the first slit of the trajectories of ions which are collected. This discriminates against ions formed near the edges of the electron beam which, on the average, possess the greatest kinetic energy of the ions getting through the first slit. Curve 3 is the proposed "over-all" efficiency curve for the spectrometer used in the present work.

[17] E. U. Condon, Phys. Rev. **32**, 858 (1928).
[18] E. U. Condon, Phys. Rev. **35**, 658A (1930).
[19] E. U. Condon and H. D. Smyth, Proc. Nat. Acad. Sci. **14**, 871 (1928).
[20] W. Bleakney, Phys. Rev. **35**, 1180 (1930); **40**, 496 (1932).
[21] J. G. Winans and E. C. G. Stueckelberg, Proc. Nat. Acad. Sci. **14**, 867 (1928).
[22] A. S. Coolidge, H. M. James and R. D. Present, J. Chem. Phys. **4**, 193 (1936).
[23] G. E. Gibson, O. K. Rice and N. S. Bayliss, Phys. Rev. **44**, 193 (1933).

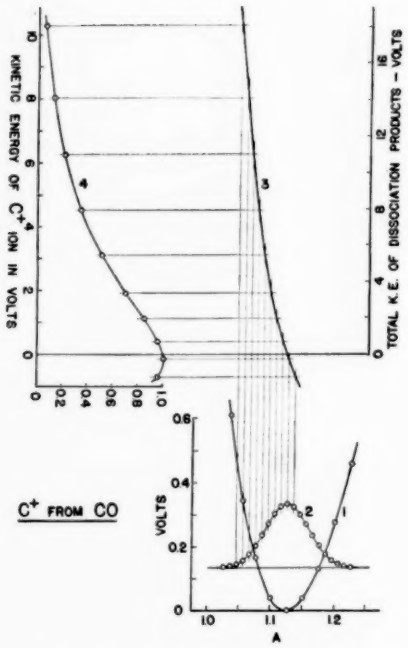

FIG. 4. Construction of the distribution in initial kinetic energy of C^+ ions from CO by the reflection method. Curve 1 is a part of the potential curve of the ground electronic state of the molecule; curve 2 is the square of the wave function of the lowest vibrational level (harmonic oscillator); curve 3 is a part of the upper potential curve to which transitions will yield curve 4, the distribution in kinetic energy. The ordinates of curves 2 and 4 are arbitrary. The position of curve 3 has been chosen so that a resultant ion peak of type I is obtained (see Fig. 5).

initial energy of the fragments of the molecule can be obtained.

The method is illustrated in Fig. 4. Curve 1 is the potential energy curve of the ground electronic state of the molecule, curve 2 is the square of the wave function (ψ_L^2), curve 3 is the upper potential energy curve. Curve 4 is then shown with ordinates representing the kinetic energy of an ion at dissociation. The ordinate of this scale will be proportional to that representing the total kinetic energy at dissociation of the molecule and will have its zero determined by the position of the asymptote (infinite nuclear separation) of the upper potential energy curve. The abscissas denote the probability of producing an ion with a given kinetic energy, and their values are taken as proportional to the value of ψ_L^2 for a particular value of r. Thus the probability is taken as proportional to the number of molecules having a nuclear separation such that when the electronic transition takes place and the molecule is raised to a new energy level, that is to a point on the upper curve, it will break up and yield an ion having a given kinetic energy. For example, in Fig. 4 the value of the probability that the C^+ ions have kinetic energy of 2 electron volts is proportional to the height of the ψ_L^2 curve at the nuclear separation value, which on curve 3 would yield an ion of that energy. In Fig. 4 the position of the upper potential energy curve is such that the most probable nuclear separation in the lower state (maximum ψ_L^2) results in zero kinetic energy of the dissociated parts. Curve 4 then has its maximum at zero kinetic energy. The values of negative kinetic energy indicated by the same construction for points of greater nuclear separation correspond to transitions in which excitation but no dissociation may take place.

The position and shape of the upper potential curve are in general not known. The position of the curve is more or less arbitrary but there are, of course, general restrictions on its shape. It is so chosen that the resultant distribution obtained by the method just described is in accord with that which may be inferred from experimental measurement of the ion peak shape. This method of "working backwards" has also been used to obtain the course of the potential curve from the observed intensity distribution in continuous spectra.[24]

Construction and classification of ion peak shapes

Curve 4 of Fig. 4 indicates the distribution in energy of the ions at the moment of formation. Those having small velocities are collected at the first slit (S_1) the most efficiently (Fig. 3). The distribution in energy of the ion current passing through S_1 may be obtained by multiplying each point of curve 4 (Fig. 4) by the value of the corresponding efficiency (Fig. 3, curve 3). Curve 3 of Fig. 5 is the resultant curve. Because of finite widths of the collecting slits and of those in the diaphragm, and the slight differences in the acceleration of ions starting at different points in the electron beam, the actual observed ion peak is broader and has no discontinuity. It is shown in Fig. 5 (curve 4). The abscissas for

[24] N. S. Bayliss, Proc. Roy. Soc. **158**, 551 (1937).

this curve are determined by changes in the values of the electric field between S_1 and S_2 (of the order of 1000 volts/cm) which, with a given magnetic field, sweeps the ion beam over the collecting slit S_3. In curve 4 of Fig. 5 the zero has been placed at the maximum and it is assumed that then the abscissas as shown measure the initial kinetic energy of the ions.

Ion current peaks of the form of curve 4 (Fig. 5) are called type I. They result when the ions formed with zero or very near zero kinetic energy are most probable. Examples are H^+ ions from H_2, N^+ ions from N_2 and N^+ ions from NO.

Figures 6 and 7 show the construction of a peak for ions which result from transition to a potential curve lying at larger nuclear separation than that of Fig. 4. The resultant peak shape possesses two maxima, one due to the maximum in the "original" distribution corresponding to the maximum transition probability, the other to the rise in the efficiency of collection by the spectrometer near zero kinetic energy. Such a peak shape, to be designated as type II, has been observed for O^+ ions from NO and is to be expected whenever ions of kinetic energy *near* zero are present but with reduced abundance when comparison is made with type I.

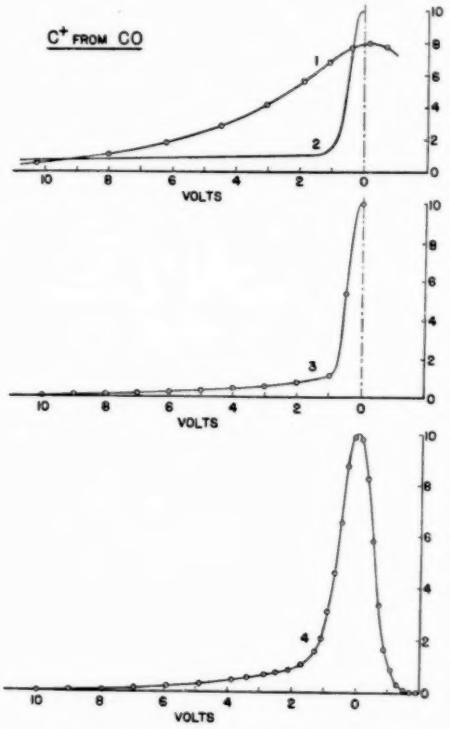

FIG. 5. Construction of the peak shape from the distribution in initial kinetic energy of C^+ from CO. Curve 1 is the distribution from Fig. 4 (curve 4); curve 2 is the instrumental efficiency curve; curve 3 is the predicted peak shape obtained by multiplying curves 1 and 2. Curve 4 is the observed peak shape. The abscissas of curve 4 are determined as they were in Fig. 2.

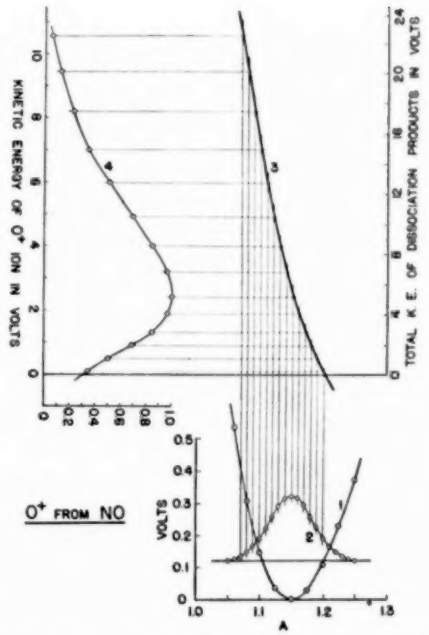

FIG. 6. Construction of the distribution in initial kinetic energy of O^+ ions from NO by the reflection method. See caption of Fig. 4 for the designation of the curves. The position of curve 3 has been chosen so that a peak of type II is obtained (see Fig. 7).

If the upper potential curve lies at still larger values of r the probability of formation of ions of very low or zero initial kinetic energy may be zero. The distribution in kinetic energy possesses a minimum kinetic energy greater than zero because the upper potential curve crosses its asymptote outside the Franck-Condon region. By virtue of the shape of the function $\psi_L^2=0$ for the ground state (curve 2 of Fig. 4) the probability of formation of ions possessing kinetic energies near the minimum is relatively low. The instrumental efficiency is relatively constant over the range of values of initial kinetic energy possessed by the ions; hence the shape of the peak, designated as type III, approximates that of the distribution at formation and the maximum appears at about the kinetic energy corresponding to the maximum transition probability. The O^+ ions which result from the dis-

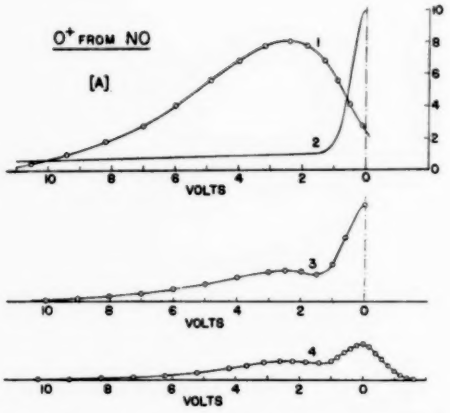

FIG. 7. Construction of the peak shape from the distribution in initial kinetic energy of O^+ from NO by method *A*. See caption of Fig. 5 for the designation of the curves.

sociation of CO exhibit a peak shape of this type (Fig. 8). This type occurs when ions of kinetic energy less than one volt (approximately) are absent.

A distribution may possess a minimum kinetic energy greater than zero for a second reason. If the potential curve to which transition takes place has a maximum at a value of r greater than that existing at transition, the total kinetic energy of the products must not be less than the height of this maximum above the asymptote. In this case there need be no restriction on the probability of formation of ions possessing kinetic energies near the minimum. If the point on the curve, transition to which results in the products of minimum energy, lies near the center of the Franck-Condon region the probability of transition to points near it is relatively large. The distribution in kinetic energy of the products then cuts off abruptly at the minimum energy.

A situation in which there is a maximum in the potential energy curve but in which the minimum kinetic energy is only a few tenths of an electron volt may appear as type I or II because of the rise of the instrumental efficiency *near* zero energies.

Variation of peak height with drawing-out field

If the ions have very little initial kinetic energy, the ion current collected will saturate at a small drawing-out field. If, however, the ions initially have velocities in random directions, more and more ions will be directed to the slit and the current will continue to increase with increasing field. Also, a small retarding field will reduce the current to zero if the initial kinetic energy is zero but ions with initial kinetic energy can be collected against a retarding field. Thus curves of ion current against the drawing-out field will yield some information of the process of formation of ions. The height of peaks of types O, I and II should not vary with the field. The height of peak type III should increase with increasing field. Figure 9 shows experimental results.

Appearance potentials and relative probability of dissociation processes

From the construction of curves for types I and II, it is evident that the peaks are formed by ions which have the least kinetic energy of those formed in the dissociation process, even though such ions are not the most abundant of those formed in the electron beam. If the upper potential energy curve is of the usual type without a maximum, the appearance potential of those ions which appear at the peak of the experimental curve locates a dissociation limit of the molecule since the initial kinetic energy of the ions is zero. Dissociation energies obtained from the appearance potentials of H^+ from H_2, N^+ from N_2, N^+

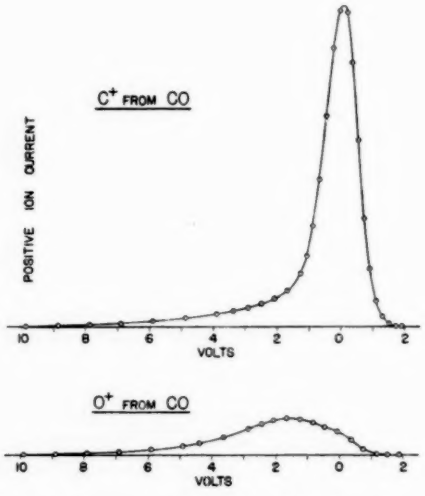

FIG. 8. Peak shapes for the C^+ and O^+ ions from carbon monoxide at 100 volts electron energy. The abscissas give ion kinetic energy in volts. Ion accelerating potential increases to the right, the maximum of the C^+ peak corresponding to about 300 volts. It is explained in the text how the scale of ion kinetic energy for each peak was calibrated.

from NO agree with those obtained from retarding potential methods and from spectroscopic data.

If comparison with other data indicates the appearance potential is higher than a dissociation limit, it must be concluded that ions of zero kinetic energy were not formed. Since peaks of type I or II are considered, the probability of formation of ions near the minimum energy must be fairly large. This situation may be explained by assuming a potential energy curve with a maximum between the F-C region and the dissociation region. Then it is possible to have a large number of ions formed with the minimum energy which may be some tenths of an electron volt above zero. Comparison of data obtained in our experiments with those from retarding potential methods and spectroscopy aids in determining the position of the zero on the abscissa scale in experimental curves (curves 4, Figs. 5, 7, 8). The location of the zero of these curves is sometimes a difficult matter but a very important one in the interpretation of the results.

The conclusion that the maximum of a peak of type I corresponds to ions of zero initial kinetic energy if such ions are formed in the process has been confirmed in another manner. A test was made to see if the maximum of the ion peak of N^+ from N_2 appears at the "position" on the scale of accelerating potential for ions of zero initial velocity and $m/e=14$. In order to avoid complications due to contact potentials and uncertainties of calibration of the voltage divider which applies the ion accelerating potential to the slit system of the spectrometer the following procedure was adopted. Argon and nitrogen were admitted into the spectrometer at the same time. The voltage interval (about 350 volts) between the maxima of the N^+ and the N_2^+ ion peaks was measured. The magnetic field was then adjusted so that the A^+ peak appeared at the position on the voltage scale previously occupied by N_2^+ and the interval between A^+ and A^{++} determined. As the ratios of the m/e values of A^+ and A^{++} and of N_2^+ and N^+ are equal these intervals should be equal if the maximum of the N^+ peak corresponds to the ion of zero initial velocity. It was found that the two voltage intervals agreed within 0.2 volt which is within the estimated experimental error.

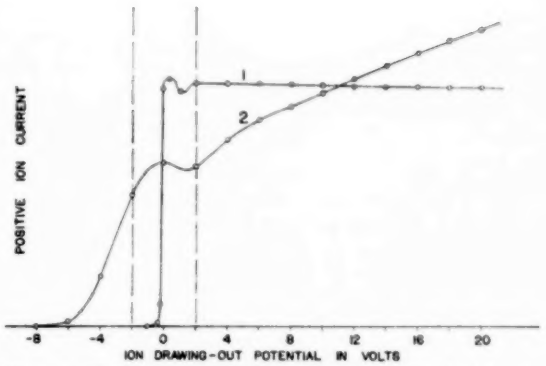

FIG. 9. Variation of peak height with the drawing-out field in the collision chamber of the mass spectrometer. The abscissas give the potential applied across the collision chamber between the back plate and the first ion slit (0.3 cm apart). Curve 1 is for CO^+ from CO (type 0) and curve 2 for O^+ from CO (type III). The curve for a peak of type I or II would approximate curve 2 for negative fields and curve 1 for positive fields. When the drawing-out field is small, stray fields apparently "reach into" the collision chamber causing peculiar focusing effects. For this reason, the shapes of the curves for potentials near zero (between the vertical dashed lines) have no significance in the present discussion.

Ions of initial velocity near zero are not formed in a process which gives rise to an ion peak shape of type III. Since ions of appreciable initial kinetic energy focus at the maximum of such a peak the appearance potential measured at the maximum may be considered only as an upper limit for the energy level of the asymptote of the potential curve. A more accurate determination of the position of the dissociation limit can be made if it is possible to determine the kinetic energy corresponding to some point on the distribution. How this was accomplished for the single process of this type observed in this work is discussed in the section of the paper which deals with CO (Process F).

The study of the shapes of ion peaks indicates that neither the height of the peak nor the area under the curve is a direct measure of the abundance of an ion. Instrumental and other factors determine the height and area. A peak of type I may be ten times as high as one of type III even though the total number of ions formed is the same in each case. Nevertheless it is possible to estimate the relative abundance of the ions formed.

EXPERIMENTAL RESULTS

In the presentation of the experimental results the following symbols will be used: $I(X)$—ioniza-

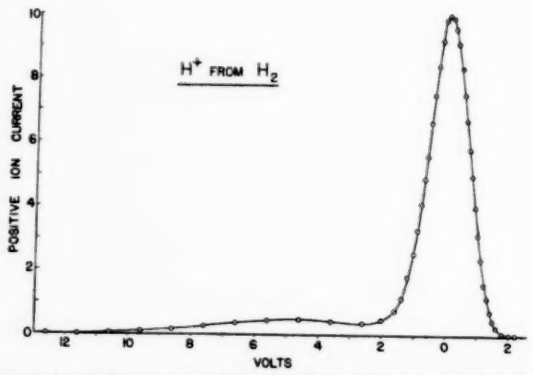

FIG. 10. H^+ ion peak from H_2 for electrons of 100 volts energy. The abscissas give the kinetic energy of the ions in electron volts (accelerating potential in volts) measured from the position of the maximum. Total accelerating potential increases to the right, that corresponding to the maximum of the peak being about 300 volts. The peak is a superposition of two peaks of types I and III.

tion potential of X which may be an ion, an atom or a molecule. $A(X^+)$—appearance potential of X^+. This is understood to refer to the product of zero initial kinetic energy unless otherwise specified. $D(X)$—heat of dissociation of X. $EA(X)$—electron affinity of X. $E(X)$—excitation energy of X.

Hydrogen

The restudy of the hydrogen molecule was undertaken primarily as a check on the operation of the mass spectrometer and the analysis of peak shapes. Bleakney[20] has demonstrated experimentally that two modes of formation of H^+ as a primary ion product from H_2 under electron impact can be distinguished. These entail transition to the $^2\Sigma_g^+$ and $^2\Sigma_u^+$ states of the molecule ion. By retarding the ions in the collision chamber of the spectrometer Bleakney showed that they possess initial kinetic energies in the ranges predicted by theory. This work was corroborated by Lozier[5] who used the retarding potential method.

From the course of the potential curves one should expect H^+ peaks of types I and III for the ions resulting from transitions to the $^2\Sigma_g^+$ and $^2\Sigma_u^+$ states of H_2^+, respectively. The resultant peak observed with the mass spectrometer (Fig. 10) is a superposition of two such peaks. It is to be distinguished from a peak of type II which may also possess a double maximum although only a single potential curve is involved.

An attempt has been made to construct from the theoretical potential curves the H^+ peak by the method described. Qualitatively the constructed and observed peak shapes agree very well. It is impossible to predict the relative heights of the two maxima of the peak, however, as the relative probability of transition to the two states at the same nuclear separation is not known. Considering this limitation, it is believed that the results of this study indicate that the essential features of the peak shape have been accounted for.

Appearance potential measurements at the maxima of the H_2^+ and H^+ peaks yielded the data:

$$A(H_2^+) = 15.4 \pm 0.1 \text{ volts},$$
$$A(H^+) = 18.0 \pm 0.2 \text{ volts}.$$

These data and the values of $D(H_2)$ and $D(H_2^+)$ predicted by them agree within experimental error with the results of previous electron impact work,[7, 20] band spectroscopic[25] and thermochemical[26] investigations and wave-mechanical calculation.[25] It is believed that data for other molecules taken in the same manner are of comparable accuracy when interpreted correctly even though knowledge of the structure of the molecule does not permit so rigorous a check as in the case of hydrogen.

Carbon monoxide[27]

A summary of data on CO is given in Table I. A number of processes in which the ions may be

TABLE I. *Summary of electron impact data for* CO. *Appearance potential in volts.*

	$A(CO^+)$	$A(CO^{++})$	$A(C^+)$	$A(O^+)$	$A(O^-)$
Hogness, Harkness* (mass spectrometer)	13.9		22.8	24	
Vaughan[2] (mass spectrometer)	13.9 ±0.2	43.0 ±1.0	22.5 ±0.2		9.5 ±1.0
Tate, Smith, Vaughan[3] (mass spectrometer)				27 ±1	
Tate, Smith[28] (total ion current)	14.1 ±0.1				
Lozier[5] (retarding potential)			20.9 ±0.1 22.8 ±0.1		9.5 ±0.1 20.9 ±0.1
Present work (mass spectrometer)	14.1 ±0.1	42.0 ±0.5	20.9 ±0.2 22.8 ±0.2	23.1 → 23.5	9.5 ±0.2 20.9 ±0.2

* T. R. Hogness and R. W. Harkness, Phys. Rev. **32**, 936 (1928).

[25] See H. Beutler and H. O. Jünger, Zeits. f. Physik **100**, 80 (1935) for a summary of values obtained for the dissociation and ionization energies of H_2 from spectroscopic observations and theoretical calculation.

[26] R. F. Bichowsky and L. C. Copeland, J. Am. Chem. Soc. **50**, 1315 (1928).

[27] A part of this work on CO was presented at the Washington Meeting of the American Physical Society, April 29, 1939. H. D. Hagstrum and J. T. Tate, Phys. Rev. **55**, 1136A (1939).

formed have been identified. These will be considered now.

Process A: $CO+e \rightarrow CO^+ + 2e$.—$CO^+$ ions were found to appear first at 14.1 ± 0.1 volts. This datum agrees very well with the results of previous work (see Table I). Further consideration of Vaughan's data by Tate and Smith[28] gave 14.0 instead of 13.9 volts.

Process B: $CO+e \rightarrow CO^{++}+3e$.—A value of $A(CO^{++}) = 42.0 \pm 0.5$ volts has been obtained. It is in substantial agreement with Vaughan's value of 43.0 ± 1.0 volts.

Process C: $CO+e \rightarrow C+O^-$.—The onset potential of the resonance process yielding O^- ions was found to be 9.5 ± 0.2 volts (Fig. 11), in good agreement with the results of previous investigations. The fact that this potential measured with the ion accelerating potential of the mass spectrometer adjusted to the maximum of the peak agrees with the extrapolated value of Lozier for ions of zero initial kinetic energy indicates that such ions are produced in the process in appreciable abundance. This result confirms Lozier's observation that O^- ions of kinetic energy from zero to approximately one volt are formed. The potential curve to which transition takes place must lie very near the asymptote in the Franck-Condon region and perhaps crosses it there. This would indicate that the curve possesses a minimum and Lozier suggests that a careful search with a mass spectrometer might reveal CO^- ions. A search was made for such ions but none could be detected. If they are formed their abundance cannot be greater than 0.01 percent of the CO^+ ion. Massey[29] suggests that in low pressure experiments of this type it will not be possible to observe the formation of negative molecular ions because they will dissociate by the reverse process before making sufficient collisions to get rid of their excess vibrational energy.

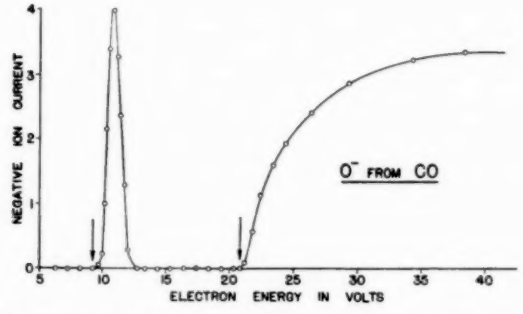

FIG. 11. Efficiency of formation of O^- ions from carbon monoxide as a function of the energy of the impacting electrons. The ion accelerating potential was adjusted to the maximum of the peak.

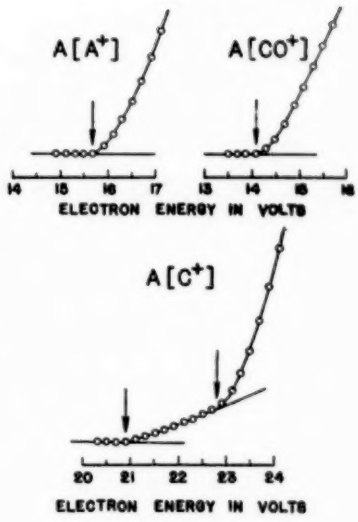

FIG. 12. Typical appearance potential curves for ions from carbon monoxide. The C^+ curve was obtained with the ion accelerating potential held constant at the value corresponding to the maximum of the peak for higher electron energies.

Process D: $CO+e \rightarrow C^+ + O^- + e$.—The first appearance potential of C^+ ions at 20.9 volts (Fig. 12) coincides within experimental error with the second appearance potential of O^- ions. (Fig. 11). This potential agrees very well with Lozier's value.

Lozier demonstrated quite conclusively that the numbers of positive and negative ions formed for electron energies between 20.9 and 22.8 volts electron energy are equal. This has been verified within experimental error in the present work for the C^+ and O^- ions. Any doubt as to the identification of the ions involved has thus been removed.

Process E: $CO+e \rightarrow C^+ + O + 2e$.—That this process is much more probable than process *D* is seen from the rates at which the C^+ ion current rises with electron energy below and above 22.8 volts. Thus the C^+ peak observed at 100 volts electron energy is made up in the main of ions from this process. The shape of the peak is shown in Fig. 8. It is seen to be of type I. The good agreement of the position of the second break at 22.8 volts in the curve for C^+ against electron

[28] J. T. Tate and P. T. Smith, Phys. Rev. **39**, 270 (1932).

[29] H. S. W. Massey, *Negative Ions* (Cambridge, 1938), p. 42.

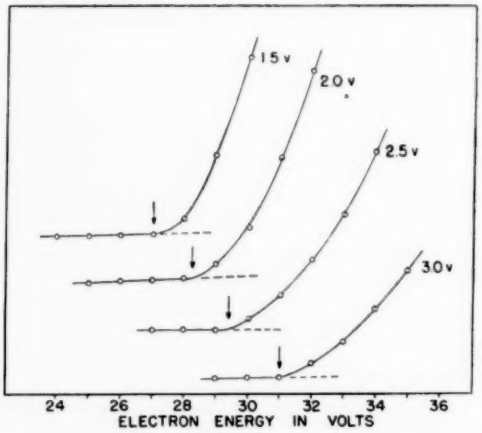

FIG. 13. One set of appearance potential curves for O^+ ions of 1.5, 2.0, 2.5 and 3.0 volts initial kinetic energy. It was found that no better data could be obtained by attempting to take readings at smaller voltage intervals because of the extremely low ion current and the fact that the position on the peak could be checked only before and after the data for each curve were obtained.

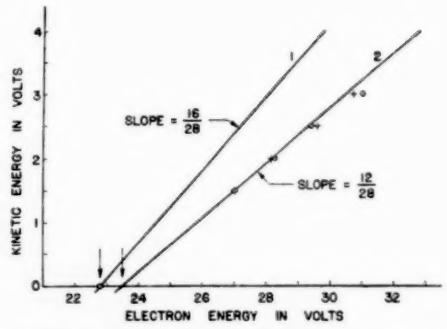

FIG. 14. Relation of the appearance potential and kinetic energy of ions from the dissociation of CO. Curve 1 is for C^+ and curve 2 for O^+. The lines are drawn with the values of slope predicted by the laws of conservation of energy and momentum applied to the dissociation process (see reference cited in footnote 7). Two sets of data are plotted for O^+. In placing curve 2 the data for lower kinetic energies were favored since they were obtained at the higher intensity portions of the peak (see Fig. 8).

energy with Lozier's extrapolated value indicates that ions of zero initial velocity are formed in the process and that for this reason the potential curve involved cannot possess a maximum. Vaughan's conclusion that the C^+ ions possess kinetic energy is untenable if it is to be interpreted as meaning that ions of zero initial kinetic energy are not formed.

Process F: $CO+e \rightarrow C+O^+ +2e$.—$O^+$ ions from CO have been observed by previous investigators but have not been studied in any detail. The only quantitative data on them were given by Tate, Smith and Vaughan[3] who report the peak to be 10 percent as high as that of C^+ at 100 volts electron energy and the appearance potential as 27 ± 1 volts. It thus appears to be of interest and importance to ascertain the reason for the low peak height and to attempt to fit energy determinations into the interpretation of other processes.

The dissociation process from which the O^+ ions result could be either $CO+e \rightarrow C^- +O^+ +e$ or $CO+e \rightarrow C+O^+ +2e$. Failure to detect C^- ions eliminates the first of these possibilities.

The O^+ peak is plotted below that of C^+ from CO to the observed relative abundance in Fig. 8. The shapes of the two peaks are entirely different, that of O^+ being of type III. It is evident that the low peak height for O^+ ions in comparison with that for C^+ ions is due to the nature of the distribution in kinetic energy of the products rather than to any significant difference in the probability of occurrence of the processes from which they result. The parts of the peaks corresponding to initial kinetic energies of more than 2 volts are about equally high. Thus the assumption that the O^+ ion is not present in any appreciable abundance because the total peak height is small is erroneous.

The location of the dissociation limit for this process requires a different technique from that used for process *E* since ions which focus at the maximum of the peak possess an unknown amount of initial kinetic energy. The scale of kinetic energy was calibrated by using as the zero point the position of the maximum of the small O^+ "impurity peak" which remained when the electron energy was reduced to a value below the appearance potential of any ions from CO. The shape of this peak and the fact that the ions result in the main from the dissociation of water vapor impurity are taken as good evidence that the peak is composed of ions possessing almost no initial velocity. The appearance potentials (Fig. 13) of O^+ ions of 1.5, 2.0, 2.5 and 3.0 volts initial kinetic energy were measured by adjusting the ion accelerating potential to the proper positions on the peak of Fig. 8.

Extrapolation of the relation of appearance potential and kinetic energy to zero kinetic energy (Fig. 14) yields 23.5 volts for the level of the dissociation limit above the ground state of

the molecule. An interesting comparison may be made here with the datum of Tate, Smith and Vaughan. Their appearance potential, presumably measured on the maximum of the peak, would, according to the lower curve of Fig. 8, be that of ions of approximately 1.5 volts initial kinetic energy. From Fig. 13 it is seen that this ion should be formed first at about 27 volts which is just the value given by Tate, Smith and Vaughan.

The low intensity of the O^+ ion current and the limitations of the method of calibration of the scale of kinetic energy make it necessary to consider the value of 23.5 volts as an upper limit. Any possible correction can be no more than a few tenths of a volt, however, and it is estimated that the true dissociation limit lies no lower than 0.4 volt below 23.5 volts.

Heat of Dissociation of CO · (D(CO))

The energy relations set up for the processes in which O^+, O^- and C^+ are formed limit the values which can be assigned to D(CO). The largest value of D(CO) compatible with the dissociation limit of process F lies in the range 9.5 to 9.6 electron volts. Interpretation[8] of various processes which led to $D(CO)=11.6$ electron volts seems untenable. The value 9.6 volts remains as the only value of D(CO) which yields a consistent interpretation of all the electron impact processes observed in CO.

We have, for example, in process D

$$A(C^+)=D(CO)+I(C)+E(C^+)+EA(O^-)+E(O^-),$$
$$20.9=9.6+11.3+0-2.2+2.2.$$

For process E we have

TABLE II. *Summary of electron impact data for* NO. *Appearance potential in volts.*

	$A(NO^+)$	$A(NO^{++})$	$A(N^+)$	$A(O^+)$	$A(O^-)$
Hogness, Lunn* (mass spectrometer)	9		22	21	
Tate, Smith[28] (total ion current)	9.5 ±0.1				
Tate, Smith, Vaughan[3] (mass spectrometer)	9.5 ±0.1	41 ±1	22 ±0.5	21	
Hanson[9] (retarding potential)			21.7 ±0.2		3.2 ×0.5
Present work (mass spectrometer)	9.5 ±0.1	41.3 ±0.3	19.9 ±0.2 21.8 ±0.2	20.5 ±0.2	7.0 ±0.3 20.0 ±0.3

* T. R. Hogness and E. H. Lunn, Phys. Rev. **30**, 26 (1927).

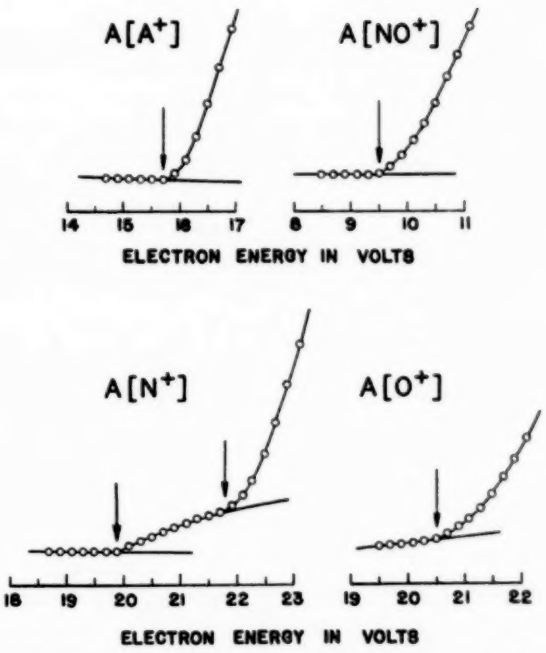

FIG. 15. Typical appearance potential curves for ions from nitric oxide. The slight slope of the O^+ curve below the break is due to amplifier drift and a small amount of ion current from dissociation of water vapor impurity.

$$A(C^+)=D(CO)+I(C)+E(C^+)+E(O),$$
$$22.8=9.6+11.3+0+1.96,$$

For process C we have

$$A(O^-)=D(CO)+E(C)-EA(O^-)+E(O^-),$$
$$9.5=9.6+0-2.2+2.2.$$

In process F the relations are

$$A(O^+)=D(CO)+I(O)+E(C)+E(O^+),$$
$$23.1=9.6+13.5+0+0.$$

The assignments of $E(C)=E(C^+)=0$ and $EA(O^-)=E(O^-)=2.2\pm0.2$ seem reasonable from spectroscopic data and earlier data on impact phenomena. It should be noted that the value $D(CO)=9.6$ volts depends on the appearance potentials in processes C, D and E which are not subject to the same error involved in $A(O^+)$. They were determined from peaks of a different type.

The value $D(CO)=9.6$ volts is not in agreement with either of two values proposed by band spectroscopists, however. Schmid and Gerö[30] interpret the three predissociation limits at 9.61,

[30] R. Schmid and L. Gerö, Zeits. f. Physik **99**, 281 (1936).

11.11 and 11.60 volts as corresponding to three dissociation limits of the molecule leading directly to $D(CO)=6.921$ volts.[31] Schmid[32] has attempted to reconcile the electron impact data of Lozier with this value of $D(CO)$ by assuming tetravalent carbon products. He calculates the level of $C^+(^4P)+O(^3P)$ as 23.5 volts above the ground state. This is outside the experimental error for $A(C^+)$ at 22.8 volts. Furthermore if $A(C^+)$ is in error it would in all probability be *higher* than the actual dissociation limit.

Herzberg,[33] on the other hand, considers only the predissication at 11.11 volts as corresponding to a dissociation limit of the molecule. The predissociation at 11.60 volts is considered to be only an upper limit for the level of some asymptote and that at 9.61 volts as accidental predissociation. Herzberg's final conclusion is that $D(CO)$ is most probably 9.144 volts[31] with the limit at 11.11 volts corresponding to $C(^3P)+O(^1D)$. It is possible to interpret only process C of the dissociation processes observed in CO under electron impact on this basis, however. This can be done by assuming unexcited O^- and C in the ^1S state. If $D(CO)=9.144$ volts it is necessary to assume an experimental error in the appearance potentials for processes D and E of about 0.5 volt. This conclusion seems a little severe on the basis of the agreement of independent electron impact experiments in H_2, N_2 and NO by different methods with each other and with band spectroscopic data which is much more conclusive than that for CO.

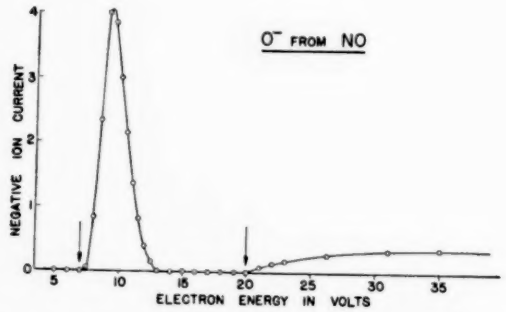

FIG. 16. Efficiency of formation of O^- ions from nitric oxide as a function of the energy of the impacting electrons. The ion accelerating potential was adjusted to the maximum of the ion peak at each reading.

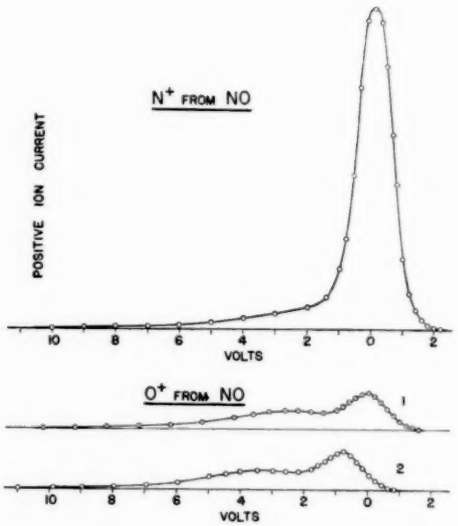

FIG. 17. Peak shapes for N^+ and O^+ ions from nitric oxide. Position 1 of the O^+ peak relative to the scale of kinetic energy corresponds to the construction of the peak by method A, position 2 to method B (see text and Fig. 7). The maximum of the N^+ peak corresponds to an accelerating potential of about 300 volts.

All thermochemical data on the heat of sublimation of carbon, $L(C)$, published prior to Jan. 1, 1934 have been reviewed by Bichowsky and Rossini[34] who conclude that the value most probably lies in the range 110 to 170 kcal. $D(CO)=9.6$ volts (221.3 kcal.) yields $L(C)=5.9$ volts (136.3 kcal.).

Goldfinger and Jeunehomme[35] have calculated vapor pressure curves for C from three values for $L(C)$ (170.2, 124.8 and 108.3 kcal.)[31] which are in agreement with the predissociation limit in CO at 11.11 volts. It was found that the direct measurements of the vapor pressure of C described in the literature lie mostly between the curves calculated for $L(C)=170.2$ kcal. and 124.8 kcal. Although $L(C)=170.2$ kcal. gives the better agreement, it was eliminated for spectroscopic reasons and $L(C)=124.8$ kcal. corresponding to $D(CO)=9.144$ volts taken as the most probable value. It should be pointed out that the value

[31] The new conversion factor of 8066.0 cm^{-1} per electron volt has been used in this paper. For this reason a number of the values cited differ slightly from those given in the original papers. See Table 2 in G. Herzberg, *Molecular Spectra and Molecular Structure, I. Diatomic Molecules* (Prentice-Hall, New York, 1939).

[32] R. Schmid, Zeits. f. Physik **99**, 274 (1936).

[33] G. Herzberg, Chem. Rev. **20**, 145 (1937).

[34] R. F. Bichowsky and F. D. Rossini, *The Thermochemistry of Chemical Substances* (Reinhold, New York, 1936).

[35] P. Goldfinger and W. Jeunehomme, Trans. Faraday Soc. **32**, 1591 (1936).

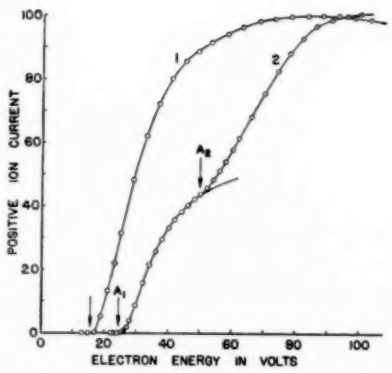

FIG. 18. Efficiency of formation of ions from N_2. Curve 1 is for N_2^+ ions and curve 2 for ions of $m/e=14$. A_1 indicates the onset potential of process C and A_2 that of process B. The ordinates of each curve have been arbitrarily chosen and have no relative significance.

$L(C)=136.3$ kcal. based on $D(CO)=9.6$ volts is perhaps in better agreement with vapor pressure measurements as it is somewhat higher than the "spectroscopic" value chosen by Goldfinger and Jeunehomme.

Nitric oxide[36]

Of particular interest in studying NO is the process $NO \rightarrow N^+ + O^-$ and the dissociation process in which O^+ is formed. The results of this paper and of earlier work are given in Table II. A number of processes have been identified.

Process A: $NO+e \rightarrow NO^+ + 2e$.—The value $I(NO)$ (Fig. 15) agrees very well with previous measurements.

Process B: $NO+e \rightarrow NO^{++} + 3e$.—$A(NO^{++})$ was found to be 41.3 ± 0.3 volts.

Process C: $NO+e \rightarrow N+O^-$.—The efficiency of formation of O^- ions as a function of electron energy is shown in Fig. 16. The onset potential of the resonance process measured at the maximum of the ion peak is 7.0 ± 0.3 volts. The fact that this potential is higher than that obtained by extrapolation by Hanson[9] indicates that ions of zero initial kinetic energy are *not* formed in the process.

Process D: $NO+e \rightarrow N^+ + O^- + e$.—This process has been identified for the first time in this work. The value of $A(N^+)$ is found at 19.9 ± 0.2 volts (Fig. 15). 20.0 ± 0.3 volts was obtained for $A(O^-)$. The appearance potential $A(N^+)$ was measured with the same ion accelerating field as was used to obtain the N^+ peak in process E and it is believed that the ions (N^+) had zero kinetic energy here as they did in process E.

The onset potential of this process is very nearly equal to the electron energy calculated from $D(NO)$[37] and $I(N)$ at which the unexcited products N^+ and O should appear. (19.84 volts).[38, 31] If Lozier's value (2.2 volts) is assumed for $EA(O)$[8] it is necessary that $E(N^+)+E(O^-)$ equal approximately 2.2 volts. The nearest state in N^+ is the ^1D at 1.90 volts. Identification of this value with the 2.2-volt excitation is a possibility but better numerical agreement is obtained if the analogy with the process $CO+e \rightarrow C^+ + O^- + e$ is carried out and the excitation assigned to the O^- ion. This excited state of O^-, lying very near the positive energy continuum, is the only one which the theory of the negative ion renders at all probable.[39]

Process E: $NO+e \rightarrow N^+ + O + 2e$.—The N^+ peak shown in Fig. 17 is to be attributed mainly to ions from this process. The shape of the peak is of type I. The appearance potential of 21.8 ± 0.2 volts (second break in the C^+ curve of Fig. 15) measured at the maximum of the peak is in better agreement with Hanson's extrapolated

TABLE III. *Summary of electron impact data for* N_2. *Appearance potential in volts.*

	$A(N_2^+)$	$A(N^+)$	$A(N_2^{++})$	$A(N^{++})$
Vaughan[2] (mass spectrometer)	15.8 ± 0.1	24.5 ± 0.1	40 ± 1(?) 47 ± 1	
Tate, Smith[28] (total ion current)	15.7			
Lozier[7] (retarding potential)		24.27 ± 0.1		
Tate, Smith, Vaughan[3] (mass spectrometer)	15.65 ± 0.1			
Present work (mass spectrometer)	15.7 ± 0.1	24.3 ± 0.2	49.5 ± 0.5	64 ± 2

[36] A part of this work on NO was presented at the New York Meeting of the American Physical Society February 24, 1940. H. D. Hagstrum and J. T. Tate, Phys. Rev. **57**, 561A (1940).

[37] $D(NO)=5.29$ volts calculated from $D(N_2)=7.384$ volts, $D(O_2)=5.082$ volts and the heat of formation of NO from thermochemistry. See G. Herzberg, *Molecular Spectra*, etc., Table 36 and R. F. Bichowsky and F. D. Rossini, reference 34.

[38] Atomic excitation and ionization energies have been taken from R. F. Bacher and S. Goudsmit, *Atomic Energy States* (McGraw-Hill, New York, 1932).

[39] For a discussion of the possibility of excited states in negative ions see O. Oldenberg, Phys. Rev. **43**, 534 (1933) (especially footnote 9 in this reference); W. W. Lozier, Phys. Rev. **46**, 268 (1934) and H. S. W. Massey, reference 29, p. 19.

value of 21.7±0.2 volts than previous mass spectrometric data. This agreement between the data of the two electron impact methods is again taken as evidence that ions of zero initial velocity are formed in the process. The N^+ product is unexcited whereas the O atomic product is in its ^1D state. The energy difference between the two breaks in the N^+ curve of Fig. 15 (1.9 volts) is thus to be interpreted as the excitation of the ^1D state rather than the electron affinity of the oxygen atom.

Process F: $NO+e \rightarrow N+O^+ +2e$.—The O^+ peak is shown in Fig. 17 drawn to the same scale used in the curve for N^+. The peak is assumed to be of type II. In curve 1 the ions which focus at the maximum are assumed to have no kinetic energy. But the appearance potential of 20.5±0.2 volts (Fig. 15) is not compatible with the known value of $D(NO)$ and excitation energies. One must assume then that the dissociation products are unexcited but have kinetic energy. The total kinetic energy turns out to be 20.5−18.9 or 1.6 electron volts of which the O^+ ion possesses 0.75 electron volt. The correct position of the O^+ peak is then that shown in curve 2 in which the maximum is at 0.75 volt.

The experimental curve 2 can be most satisfactorily constructed from the curve showing the distribution in kinetic energy of the ions at the instant of formation by assuming that the upper potential energy curve has a maximum of 1.6 volts.

Herzberg and Mundie[40] have assumed a potential maximum of 1.3 volts to explain a predissociation limit. It appears that the possible existence of potential curves with maxima as high as is necessary to postulate here is not in doubt.

TABLE IV. *Summary of electron impact data for* O_2. *Appearance potential in volts.*

	$A(O_2^+)$	$A(O_2^{++})$	$A(O^+)$	$A(O^-)$
Hogness, Lunn* (mass spectrometer)	13		20	
Kallmann, Rosen** (mass spectrometer)	13		19.5	
Tate, Smith[28] (total ion current)	12.5			6
Lozier[8] (retarding potential)				2.9±0.2 12.0±0.2
Present work (mass spectrometer)	12.3±0.1	50.0±0.5	19.2±0.2	3.0±0.4 18.9±0.4

* T. R. Hogness and E. G. Lunn, Phys. Rev. **27**, 732 (1926).
** H. Kallmann and B. Rosen, Zeits. f. Physik **61**, 61 (1930).

[40] G. Herzberg and L. Mundie, J. Chem. Phys. **8**, 263 (1940).

Nitrogen

Data from previous electron impact studies in N_2 are given in Table III. Restudy of this molecule with a mass spectrometer was undertaken to extend the experimental study of peak shapes and to obtain, if possible, a definite interpretation of the increases in the efficiency of production of ions of $m/e=14$ observed by Vaughan.[2]

Process A: $N_2+e \rightarrow N_2^+ +2e$.—The value of 15.7±0.1 volts obtained for $I(N_2)$ is in agreement with previous electron impact data listed in Table III and with the value of 15.581 volts determined from the limit of a Rydberg series of bands in the molecular spectrum.[41, 31]

Process B: $N_2+e \rightarrow N_2^{++}+3e$.—The efficiency of formation of ions of $m/e=14$ as a function of electron energy is shown in Fig. 18. The second break at 49.5±0.5 volts does not agree very well with the position of either break reported by Vaughan[2] but is undoubtedly to be identified with the more pronounced break in his curve at 47 volts. It is believed that the first break in Vaughan's curve at 40 volts may be the onset of the formation of CO^{++} ions. CO was an acknowledged impurity in the apparatus. Furthermore the energy difference between the breaks (7 volts) is just the difference found in this work between $A(CO^{++})$ and the second break in curve 2 of Fig. 18. No definite identification of the ionization or dissociation process responsible for this increase in the ion current has as yet been made. It will be indicated in the discussion of process *C* that the break of 49.5 volts may now be ascribed to the onset of double ionization of the molecule. Such a process is to be expected from the results for other molecules.

Process C: $N_2+e \rightarrow N^+ +N+2e$.—The peak at $m/e=14$ for 100-volt electrons is of type I and is very similar in appearance to the peaks for C^+ from CO and N^+ from NO. (see Figs. 8 and 17). The appearance potential measured at the maximum of the peak is 24.3±0.2 volts. Agreement with Lozier's extrapolated value of 24.27 volts[7]

[41] R. S. Mulliken, Phys. Rev. **46**, 144 (1934); A. van der Ziel, Physica **4**, 373 (1937); R. E. Worley and F. A. Jenkins, Phys. Rev. **54**, 305 (1938).

indicates that ions of zero initial velocity are formed.

The ion peak at 100 volts electron energy is also made up of ions from the process which begins at 49.5 volts. These ions may be either N_2^{++} or N^+ from a second mode of dissociation of the molecule. The efficiency of formation of ions of 2 volts initial kinetic energy as a function of electron energy was determined by setting the ion accelerating potential at a value 2 volts less than that corresponding to the maximum of the peak. The curve shows no second break at any point and resembles curve 1 of Fig. 18. This result indicates that the process starting at 49.5 volts is double ionization of the molecule. If the ions were N^{++} a second break should have been observed at about 53.5 volts electron energy in the efficiency curve for 2 volt ions.

Process D: $N_2+e \rightarrow N^{++}+N+3e$.—An extremely small ion peak was observed at the ion accelerating potential corresponding to $m/e=7$. The abundance of the ion relative to N_2^+ is only 0.006 percent. These ions could either be N^{++} resulting from dissociation of the molecule or N_2^{++++}. Since no N_2^{+++} ions were found at the $m/e=9.35$ position it is likely that the ions of $m/e=7$ are N^{++}. Furthermore the shape of the ion peak appears to be of type III indicating that the ions possess considerable initial kinetic energy. This could be possible only if the ions are products of dissociation rather than multiple ionization. The appearance potential of the ions at the maximum of the distribution was found to be 64 ± 2 volts. Lack of knowledge of the kinetic energy of the ions precludes any further interpretation of the process.

Oxygen[42]

The work on oxygen revealed the formation of O_2^{++} and O^{++} and gave additional information on processes in which other ions were formed. The results of this and other recent experiments are shown in Table IV.

Process A: $O_2+e \rightarrow O_2^+ + 2e$.—A value of 12.3 ± 0.1 volts was obtained for $I(O_2)$. This is lower than the value of 12.5 volts obtained by Tate and Smith[28] but is in better agreement with the value of 12.2 volts obtained by means of the cycle $I(O_2)=D(O_2)+I(O)-D(O_2^+)$ and spectroscopic determinations of $D(O_2)$, $I(O)$ and $D(O_2^+)$.[43]

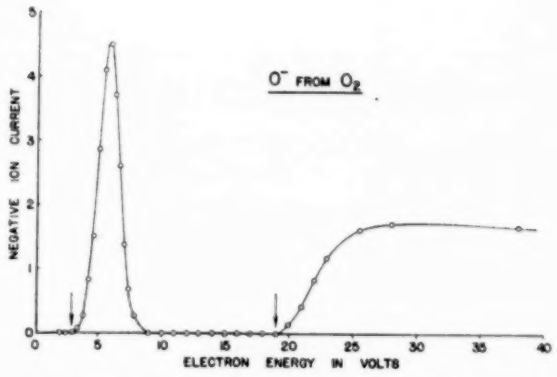

FIG. 19. Efficiency of formation of O^- ions from oxygen. The spectrometer was adjusted to collect ions of zero initial kinetic energy.

Process B: $O_2+e \rightarrow O_2^{++}+3e$.—The relative efficiency of formation of ions of $m/e=16$ from O_2 by electrons of energies up to 100 electron volts has been measured. The curve is similar to that for ions of $m/e=14$ from N_2 shown in Fig. 18 (curve 2). In this case, however, the second break occurs at 50.0 ± 0.5 volts. It has been demonstrated by the method used for process *B* in N_2 that this break indicates the onset of the production of O_2^{++}.

Process C: $O_2+e \rightarrow O+O^-$.—The efficiency of formation of O^- ions as a function of electron energy is shown in Fig. 19. The first appearance potential at 3.0 ± 0.4 volts is undoubtedly to be identified with the value of 2.9 volts obtained by extrapolation by Lozier[8] for ions of zero initial kinetic energy. At first sight this result appears to contradict Lozier's observation that ions of kinetic energy less than 1.3 volts are not formed. It is possible, however, that the ions observed in this work and those observed by Lozier result from transitions to different potential curves having the same asymptote. Massey[44] has interpreted the resonance process observed by Lozier as transition to the unstable Σ_u state of O_2^-. It is suggested that the process observed in

[42] A part of this work on O_2 was presented at the Washington Meeting of the American Physical Society, April 26, 1940. J. T. Tate and H. D. Hagstrum, Phys. Rev. **57**, 1071A (1940).

[43] R. S. Mulliken and D. S. Stevens, Phys. Rev. **44**, 720 (1933).

[44] H. S. W. Massey, reference 29, pp. 28 and 52.

this work with a mass spectrometer involves transition to the Π_u state. If the potential curve for this state has the position proposed by Massey ions of zero initial kinetic energy could be formed. Furthermore if the ions from this process possess initial kinetic energies no greater than a fraction of a volt they would not be observed by the retarding potential method.

Process D: $O_2+e\rightarrow O^+ + O + 2e$.—The shape of the O^+ ion peak at 100 volts electron energy is of type I. Ions of kinetic energy *near* zero are relatively numerous. The appearance potential measured at the maximum of the peak (19.2 ± 0.2 volts), however, is 0.5 volt greater than the potential at which ions of zero initial velocity should appear. $[D(O_2)+I(O)=5.08+13.62=18.7$ volts]. On the basis of the accuracy of similar measurements in other molecules this difference is considered to be well outside the experimental error. It cannot be attributed to excitation of the products, as neither O nor O^+ possesses an appropriate state. The appearance potential must then correspond to ions of 0.25 volt initial kinetic energy. The peak shape analysis is compatible with a potential curve which has a maximum 0.5 volt above the asymptote (see the discussion of process *F* in NO).

Process E: $O_2+e\rightarrow O^+ + O^- + e$.—The second appearance potential of O^- ions from O_2 is 18.9 ± 0.4 volts. (Fig. 19). This value is 0.2 volt higher than the potential energy of the products $O^+ + O$ above the ground state of O_2. There can, however, be little doubt that two values should be identified. The accuracy of the datum for this process is not to be compared with that for process *D* which is about 20 times as probable.

Since it is not possible to identify the appearance potential with any other dissociation limit of the molecule, the products $O^+ + O^-$ are excited by very nearly the amount $EA(O)=2.2$ volts. Since the lowest state of O^+ is the $^2D^0$ at 3.3 volts the O^- ion must assume all of this energy. This is an additional example of the formation of the O^- ion in the "loosely bound" state.[39]

The curve of O^+ ion current as a function of electron energy exhibits only the single break at 19.2 volts which has been identified with process *D*. Since O^- ions from process *E* are observed at 18.9 volts one questions why O^+ ions which are formed in equal numbers in the process are not observed at the same potential. This is to be explained as follows. The measurement of $A(O^+)$ was made at the maximum of the O^+ peak which has been shown to correspond to ions of 0.25 volt kinetic energy. When the electron energy was varied the ion accelerating potential was not changed so that ions of 0.25 volt kinetic energy were being collected when the onset potential of process *E* was measured. Since the dissociation limits for $O^+(^4S^0)+O(^3P)$ and $O^+(^4S^0)+O^-$ (excited by 2.2 volts) almost coincide, only one appearance potential should be observed for O^+ ions of any initial velocity.

Process F: $O_2+e\rightarrow O^{++}+O+3e$.—An extremely small ion peak was observed at the $m/e=8$ position. Its abundance was of the order of 0.01 percent of O_2^+. Failure to find any ions at the position corresponding to O_2^{+++} indicates that the ions of $m/e=8$ are more likely O^{++} than O_2^{++++}. No appearance potential or peak shape measurements were attempted. Because of the effect of O_2 on the filament of the spectrometer the gas pressure and the electron beam intensity could not be run high enough to make such measurements possible.

Acknowledgments

The authors wish gratefully to acknowledge the work of Dr. A. Hustrulid on the design and construction of the electromagnet and control equipment and the courtesy of Dr. A. O. Nier in arranging for the construction of the 1000-volt stabilized rectifier set. Many thanks are due Dr. E. L. Hill for a number of helpful discussions during the course of the work. Help and advice of a technical nature were very kindly supplied by Messrs. E. F. Greinke, W. B. Haliday, R. B. Thorness and D. Miller.

Experimental Study of the Diffuse Scattering of X-Rays by Potassium Chloride Crystals

STANLEY SIEGEL
Ryerson Physical Laboratory, University of Chicago, Chicago, Illinois
(Received December 23, 1940)

Diffusely scattered radiation has been studied with a KCl crystal and copper radiation. Observations have been made in the immediate region of a strong reflection. The shapes and half-widths of the maxima have been studied as functions of the direction of incidence. Observations have been found to agree with the theory.

GENERAL

AT the December, 1939, meeting of the American Physical Society in Chicago, W. H. Zachariasen proposed a new theory of the diffuse scattering of x-rays by crystals. In one aspect of the theory, it was predicted that the diffusely scattered x-radiation would appear as sharp diffraction maxima. In a subsequent paper at the same meeting, S. Siegel and W. H. Zachariasen reported an experimental study of these maxima. The results of the theory[1] and experiment[2] have been published.

The difference between this theory and the earlier work of Debye, as well as the experimental studies by Jauncey and his collaborators, has already been treated.[1]

The existence of streaks in Laue photographs has been known for many years, and in 1923, Faxén[3] suggested that these streaks might be caused by a thermal effect in the crystal. Wadlund[4] observed very prominent streaks in some photographs and Zachariasen[5] interpreted these as being due to a two-dimensional lattice effect. Recently Preston[6] has shown the effect of temperature on these streaks, thus confirming Faxén's suggestion. Preston observed streaks when general radiation was used; however, when monochromatic radiation was used, maxima, similar to Laue spots, appeared. Preston interpreted these on the basis that the thermal vibrations of the lattice break the crystal into groups composed of an atom and its nearest neighbors, and these thermal motions change the interatomic distance from one group to another, thus producing new maxima. Raman, apparently unaware of Preston's work, or of the work carried out at Ryerson Laboratory, published photographs showing these spurious maxima.[7] He interpreted the maxima as a specular reflection of x-rays resulting from stratifications of density in the crystal which are not static but dynamic in character. Other articles have since appeared. Knaggs and collaborators[8] have published photographs of these maxima. Lonsdale and collaborators[9] have made a detailed qualitative study of this effect. The conclusions reached by them are those predicted by theory, many of the results however, having been already studied quantitatively. More recently, another paper by Raman and Nilakantan has appeared.[10]

Although the agreement between theory and observations in our original experiment was quite good, there was some discrepancy between theoretical and observed widths of the diffuse maxima. Thus it was decided to carry out the observations in more detail, to extend them as close as possible to the Bragg angle, and to increase the accuracy of observations with better equipment. The original experiment was performed with a crystal of sodium chloride. Since the theory was developed for crystals containing atoms of only one kind, a good approximation to such a case would be potassium chloride, which was used throughout the present experiment.

[1] W. H. Zachariasen, Phys. Rev. **57**, 597 (1940).
[2] S. Siegel and W. H. Zachariasen, Phys. Rev. **57**, 795 (1940).
[3] H. Faxén, Zeits. f. Physik **17**, 266 (1923).
[4] A. P. R. Wadlund, Phys. Rev. **53**, 843 (1938).
[5] W. H. Zachariasen, Phys. Rev. **53**, 844 (1938).
[6] G. D. Preston, Proc. Roy. Soc. **172**, 116 (1939).
[7] C. V. Raman and P. Nilakantan, Nature **145**, 667 (1940); Proc. Ind. Acad. Sci. **11**, 379 (1940).
[8] I. E. Knaggs, K. Lonsdale, A. Müller, A. R. Ubbelohde, Nature **145**, 820 (1940).
[9] K. Lonsdale, I. E. Knaggs, H. Smith, Nature **146**, 332 (1940).
[10] C. V. Raman and P. Nilakantan, Proc. Ind. Acad. Sci. **12**, 141 (1940).

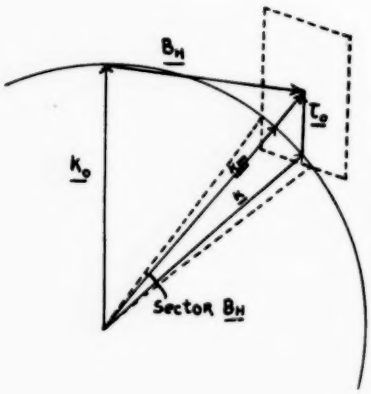

FIG. 1. A section of the reciprocal lattice.

METHODS FOR OBSERVING THE MAXIMA

As the theory indicates, the streaks are produced by the continuous radiation in the x-ray beam while the spots are individual diffraction maxima due to the characteristic radiation. In the present paper only the diffuse spots will be dealt with. These maxima are observed whenever Bragg's law is nearly satisfied.

Figure 1 shows the conditions under which they may be observed. This figure and the following description have been given in Zachariasen's paper.[1] Vectors $\mathbf{k}_0$ and $\mathbf{k}$ are the directions of incidence and scattering of the x-ray beam. $|\mathbf{k}_0| = |\mathbf{k}| = 1/\lambda$. $\mathbf{B}_H$ is a vector in the reciprocal lattice, and its shortest separation from the vector $\mathbf{k}-\mathbf{k}_0$ is τ_0. Let $\mathbf{k}$ vary. Its terminus will describe a sphere of radius $1/\lambda$ about the terminus of $-\mathbf{k}_0$, thus producing the sphere of reflection. The points on the sphere of reflection which are closer to $\mathbf{B}_H$ than to any other lattice point define a sector of the solid angle 4π, so that the same vector $\mathbf{B}_H$ is associated with all directions $\mathbf{k}$ within the sector. As $\mathbf{k}$ varies within a sector, τ_0 varies with it since $\mathbf{k}-\mathbf{k}_0+\tau_0=\mathbf{B}_H$. Considering $\mathbf{k}_0$ and $\mathbf{B}_H$ to be fixed, τ_0 becomes a minimum value, $\tau_{\min}$ when $\mathbf{k}$ is parallel to $\mathbf{B}_H+\mathbf{k}_0$. Thus $\tau_{\min}=|\mathbf{B}_H+\mathbf{k}_0|-|\mathbf{k}|$ or $\lambda\tau_{\min}\approx-\Delta\sin 2\theta_B$, where θ_B is the Bragg angle and $\theta_i\equiv\theta_B+\Delta$, Δ being a small deviation from the Bragg angle. The intensity of the scattering reaches a maximum whenever τ_0 is a minimum, and the direction of the intensity maximum, $\mathbf{k}_m$, is $[1+\lambda\tau_{\min}]\mathbf{k}_m=\mathbf{B}_H+\mathbf{k}_0$. The scattering angle corresponding to the maximum is shown to be $2\theta_m\approx 2\theta_B+2\Delta\sin^2\theta_B$. For scattering directions $\mathbf{k}$ near a maximum $\mathbf{k}_m$, $(\lambda\tau_0)^2=(\lambda\tau_{\min})^2+\chi^2$ where χ is the angle between $\mathbf{k}$ and $\mathbf{k}_m$. The intensity distribution is symmetrical about the maximum, and the half-width at half-maximum is $\chi_{\frac{1}{2}}\approx\lambda|\tau_{\min}|=|\Delta|\sin 2\theta_B$.

Thus, in a transmission photograph there will always be some reflection planes for which $\tau_{\min}$ will give appreciable intensity, enough to be conveniently recorded.

Transmission photographs were obtained by Preston and later by Raman. They obtained Laue photographs using apparently large pinholes to define the primary beam, and employing sensitizing screens to hasten recording. But for quantitative work it is necessary to use a narrow pinhole or slit to keep the divergence of the beam at a minimum and to avoid the use of sensitizing screens, for such screens widen the spots, causing them to become too diffuse for any width or intensity measurements. The author tried to obtain transmission photographs using a small pinhole, monochromatic copper radiation, and a thin KCl crystal. One would expect weak reflections with Cu $K\alpha$ and KCl, except at a scattering angle of 90°, in which case the absorption would become quite large. After a 36-hour exposure only very faint spots were discernible. The transmission method does not appear very amenable to a quantitative study.

The best method for observation is obtained by reflecting the primary beam from the crystal surface and making observations on a strong reflection. In this case the crystal can be set to produce any desired $\tau_{\min}$ values, and, depending on the nature of the crystal surface, observations can be made on diffuse maxima having relatively large intensity values. It must be remembered, however, that in any method of observation, the divergence of the primary beam must be smaller than the widths of any of the observed diffuse maxima. This immediately rules out the use of wide slits or sensitizing screens, and gives rise to small recording intensities. This point will be elaborated.

APPARATUS AND EXPERIMENT

A Bragg spectrometer was used in making observations. All such observations could be duplicated to within 1′ of arc, so that any error was less than that value. The beam was defined

by two slits separated a distance of 8.0 cm. The width of each slit was 0.005 cm, the height being 0.3 cm. The distance between the second slit and crystal was 5.0 cm, and between crystal and photographic plate, 6.04 cm. A copper x-ray tube was used throughout the experiment and the radiation was filtered with a nickel foil. Special care was taken in orienting the crystal so that the same facial area would always receive the same illumination. This was accomplished by the usual optical methods. The photographic plate was mounted normal to the incident beam.

Before observations of any kind are made, it is of primary importance to have as "perfect" a crystal surface as possible. The theory calls for a well-defined beam. The divergence of the beam reflected from the crystal face must, of course, be narrower than the widths of any of the recorded maxima. The maxima are sharpest at the Bragg angle and become broad and diffuse as the crystal is rotated from its Bragg position. Hence the narrowest maximum is determined by the point of observation closest to the Bragg angle for the characteristic radiation producing the maximum. Observations cannot be made at the Bragg angle, for the diffuse temperature maximum and the Bragg reflection coincide. Thus the crystal is slightly rotated away from its Bragg angle so that the Bragg reflection is completely suppressed and will not interfere with the emitted temperature maximum. It is found however, that most crystal surfaces are rough and warped, and this allows the Bragg reflection to persist over quite an angular range about the Bragg angle.

Experimental difficulties have been encountered at this point. In the original experiment with NaCl it was found that the Cu $K\alpha$ line reflected from the (200) face could persist even though the crystal was rotated 60′ from its Bragg position. The diffuse maxima cannot be studied under such conditions for they are very nearly superimposed upon the persistent Cu $K\alpha$ line, and it was only by properly etching the surface that the line radiation disappeared when the crystal was 30′ from the Bragg position. If the intensity of the line radiation is plotted as a function of the deviation of the crystal away from the Bragg position for the line, then one obtains a "surface distribution curve." Etching the surface produces "surface distribution curves" of various shapes and widths. Large primary slits allow illumination of a larger facial area, and this increases the persistence of the Bragg reflection.

Therefore, if observations are to be made on the sharp intense temperature maxima near the Bragg angle, a good crystal surface showing a rapid cut-off of the Bragg reflection must be used. Such a surface will exhibit a narrow distribution curve. After determining the point of observation closest to the Bragg angle, slit widths can be approximately adjusted to account for the narrowest diffuse maximum which will be emitted at that point.

In the present experiment an extraordinary KCl crystal section was cleaved from its parent. The parent was an artificial crystal. The cleavage (200) surface was so perfect that the Bragg angles for each component of the Cu $K\alpha$ doublet were quite sharply determined. Figure 2 shows the appearance of the doublet on rotation of the crystal through the Bragg angles for the doublet. In Fig. 2(a) $K\alpha_1$ is strongly reflected while $K\alpha_2$ is barely visible. In Fig. 2(b) $K\alpha_2$ has increased in intensity so that its intensity is greater than that of $K\alpha_1$. Figure 2(c) shows that $K\alpha_1$ has still decreased in intensity. The angles indicated in the figure are arbitrary. A surface distribution curve for this crystal has been made. Two curves are possible, one for each component of the doublet. The deviation of the crystal away from the average Bragg angle for the doublet is indicated by Δ. For $\Delta=6'$ the intensity of the

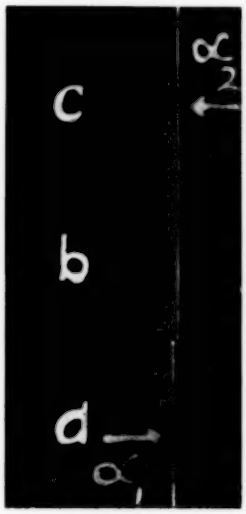

FIG. 2. Showing the change in intensity of each component of the Cu $K\alpha$ doublet over a three-minute interval in the crystal angle. These lines are magnified. The lines tend to break up when the crystal is moved too far from the Bragg positions.

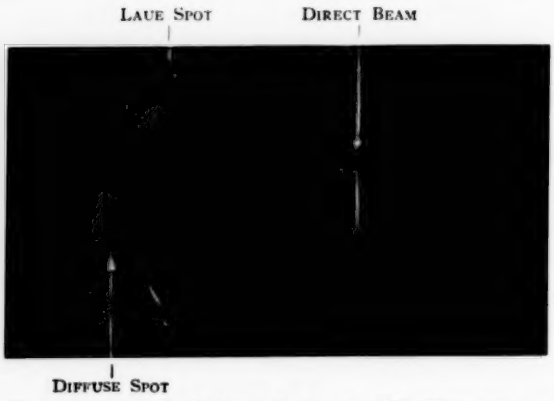

FIG. 3. Typical photograph for $\Delta = 29'$. The exposure time is 32 hours. The diffuseness of the temperature maximum can be seen extending into the Laue spot. A diffuse temperature halo can be seen surrounding the direct beam.

emitted doublet became weak enough to make observations on the temperature maximum. A 5-hour exposure on the photographic plate yielded a temperature maximum and only a very faint doublet which did not interfere.

The necessity for such a narrow beam made the use of the ionization-chamber method impossible for recording the intensities of the diffuse maxima. For studying the widths of the lines, the analyzing slit in front of the ionization chamber must measure the differential intensity and must thus be narrower than the primary slits. Even then the intensity of a diffuse line for $\Delta = 40'$ say, may be about 10^{-4} that of the Cu $K\alpha$ line emitted at the Bragg angle.

In making observations, the crystal was oriented so that the cleavage face would reflect at the average Bragg angle for the Cu $K\alpha$ doublet. All diffuse maxima were then due to the line radiation. The intensity of the continuous radiation is small in comparison with that of the Cu $K\alpha$ lines, so that the diffuse scattering of the continuous radiation can be neglected. Since the crystal was quite perfect, observations began for $\Delta = 6'$ and extended up to $\Delta = 41'$. For $\Delta = 6'$ the exposure time to produce the maximum was 5 hours, and for $\Delta = 41'$ the exposure time was 71 hours. The exposure time varies approximately as $1/\Delta^2$. Thus any observations beyond $\Delta = 41'$ would require extremely long exposures.

EFFECT OF TEMPERATURE

All observations in this experiment were made at room temperature. However, the diffuse maxima have been studied over a wide range of temperatures. Lonsdale and workers have observed them at liquid-air temperatures. They find the diffuse spot pattern disappears almost completely at that temperature. Raman and Nilakantan have observed them from room temperature up to 275°C and find an increase in intensity at higher temperatures. Preston has made observations at 500°C and finds increased intensity. The observations include a variety of crystals.

EXPERIMENTAL RESULTS

Figure 3 shows a typical photograph. For this case $\Delta = 29'$ and the exposure time is 32 hours. The diffuseness of the temperature maximum may not be apparent from the reproduction given, but a photometer tracing reveals that it extends well into the Laue spot next to it. The geometrical patterns are the Laue reflections. The Laue reflection next to the diffuse line is very uniform and regular, indicating the quality of the crystal face.

According to theory, the direction of scattering corresponding to an intensity maximum of the diffuse radiation lies in the plane of incidence, and the scattering angle is $2\theta_m = 2\theta_B + 2\Delta \sin^2 \theta_B$.

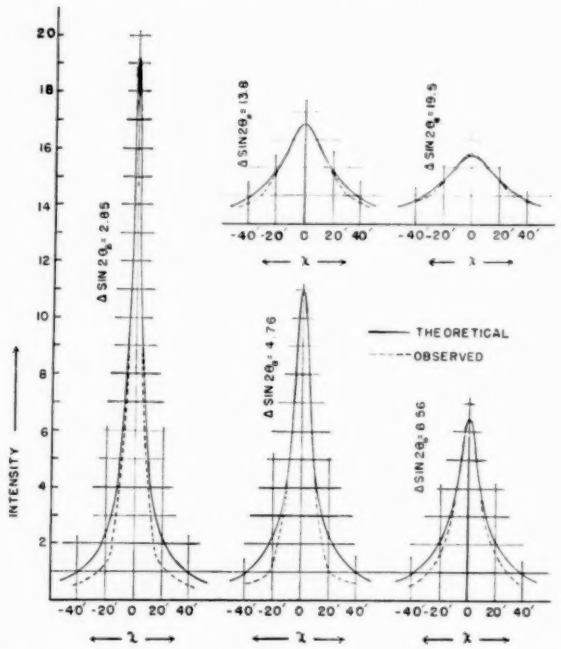

FIG. 4. Shape of the diffraction maxima for different values of $|\Delta|$.

If the incident beam is a narrow pencil, the intensity near a maximum is

$$J_2=\frac{K}{(\Delta \sin 2\theta_B)^2+\chi^2+\varphi^2},$$

where χ and φ are the angular deviations from the maximum in the plane of incidence and normal to it. If Δ, χ, and φ remain small, K can be treated as a constant. However, in this experiment a slit was used. The intensity measurements were made in the plane of incidence, so that the above equation must be integrated with respect to φ. The result is

$$J_2 \propto \tan^{-1}(\varphi_m/y)/y, \quad y\equiv[(\Delta \sin 2\theta_B)^2+\chi^2]^{\frac{1}{2}},$$

where $\varphi_m=l/2R$ and l is the height of the slit. R is the distance from the crystal to the point of observation. In the present experiment φ_m was 85.2′.

Figure 4 shows the shape of the diffuse temperature maxima for various values of $\Delta \sin 2\theta_B$, θ_B being the average Bragg angle for Cu $K\alpha_{1,2}$. The experimental curves were calculated from photometer tracings of the plates. The agreement between observed and theoretical shapes of the maxima is quite good.

In Fig. 5 $\chi_{\frac{1}{2}}$ represents the half-widths at half-maximum. $\chi_{\frac{1}{2}}$ is plotted as a function of $\Delta \sin 2\theta_B$. The circles represent single measurements. In some cases it was necessary to average the values obtained from more than one tracing. These latter points are indicated by crosses. According to theory the maxima do not appear at an angle $2\theta_B$ but at an angle $2\theta_B+2\Delta \sin^2 \theta_B$. This means the lines are shifted by a matter of some seconds. This has been observed on some of the plates, but it is too small to measure accurately. It will change the experimental half-widths by a very small amount only.

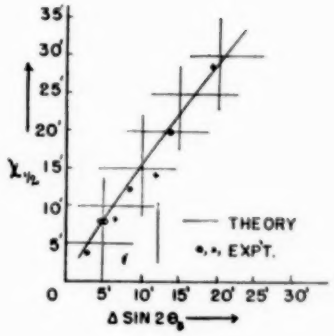

FIG. 5. Variation of half-width with $|\Delta|$.

SUMMARY

All measurements have been made on maxima due to the line radiation present in the incident beam, and only a simple crystal, KCl, has been studied. The crystal has been found to exhibit a perfect surface for this study. The observations extend from $\Delta=\pm 6'$ to $\Delta=\pm 41'$. The shapes and widths of the maxima have been found to agree quite well with the theory.

A study of the variation of the peak intensities of the maxima with $\Delta \sin 2\theta_B$ has previously been made.[2] This variation of intensity is the background present about each reflection in an oscillation photograph. For every Laue reflection there is associated with it a diffuse temperature maximum. However, maxima may arise in directions other than those of the Laue directions in the manner indicated. The intensity of the maxima has been shown to increase with increased rise in temperature. The theory indicates that there should be a slight increase in intensity of the diffuse radiation in a region about the *zero* angle of scattering. Figure 3 shows that it is manifest as a halo about the transmitted direct beam.

The author wishes to thank Dr. Zachariasen for suggesting the problem and for his valuable aid and criticism during the investigation.

The Measurement of Self-Diffusion in Zinc*

FLOYD R. BANKS**
Randal Morgan Laboratory of Physics, University of Pennsylvania, Philadelphia, Pennsylvania
(Received October 3, 1940)

Measurements of self-diffusion along the *C* axis of zinc single crystals have been carried out. Long-lived radioactive Zn^{65} was used as an indicator. Measurements were made at six different temperatures, enabling a determination of the activation energy, which is 19,600 calories per mol. The diffusion coefficient at 410.4°C is 9.89×10^{-4} cm²/day.

INTRODUCTION

DIFFUSION in metals is important both to the metallurgist and to the physicist.[1] It is important to the former because phenomena such as carburization of steel, production of corrosion- and heat-resisting substances, rates of hardening and transformation, and heat treatment of castings, all depend on diffusion rates. Self-diffusion is especially important because of the information it may reveal concerning creep in solids. It is important to the physicist because it will elucidate the mechanism of rate processes in solids, since it involves atomic movements.

Inquiries into the subject of self-diffusion (in which the atoms of a lattice are replaced by atoms of their own kind) led von Hevesy[2] and his collaborators to the use of radioactive isotopes as indicators. The property of radioactivity of an atom *A* permits its labeling or "tagging" and hence affords a means of studying its progress through the lattice of nonradioactive solvent *A*. By such means Hevesy, Seith, and Keil[2] studied self-diffusion in lead and Seith and Keil[3,4] studied self-diffusion in lead and bismuth, with thorium B (which is an isotope of lead) and thorium C (which is an isotope of bismuth).

Prior to the advent of artificial radioactivity the use of radioactive isotopes as indicators in studies of self-diffusion was limited to the heavier elements since these were the only ones which had active isotopes in nature. With artificially produced radioactive isotopes, however, means of studying the lighter elements, such as zinc and copper (elements of special interest to the metallurgist) are available. Self-diffusion in gold[5,6] and copper[7,8] has been studied by using artificial radioactive isotopes. The present paper deals with self-diffusion in zinc.

DESCRIPTION AND DISCUSSION OF PRESENT INVESTIGATION

Radioactive Zn^{65} is used as an indicator in this study. It is electrolytically deposited on a flat, polished, and etched surface of a single crystal of high purity zinc; the sample is then held for a fixed time at an elevated temperature to allow diffusion to proceed in the crystal, and finally cut into sections on a lathe at room temperature. The activity of each section is measured with a Geiger counter or an electroscope. From the weight of each section, the thickness can be computed, and from the thickness and activity the diffusion coefficient is obtained.

Zn^{65} (half-life eight months) can be obtained free from inactive Zn by proton bombardment of copper: $Cu^{65}(p, n)Zn^{65}$. The Zn^{65} produced by this proton-neutron reaction emits positrons and conversion electrons of a strong gamma-ray. Zn^{65} can also be produced from Zn^{64} by deuteron bombardment: $Zn^{64}(d, p)Zn^{65}$.

It is not possible to determine the diffusion coefficient by a method such as that of Hevesy,

* This investigation has been carried out in cooperation with Dr. H. M. Day, Research Laboratory of the General Electric Company, Schenectady, New York. The preparation of accurately oriented, strain-free single crystals, and the precision heat treatments will be described in publications dealing with other phases of the diffusion problem.

** Now at Morgan State College, Baltimore, Maryland.

[1] R. F. Mehl, Trans. A. I. M. E. Inst. of Metals Div. **122**, 11 (1936).

[2] Hevesy, Seith and Keil, Zeits. f. Physik **74**, 197 (1932).

[3] W. Seith, Zeits. f. Elektrochemie **39**, 538 (1933).

[4] W. Seith and A. Keil, Zeits. f. Metallkunde **25**, 104 (1933).

[5] A. Sagrubskij, Physik. Zeits. Sowjetunion **12**, 118 (1937).

[6] H. A. C. McKay, Trans. Faraday Soc. **34**, 345 (1938).

[7] B. V. Rollin, Phys. Rev. **55**, 231 (1939).

[8] Steigman, Shockley and Nix, Phys. Rev. **56**, 13 (1939).

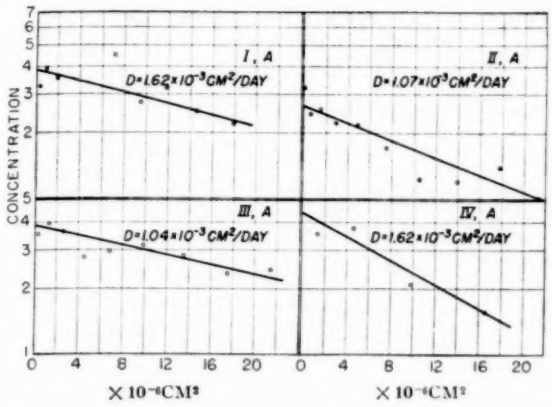

FIG. 1. Counter measurements on crystals of group *A*. Logarithm of concentration for each section plotted against square of mean depth in crystal. Temperature of heat treatment—412.5°C; time of heat treatment—12.5 hours for crystals I and II, 24 hours for crystal III, 6 hours for crystal IV; number of sections—ten, ten, ten, and six, respectively.

Seith and Keil,[2–4, 9] *viz.*, evaporation of Zn^{65} onto the surface of a crystal of ordinary zinc and measurement of the radioactive decay before and after diffusion, because there is no fixed range for electrons. It is possible, however, to solve the diffusion equation and take into account the approximately exponential character of the absorption of a continuous energy spectrum of electrons (the emitted radiation) in the substance employed, as Steigman, Shockley and Nix[8] did. This would lead to a very uncertain interpretation of the data in the case of Zn^{65}, for the ionizing radiation from this radioactive element is complicated by the emission of strong gamma-radiation. Methods may be devised, however, which do not depend on calculating the amount of diffusion which occurs from the decrease in intensity of the radiation measured at the surface. The procedure outlined at the beginning of this section is such a method.

Zn^{65} is separated from the copper from which it is produced by dissolving the surface of the copper containing the Zn^{65} in 1−1 nitric acid. Chlorides are made of the Zn^{65} and copper, and the copper precipitated by hydrogen sulphide from a 0.3 normal HCl solution. Actually, there will be more copper ions present in the filtrate than Zn^{65} ions, because of the degree of efficiency of the precipitation process and because there is such a small quantity of Zn^{65} initially. Several precipitations are made until further bubbling of hydrogen sulphide through the solution brings down no more copper. The precipitate is tested in each case for its activity to ascertain whether any of the Zn^{65} is brought down with the copper. After this procedure practically all of the Zn^{65} remains in the solution, which is then concentrated down to dryness, and the residue dissolved in 5 cc of water. This solution serves as the electrolyte in the electrolysis process.

Single crystals were grown from high purity Zn and were used in the form of cylinders about 0.5 inch in diameter and 0.3 inch long. All the crystals had the same crystallographic orientation (diffusion interface perpendicular to the *C* axis), and their flat, etched, and polished surfaces were perfect reflectors. Each crystal served as the cathode during the electrolysis, a portion (0.5 cc in 3 cc of water) of the Zn^{65} solution mentioned above was the electrolyte, and a spiral platinum wire was the anode. The time of the electrolysis varied from forty-five minutes to six hours, the average voltage used was 4.5 volts, the average current 10 milliamperes. None of these factors seemed to be critical. During the electrolysis the crystals generally became tarnished.

A rotating cathode was used to provide stirring of the electrolyte to have a uniform distribution of the Zn^{65} ions throughout the solution, to prevent bubbles from gathering on the surface of the cathode, and to permit selective deposition of Zn^{65} in the presence of copper. A rotating cathode[10, 11] is indispensable for selective deposition of Zn^{65}, for it is well known that copper will plate out before zinc. A high speed rotating cathode obviates this. Also, the cathode was dipped in and out of the solution during the electrolysis to prevent the formation of bubbles, for they would destroy the intimacy of the contact between the surface of the zinc crystal and the Zn^{65}.

After electrolysis the impregnated crystals were held for a fixed time at elevated temperatures to allow diffusion to proceed. Variations in temperature during the course of the heat

[9] G. v. Hevesy and W. Seith, Zeits. f. Physik **56**, 790 (1929).

[10] C. G. Fink and F. A. Rohrman, Trans. Am. Electrochem. Soc. **58**, 403 (1930).

[11] J. Steigman, Phys. Rev. **53**, 771 (1938).

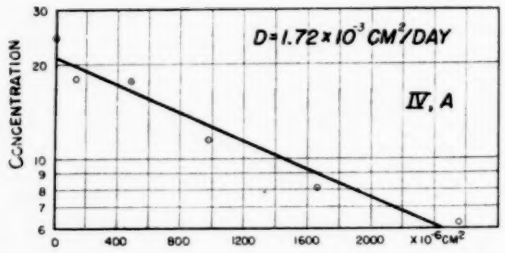

FIG. 2. Electroscope measurements on crystal IV, group *A*. Logarithm of concentration for each section plotted against square of mean depth in crystal. Temperature of heat treatment—412.5°C; time of heat treatment—6 hours; number of sections—six.

treatment were always less than 0.1°C. At room temperature the crystals were cut into sections approximately 0.002 inch thick on a lathe, the cut being parallel to the original face. The sections were in the form of ribbons, as cut by the lathe tool. It was not necessary to have the section of predetermined or accurately equal thickness; for each section was weighed, and the thickness computed from the weight, the known density of zinc (taken here to be 7.10 g/cc), and the area of the face from which the sections were turned. General freedom from edge effects was ensured by turning off the cylindrical surface of the crystal to a depth of approximately 0.005 inch before the sections were taken off.

The activity of each section was measured either with a Lauritsen[12] electroscope or with a Geiger-Müller counter. For the electroscope measurements each section was placed in the electroscope can. Most of the measurements were made with a thin glass-walled Geiger counter, directly under which each section was placed (in a small pill box) in approximately the same position. The background of this counter was approximately 17 counts per minute. After diffusion the activities of the first sections were at least 100 counts per minute above the background, the activities of the last sections at least 5 counts per minute above the background. About 2000 counts per section were taken, so that the precision ranged from one percent for the first sections to nine percent for the last.

It was not necessary to compare each measurement with a standard to allow for radioactive decay, as McKay[6] and Steigman, Shockley, and Nix[8] did. Because of the long half-life of Zn^{65} (eight months) the decay during any series of measurements is negligible. Also, it was not necessary to correct for the absorption of electrons in matter since each section was only approximately 0.002 inch thick (except for crystal IV, group *A*, where each section was 0.004 inch thick), and geometrically similar to every other section.

The electroscope and Geiger-counter measurements provided independent methods of determining the respective activities (and hence diffusion coefficients D) and the close agreement between these two methods (e.g., see results of crystal IV, group *A*) was construed to indicate reliability of the present technique in the study of the phenomenon in question.

The diffusion equation is

$$\partial c/\partial t = D\partial^2 c/\partial x^2 \qquad (1)$$

if there is no evaporation to or from the surface. Here c is the concentration of Zn^{65}, t the time for

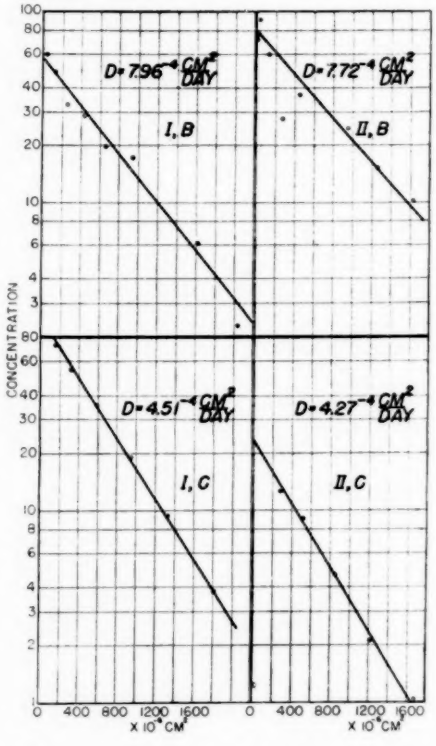

FIG. 3. Counter measurements on crystals of groups *B* and *C*. Logarithm of concentration for each section plotted against square of mean depth in crystal. Temperature of heat treatment—400°C and 374.4°C, respectively; time of heat treatment—6 hours and 7.5 hours, respectively; number of sections—ten.

[12] C. C. Lauritsen and T. Lauritsen, Rev. Sci. Inst. **8**, 438 (1937).

the diffusion, x the axial coordinate in the sample, and D the diffusion coefficient. D is assumed to be independent of c. The solution of this equation is given in this form:

$$c=(\pi Dt)^{-\frac{1}{2}}\exp\left[-x^2/4Dt\right], \tag{2}$$

in which the initial thickness of the active layer is assumed infinitesimal. If ln c is plotted against $\bar{x}^2$, which represents the square of the average depth of the section considered below the surface of the crystal, a straight line results of intercept $-\ln(\pi Dt)^{\frac{1}{2}}$, and of slope $-\frac{1}{4}Dt$. Thus, if c and x are known, D can be obtained directly from the graph, for a given t. The concentration in each section is obtained in relative units from the activity by dividing by the thickness of the section ($c_n=A_n/t_n$). This introduces an error of less than 1 percent (for the small distances dealt with in the experiment), which is well under the experimental error.

From Eq. (2)

$$Dt=\frac{\bar{x}_1^2-\bar{x}^2}{4\ln(c/c_1)}. \tag{3}$$

From the half-value of the concentration, i.e., the point where the concentration has fallen to one-half of its original value we have

$$Dt=0.361\bar{x}_{\frac{1}{2}}^2, \tag{4}$$

where $\bar{x}_{\frac{1}{2}}^2$ is the square of the abscissa where the half-value ordinate occurs.

$\bar{x}_{\frac{1}{2}}^2$ is determined from the graph (of ln c *vs.* $\bar{x}_n^2$) and t is known. Therefore D is obtained directly.

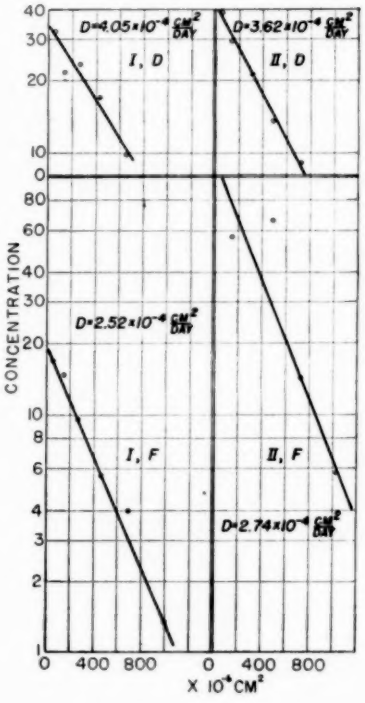

FIG. 4. Counter measurements on crystals of groups D and F. Logarithm of concentration for each section plotted against square of mean depth in crystal. Temperature of heat treatment—364.7°C and 355°C, respectively; time of heat treatment—8 hours and 9 hours, respectively; number of sections—ten.

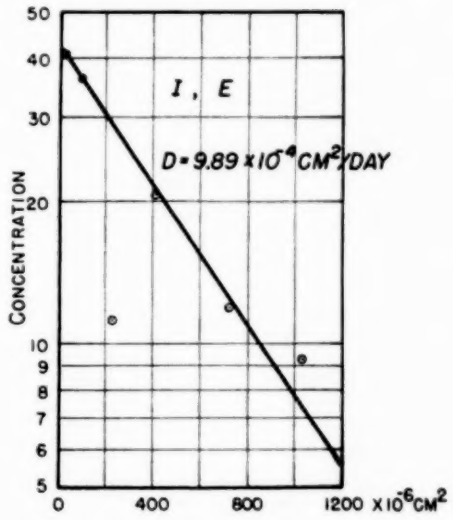

FIG. 5. Counter measurements on the only crystal of group E. Logarithm of concentration for each section plotted against square of mean depth in crystal. Temperature of heat treatment—410.4°C; time of heat treatment—3.5 hours; number of sections—ten.

RESULTS

The rate of diffusion was determined at six different temperatures for six groups of single crystals: Group A consisted of four crystals, group E, one, and all other groups of two crystals each.

Figure 1 displays the graphs of the counter measurements for the crystals I–IV of group A. Figure 2 is the graph for crystal IV, group A, for electroscope measurements. The agreement between the counter and electroscope measurements on the sections of this crystal is quite satisfactory. Figures 3, 4, and 5 are the graphs for crystals of groups B, C, D, E, and F.

The temperature dependence of D is given by

$$D=Ae^{-Q/RT}, \tag{5}$$

where A is the activation constant, Q the activation energy, R the gas constant, T the absolute temperature, and e is the logarithmic base.

$$\ln D=\ln A-(Q/RT). \tag{6}$$

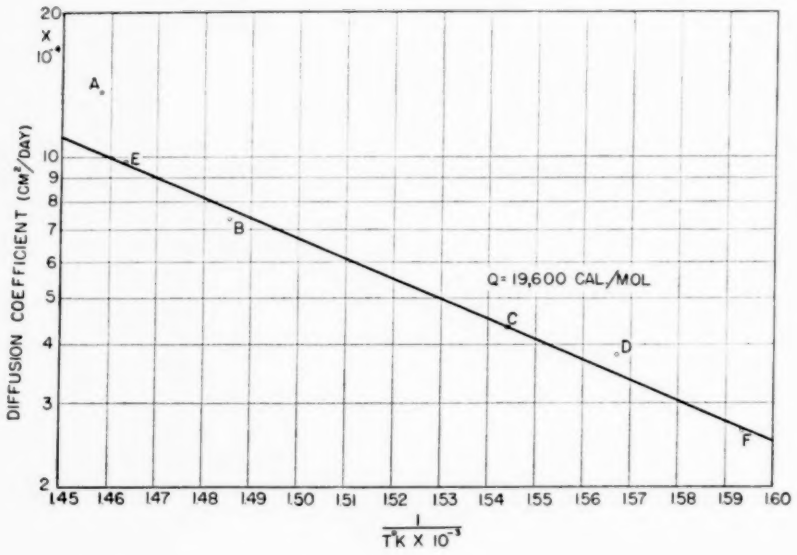

FIG. 6. Diffusion coefficient as a function of reciprocal temperature. The crystals of group *A* were heat treated before the precision furnance control had been developed.

If ln D is plotted against $1/T$ a straight line of intercept ln A, slope $-Q/R$ results. Q, the activation energy is obtained directly from the graph. Figure 6 shows the temperature dependence of D (a plot of D against $1/T$). The value obtained for Q is 19,600 cal./mol.

Q can be calculated also from the Dushman-Langmuir[13] equation

$$D = Q/Nh\delta^2 e^{-Q/RT},$$

where δ is the interatomic distance, N is Avogadro's number, h is Planck's constant, D the diffusion coefficient, Q the activation energy, R the gas constant, T the absolute temperature, and e the logarithmic base. The average calculated value of Q is 22,200 cal./mol.

Discussion of Results

Different boundary conditions prevailing at the interface between the diffusing solute and the ordinary zinc crystal will alter the results because of the possibility of the trapping of active zinc on the surface. Some of the plated zinc may be in good contact and start to diffuse immediately, some may be in poor contact and start to diffuse later, and some may not start at all. As a matter of fact, it is seen from the graphs that the first point of the curve for each crystal seems to be somewhat high. It is assumed that the greater part of the diffusion takes place normally. Justification for this assumption is in the agreement between the experimental and theoretical curves.

Possible sources of error in the determination of D are: (1) variations in the temperature of heat treatment (practically negligible since the furnace control was good to 0.1°C; (2) errors in weighing (less than 1 percent); (3) slightly different geometric orientations of the sections with respect to the counter in measuring activities; (4) assumption of independence of D and concentration c; (5) assumption that the thickness of the initial layer is not comparable with the depth of penetration (and hence the evaporation is not important); (6) statistical fluctuations in the counts made on each section; (7) location of the average line through the points; and (8) variation in time at the temperature of the heat treatment (a maximum of 3 percent).

Conclusion

The method described presents a very satisfactory way of determining the coefficient of self-diffusion D, and the activation energy Q, in zinc. It is especially useful in that it provides a simple and direct procedure for getting an average value for D.

The author expresses his gratitude to Professor Louis N. Ridenour, who initiated the experiment and under whose guidance the work de-

[13] S. Dushman and I. Langmuir, Phys. Rev. **20**, 113 (1922).

scribed here was carried out, to Dr. Harry M. Day, of the Research Laboratories of the General Electric Company, who prepared all of the crystals and performed the heat treatments, to Professors Frederick Seitz and Enos Witmer for their valuable discussions; and to the workers of WPA Project No. 21637 for assistance.

Gifts of Zn^{65} are very gratefully acknowledged from the following: Professor M. G. White, Palmer Physical Laboratory, Princeton University; Dr. A. J. Allen, late of the Biochemical Research Foundation of the Franklin Institute; and Professor Luis W. Alvarez, Radiation Laboratory, University of California.

FEBRUARY 15, 1941 PHYSICAL REVIEW VOLUME 59

The *L*-Emission Bands of Sodium, Magnesium and Aluminum

WILLOUGHBY M. CADY AND D. H. TOMBOULIAN
Cornell University, Ithaca, New York

(Received December 21, 1940)

The radiation emitted when conduction electrons fill vacancies in the *L* shell is spread over a band whose shape represents the energy distribution of the conduction electrons. This band has been studied spectrophotometrically for pure sodium, magnesium and aluminum. The observed shapes are in general agreement with theoretical predictions and confirm the results of previous experimental studies. In each case a "tail" has been observed at the low frequency end of the band, for which alternative explanations are offered. With the x-ray continuum as a standard of intensity, the total intensity of the *L* band increases nineteen-fold from sodium to aluminum.

THE electronic structure of a metal can be investigated by a study of the x-radiation emitted by the metal when one of its conduction electrons falls into a vacancy in an inner shell. Since the conduction electrons have energies throughout a range of several electron volts, this x-radiation is a band of corresponding width. The distribution in energy of the intensity in this band is related to the distribution in energy of the conduction electrons; thus the definite upper limit of the energy of the conduction electrons is evidenced by the fact that the x-ray emission band is sharply bounded at its high frequency end.

X-ray bands of this origin have been observed repeatedly. The recent work of Bearden and collaborators[1] provides examples in the region of 1.5A. In principle, it is preferable to observe the structure of the bands emitted in the ultra-soft x-ray region ($\lambda > 10$A), for here the frequency of the radiation is not large in comparison with the frequency spread of the emission band and high resolution technique is not necessary. Of several reports of bands emitted in this region, those of O'Bryan and Skinner[2] and of Skinner[3] are outstanding in that they present and discuss reliable photometric descriptions of the radiation from very clean surfaces of certain metals. In the emission of ultra-soft x-rays, the surface of the target must be extremely clean, since all photons except those from the surface are absorbed in the target. Foreign elements on the target not only introduce their own characteristic spectra, but also affect the characteristic radiation of the target element itself. The numerous reports of ultra-soft x-rays by Siegbahn and Magnusson[4] and others at Uppsala must be regarded as qualitative, since their targets were admittedly contaminated with carbon, nitrogen and oxygen.

The present work was undertaken as an attempt to confirm and extend previous work in the photometry of the band of radiation emitted as conduction electrons fall to L_{II} or L_{III} levels made vacant by electron bombardment.

[1] H. Friedman and W. W. Beeman, Phys. Rev. **58**, 400 (1940).

[2] H. M. O'Bryan and H. W. B. Skinner, Phys. Rev. **45**, 370 (1934).

[3] H. W. B. Skinner, Prog. Rep. Phys. Soc. **5**, 257 (1939).

[4] M. Siegbahn and T. Magnusson, Zeits. f. Physik **62**, 435 (1930); **87**, 291 (1934); **88**, 559 (1934); **95**, 133 (1935).

Experimental

The vacuum spectrograph comprised a glass grating of radius of curvature about 1.5 meters and effective width 2.5 cm, ruled with 30,000 lines per inch and adjusted for about 5.7° grazing angle of incidence; a vertical slit, made of two fragments of a razor blade; and a plateholder, embracing the wave-length range from zero to about 740A, which could be raised or lowered without breaking the vacuum. (This motion of the plateholder caused no wave-length displacement of spectrum lines, within the wave-length accuracy demanded in the present work.) A horizontal slot before the plate made it possible successively to bring adjacent zones of the plate into the same part of the x-ray beam, and an externally controlled shutter was used to begin and end the exposures. The dispersion varied from about 1.0A/mm at 100A to 2.2A/mm at 740A.

The x-ray tube was similar to that of O'Bryan and Skinner.[2] It consisted of a 2-liter Pyrex bulb having arms with tapers into which were inserted the filament and target assemblies. The x-ray filament was a tungsten helix, 2 cm long, wound on a 60-mil mandrel out of 10-mil wire 40 cm in length. The filament was partly surrounded by a tantalum shield to prevent direct illumination of the slit by the filament. An evaporator for aluminum, inserted in a third sidearm, consisted of a 20-mil tungsten filament in the form of a helix, the coils of which were charged with small loops of aluminum wire; magnesium was evapoated from tungsten baskets, while in the case of sodium a special distilling furnace was employed. The metals used in coating the target were of high purity. In no case was the impurity content greater than 0.1 percent.

The target was a thin-walled copper tube of square section. It was free to rotate so that any one of the four faces could be placed in position for the exposure, the target being so turned that the radiation entering the slit made an angle of 45° with the normal to the face in use. The target was placed at 6 mm from the filament and 14 cm from the spectrograph slit, which was protected by a "fore-slit." None of the grease (Apiezon *L*) used to lubricate the tapers at the three arms was nearer than 15 cm from the target; therefore the grease was not appreciably warmed by the heat of the filament. During all aluminum and magnesium runs the target was water cooled.

In the case of sodium it was necessary to keep the target temperature below 0°C in order to prevent the sodium from melting. This was accomplished by circulating a liquid (alcohol), cooled in passing through a copper coil surrounded by solid carbon dioxide and alcohol. The circulation was maintained by a gear pump. The temperature of the alcohol leaving the target assembly was about −45°C. Provision was made for keeping the greased taper of the target near room temperature in order to prevent "freezing" of the metal to the glass.

Procedure

The x-ray exposures were so planned that the relative intensity could be found as a function of the distance along the length of the spectrogram. The target was bombarded for a couple of hours to outgas it, the shutter being closed; two or three times during this conditioning the target was coated by heating the evaporator. When the ionization gauge read about 4×10^{-6} mm Hg, the target was recoated and the shutter opened to begin the exposure. During the exposure, the tube was connected directly to a transformer giving 1450 volts, r.m.s.; by adjustment of the filament current (about 5.4 amp. a.c.) the d.c. milliammeter in series with the target was held at 200 ma.

In the case of aluminum, the exposure time was 50 minutes with the plateholder up, and 100 minutes with the plateholder down; for an additional 50 minutes the plateholder was up and the target potential was off, to equalize the slight light fog from the x-ray filament upon the two zones of the plate. There was no visible fouling of the target, but to insure ideal surface conditions the target was recoated at 5-minute intervals. (It was found that aging the aluminum target for 10 minutes gave a general reduction of the intensity by a few percent, with no obvious change in the wave-length distribution of relative intensity.) Since during the exposures the pressure fell typically from 4×10^{-6} to 1×10^{-6} mm Hg, it was considered necessary to break up the total of 200 minutes of exposure into ten

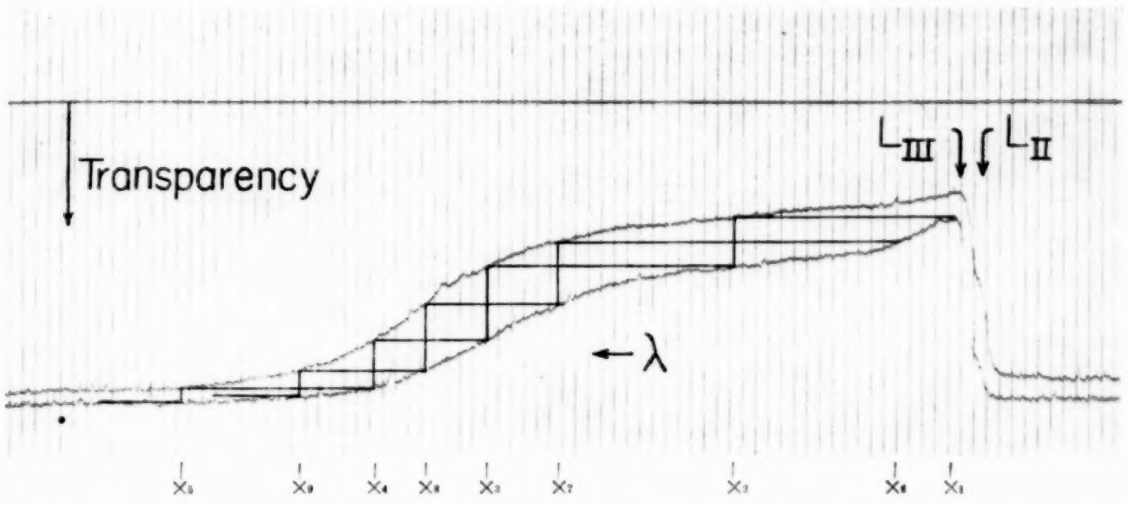

FIG. 1. Densitometer curves of a one-hour and a two-hour exposure of the aluminum *L* band on the same plate, illustrating the sensitometric method. The wave-length range is 162 to 218A.

cycles to prevent favoring either the "up" or the "down" portions. During each cycle the plateholder was up (with x-rays turned on) for 5 minutes, up (with x-rays off) for 5 minutes, and down (with x-rays on) for 10 minutes. This routine, here described for aluminum, provides two juxtaposed exposures which have had the same treatment as regards light fog, and which differ only in respect to their x-ray illumination. Two good aluminum plates were made in this way.

The seven good magnesium plates were exposed by a routine similar to the above, but there were six cycles of 4 times 10 minutes each, giving x-ray exposure times of 60 and 120 minutes; the target was recoated at 10-minute intervals. For sodium, all four faces were simultaneously coated at hourly intervals, so that each face was used for 15 minutes before recoating; there were eight one-hour cycles, and the four target faces were in each cycle used in sequence, permuted variously to avoid beginning each cycle with the same face. Thus on each sodium plate the x-ray exposure times were 120 and 240 minutes; two plates were so made, the tube current being limited to 100 ma to prevent the coating of sodium from melting.

The respective slit widths for sodium, magnesium and aluminum were roughly 0.32 mm, 0.12 mm, 0.08 mm. The wave-length at the peak of the sodium band was determined by comparison with the line spectrum of air from a disruptive capillary discharge to which the plate was exposed after the x-ray tube had been removed. Ilford QI plates were used in all photometric runs. These seem nearly as sensitive as Schumann plates, and their sensitivity is fairly free of local irregularities.

The photometric process by which the intensity distribution in the band was determined from the spectrogram is reminiscent of a method used by Skinner and Johnston[5] for comparing spectrum line intensities. The process depends on the assumption that the plate sensitivity is independent of wave-length throughout the band and also that the reciprocity law is valid. No assumption need be made as to the characteristic curve of the plate; in fact, the characteristic curve is deduced in the course of this process.

Densitometer curves from the two exposures on the same plate are recorded together as in Fig. 1. Since the exposures stand in the ratio 2:1, it may be seen that the intensity at the point x_2 on the faint trace is half the intensity at x_1, that the intensity at x_3 is half the intensity at x_2, etc. On the basis of these observations a preliminary characteristic curve may be sketched, showing the relation between the intensity and the transparency of the fainter exposure. (For convenience the deflection of the densitometer galvanometer

[5] H. W. B. Skinner and J. E. Johnston, Proc. Roy. Soc. **A161**, 420 (1937).

may be used in place of transparency.) A second preliminary characteristic curve may similarly be obtained from the points x_6, x_7, etc., x_6 being arbitrarily chosen. The final characteristic curve may then be obtained by superposing two or more such preliminary curves. The galvanometer deflection is now tabulated as a function of distance along the plate; with the aid of the characteristic curve these data now yield values of $I(x)$, the relative intensity per unit distance along the plate.[6] The values of $I(x)$ when multiplied by dx/dV give $I(V)$; here V is the energy in electron volts of the photons incident at any position x on the plate and $I(V)$ is the relative intensity of the radiation in the band per electron-volt interval. The quantity dx/dV is related to the dispersion of the spectrograph. It must be pointed out that this scheme of photometry gives results which represent the x-radiation only and are not influenced by uniform light fogging.

TABLE I. *Intensity distribution in the L bands.*

Sodium		Magnesium		Aluminum	
V	$\nu^{-3}I(V)$	V	$\nu^{-3}I(V)$	V	$\nu^{-3}I(V)$
25.00	1.6	39.5	1.1	58.0	4
25.50	2.4	40.0	1.3	59.0	6
25.75	5.6	40.5	2.0	60.0	9
26.00	7.5	41.0	4.2	61.0	13
26.25	9.4	41.5	6.6	62.0	21
26.50	12	42.0	10	63.0	33
26.75	14	42.5	17	64.0	48
27.00	18	43.0	27	65.0	60
27.25	21	43.5	39	66.0	67
27.50	28	44.0	52	67.0	71
27.75	41	44.5	65	68.0	71
28.00	53	45.0	75	69.0	69
28.25	64	45.5	81	70.0	67
28.50	74	46.0	86	70.5	68
28.75	81	46.5	89	71.0	71
29.00	87	47.0	91	71.5	82
29.25	94	47.5	91	72.0	100
29.50	97	48.0	89	72.2	97
29.75	100	48.4	85	72.4	73
30.10	97	48.8	87	72.6	29
30.20	93	48.9	92	72.8	12
30.25	79	49.0	97	73.0	2
30.30	61	49.1	100	73.5	1
30.35	40	49.2	83	74.0	0
30.40	25	49.3	43		
30.45	17	49.4	15		
30.50	11	49.5	7.3		
30.55	6.1	49.6	3.9		
30.70	3.7	50.0	1.1		
31.25	1.9	50.4	0.4		
31.75	0.8	51.0	0.4		

[6] This "staircase" method, originated by Professor L. G. Parratt for a somewhat different purpose, is described by him in a paper now in preparation.

Results

For each element there has been observed a characteristic band superimposed on a continuous background. (This background is assumed to be the true x-ray continuum, although it may be due in part to x-rays scattered from the grating.) The results on these spectra, averaged for each element, are presented in Tables I and II and Fig. 2. Table I gives, for several values of V, the intensity distribution as $\nu^{-3}I(V)$ where ν is the frequency of the L radiation; the continuous spectrum, evident on both sides of the L band, has been subtracted off. From the work of Jones, Mott and Skinner[7] and Skinner,[3] it is expected that the curve $\nu^{-3}I(V)$ *vs.* V for an $L_{II\ III}$ band will be parabolic near the low frequency end of the band. These curves are shown for sodium, magnesium and aluminum in Fig. 2, together with the parabolas that best fit them. The curves resemble those of Skinner.[3]

Certain numerical characteristics are compiled in Table II. For sodium, λ(peak) is the wave-length for the greatest value of $I(\lambda)$, which is the relative intensity per unit wave-length interval; while the quantity designated as V(peak) is the photon energy when $I(V)$ is maximum. For the remaining elements V(peak) is calculated directly from the published values of λ(grenze) which are here listed as λ(peak). "Maximum V, extrapolated" is the intercept of the steepest tangent to the high V end of the $\nu^{-3}I(V)$ curve. "Band width" is defined as the separation between this intercept and the foot of the "best parabola." For comparison, there are also listed the data of O'Bryan and Skinner[2] as

TABLE II. *Summary of results.*

		Sodium	Magnesium	Aluminum
λ (peak)	(A)	407.6±0.4	250.20*	170.49**
V (peak)	(ev)	29.9	49.1	72.0
Maximum V, extrapolated	(ev)	30.4	49.4	72.8
V at foot of best parabola	(ev)	27.3_5	43.0	62.2
λ at tip of tail	(A)	487	307	212+
V at tip of tail	(ev)	25.2	40	58−
Band width (observed)	(ev)	3.05±0.10	6.4	10.6
Band width (Skinner)[3]	(ev)	3.0±0.2	7.6±0.3	13.2±0.5
Sommerfeld band width[3]	(ev)	3.2	7.3	11.9
Area ratio (tail to total band)		0.10_4	0.06_5	0.07_3
Intensity ratio (peak to continuum)		1.7	7	11
Intensity ratio (total band to continuum)		4.2	34	78

* M. Siegbahn and T. Magnusson, Zeits. f. Physik **87**, 291 (1934).
** M. Siegbahn, Ergeb. d. exakt. Naturwiss. **16**, 123 (1937).

[7] Jones, Mott and Skinner, Phys. Rev. **45**, 379 (1934).

recalculated by Skinner,[3] and band width predictions on the basis of the Sommerfeld free electron model.

The tail at the low energy end of the bands, reported also by O'Bryan and Skinner, is interesting. Table II gives a comparison of the area, (measured on the $\nu^{-3}I(V)$ graph, between the curve and the best parabola) of the tail with the total area under the $\nu^{-3}I(V)$ curve. This ratio of areas is roughly independent of atomic number. The origin of the tails is uncertain. Skinner[3] suggests that they are caused by a softening of the radiation in the band, as by the Raman effect. Seitz[8] attributes them to "excitation levels," i.e., to extra levels below the valence band, that occur wherever a completed shell of an atom has been ionized; since this is, of course, the case at each point in the lattice where a photon is produced, the excitation states might affect the emission band.

It may be pointed out that thermal fluctuations in the lattice constant might, according to the Sommerfeld theory, cause a diffuseness at the foot of the parabola, observed as a tail. Alternatively one may propose a double jump hypothesis to account for the tails: that as one conduction electron falls to the ionized L shell a second conduction electron jumps into an unoccupied conduction level; in this "semi-Auger" process a photon is emitted, of which the energy is less than the energy loss of the first electron.*

The bands have very unequal intensities for the different elements. A convenient measure for the relative intensities of the bands is afforded by the continuous spectrum, since the continuum is not expected to vary greatly among the present three elements. The maximum $I(V)$ is seen in Table II to increase rapidly in relation to the continuum, with increasing atomic number. It is, perhaps, of theoretical interest to compare, for each element, the total band intensity $\int I(V)dV$ with the intensity per volt of the continuous spectrum. This ratio is also seen to increase greatly with atomic number. This increase is to be expected; in fact a semi-quantitative calculation involving the radiative transition probability, Auger effect and ionization probability affords a prediction that the foregoing ratio shall, between sodium and aluminum, show a 12-fold increase.

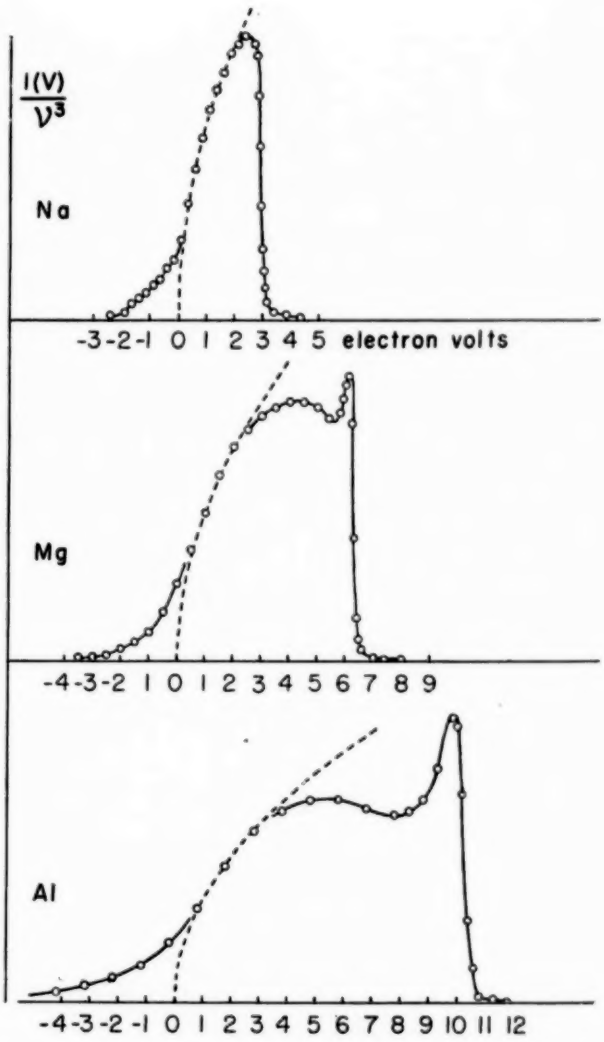

FIG. 2. Intensity distribution in the L bands corrected for continuum, divided by ν^3. The dotted curves are the parabolas which best fit the data. The zero of the energy scale is at the foot of the parabolas.

It is a pleasure to acknowledge helpful conversations with Professor Debye and Professor Parratt, and the assistance generously given by Professor Bethe in the interpretation of the bands. The design and operation of the x-ray tube were influenced by the good advice of Professor H. M. O'Bryan of Georgetown University.

[8] F. Seitz, *Modern Theory of Solids* (McGraw Hill, 1940), p. 438.

* *Note added in proof.*—A semi-Auger process, independently considered by Skinner and the authors, (H. W. B. Skinner, Phil. Trans. Roy. Soc. **A239**, 95 (1940)) (above) as resulting in the tails that appear on the low energy side of the emission bands, is rejected by Skinner in favor of an alternative hypothesis on the ground that this process would produce tails at both sides of the bands. This rejection is however invalid: the semi-Auger process can decrease but never increase the energy of an emitted photon.

Term Values in V II and Mn II

D. S. BOWMAN
Allegheny College, Meadville, Pennsylvania
(Received December 23, 1940)

The term values for d^3s and d^5s have been calculated in Russell-Saunders coupling. For some of the terms of the same kind in d^5s, only the sum of the energies is obtained. The first approximation to the separations of the levels is also found for d^3s. The theoretical formulas including Ostrofsky's results for d^4 are then applied to the observed values of V II and Mn II.

THE term values for d^3s and d^5s have been calculated in Russell-Saunders coupling. Only the center of gravity of the levels with different values of J belonging to a single term have been found in d^5s. In d^3s the separations of the levels have also been calculated. Separate values have been found for each of the terms in d^3s. Terms of the same kind in d^5 lead to energy sums in d^5s rather than to the separate energies of each term. There are three cases, ^2D, ^2F, and ^2G, in d^5 for which more than one term of the same kind arises. When an s electron is added, singlet and triplet terms in d^5s are obtained from these terms of d^5. Separate energies have not been found for these singlets and triplets. Only the sum of the energies of those terms of the same kind is obtained.

The formulas for the energies in terms of the Slater-Condon Fs and Gs were then used to find the term values in V II $3d^34s$ and Mn II $3d^54s$. It was to assist in the analysis of these spectra that the calculations were made. Now that the analysis of V II has been completed by Meggers and Moore,[1] it seemed desirable to present the theoretical calculations also. The septet and quintet terms of Mn II have all been found by Curtis,[2] and the theory gives in addition the positions of the singlets and triplets. To aid in the analysis further, Ostrofsky's[3] formulas were used to calculate the missing terms in V II $3d^4$ with parameters found from the observed values of V II $3d^4$.

The terms in Russell-Saunders coupling can be calculated by the standard method given by Slater.[4] Van Vleck[5] has given a different method

[1] W. F. Meggers and C. E. Moore, J. Research Nat. Bur. Stand. **25**, 83 (1940).
[2] C. W. Curtis, Phys. Rev. **53**, 474 (1938). I am grateful to Dr. Curtis for permission to include the unpublished ^5F term.
[3] M. Ostrofsky, Phys. Rev. **46**, 604 (1934).
[4] J. C. Slater, Phys. Rev. **34**, 1293 (1929).
[5] J. H. Van Vleck, Phys. Rev. **45**, 405 (1934).

TABLE I. *Term values of d^3s for* V II.

	Wave Numbers Obs.	Calc.
$^1P=F_0-6F_2-12F_4$	22273.54	22898
$^3P=F_0-6F_2-12F_4-2G_2$	20237.81	20228
$^3P=F_0-147F_4+G_2$	19147.03	19214
$^5P=F_0-147F_4-3G_2$	13646.67	13873
$^1D=F_0+5F_2+3F_4+(193F_2^2-1650F_2F_4+8325F_4^2)^{\frac{1}{2}}$	——	50274
$^3D=F_0+5F_2+3F_4+(193F_2^2-1650F_2F_4+8325F_4^2)^{\frac{1}{2}}-2G_2$	44139.29	47603
$^1D=F_0+5F_2+3F_4-(193F_2^2-1650F_2F_4+8325F_4^2)^{\frac{1}{2}}$	25191.08	24535
$^3D=F_0+5F_2+3F_4-(193F_2^2-1650F_2F_4+8325F_4^2)^{\frac{1}{2}}-2G_2$	20600.84	21865
$^1F=F_0+9F_2-87F_4$	34228.79	34058
$^3F=F_0+9F_2-87F_4-2G_2$	30637.30	31388
$^3F=F_0-15F_2-72F_4+G_2$	8903.58	8054
$^5F=F_0-15F_2-72F_4-3G_2$	2926.16	2713
$^1G=F_0-11F_2+13F_4$	19112.93	19178
$^3G=F_0-11F_2+13F_4-2G_2$	16446.05	16508
$^1H=F_0-6F_2-12F_4$	23391.09	22898
$^3H=F_0-6F_2-12F_4-2G_2$	20302.57	20228

$F_0=3F_0(nd, nd)+3F_0(n's, nd)=31155.58$, $F_2=F_2(nd, nd)=1195.557$
$F_4=F_4(nd, nd)=90.31642$, $G_2=G_2(n's, nd)=1335.338$

TABLE II. *Separations of the levels of the terms of d^3s for* V II, *given in wave numbers. The subscript on the left of the terms indicates the number of terms of the same kind which occur. The sum of the separations of the two ^2P, ^2D and ^2F terms are given. $\zeta_{nd}=154$.*

		Obs.	Calc.
$^5F_5$	$5/4\zeta_{nd}$	194.58	193
4	$4/4\zeta_{nd}$	159.46	154
3	$3/4\zeta_{nd}$	121.75	116
2	$2/4\zeta_{nd}$	82.19	77
1			
$^3P_3$	$3/4\zeta_{nd}$	146.88	116
2	$2/4\zeta_{nd}$	83.02	77
1			
$^3H_6$	$6/10\zeta_{nd}$	83.03	92
5	$5/10\zeta_{nd}$	37.87	77
4			
$^3G_5$	$15/20\zeta_{nd}$	111.49	116
4	$12/20\zeta_{nd}$	80.54	92
3			
z^3F_4	$4/3\zeta_{nd}$	228.10	205
3	$3/3\zeta_{nd}$	170.33	154
2			
z^3D_3	$3/6\zeta_{nd}$	−55.03	77
2	$2/6\zeta_{nd}$	53.37	51
1			
z^3P_2	$6/4\zeta_{nd}$	219.94	231
1	$3/4\zeta_{nd}$	−62.16	116
0			

TABLE III. *Term values in* V II *$3d^4$ from Ostrofsky's formulas. The plus sign written as a superscript on the right indicates the higher of two terms of the same kind, the minus sign the lower.*

	Wave numbers Obs.	Calc.		Wave numbers Obs.	Calc.
$^1S^+$	—	61919	$^1G^-$	17704.72	18560
$^1D^+$	44451.73	44843	^1I	18985.24	18188
$^1G^+$	36218.81	35589	^3D	18110.74	17854
$^3F^+$	30096.11	29842	^3G	14365.92	14399
$^3P^+$	31962.80	29765	$^3P^-$	11502.76	13847
^1F	26633.56	25590	$^3F^-$	13352.50	13769
$^1D^-$	20774.66	23124	^3H	12427.79	11932
$^1S^-$	19696.34	20208	^5D	0.00	−580

$F_0=5318.86$, $F_2=869.862$, and $F_4=75.2701$.

of arriving at the same results, and in addition shows how to find the terms of a^ks from those of a^k. Thus d^3s may be most simply found from d^3, which has already been calculated[6] by the methods of both Slater and Van Vleck. These calculations included the separation of the two ^2D terms. The separations of the different levels of d^3s are included as they were used in identifying the ^3F terms. These levels are calculated from the diagonal matrix elements of spin-orbit interaction by Goudsmit's method.[7] The nondiagonal elements of spin-orbit interaction between the different terms in Russell-Saunders coupling are neglected.

Similarly d^5s may be found from d^5. In order to find the terms of d^5 from those given for d^5s in Table IV, the $G_2(n's, nd)$ parameters which

[6] C. W. Ufford and G. H. Shortley, Phys. Rev. **42**, 167 (1932). Robert Serber, Phys. Rev. **45**, 461 (1934).
[7] S. Goudsmit, Phys. Rev. **31**, 946 (1928).

TABLE IV. *Term values of d^5s applied to* Mn II *$3d^54s$. The subscript on the left of the terms indicates the number of terms of the same kind which occur. Where more than one term of the same kind is indicated, the formulas represent the sum of the energies of the terms of the same kind.*

	Wave numbers Obs.	Calc.
$^2I=F_0-24F_2-90F_4-3G_2$		38711
$^1I=F_0-24F_2-90F_4-G_2$		41884
$^2H=F_0-22F_2-30F_4-3G_2$		46913
$^1H=F_0-22F_2-30F_4-G_2$		50086
$^3G=F_0-25F_2-190F_4-4G_2$	27571	26620
$^3G=F_0-25F_2-190F_4$		32965
$z^3G=2F_0-10F_2-300F_4-6G_2$		117970
$z^1G=2F_0-10F_2-300F_4-2G_2$		124315
$^3F=F_0-13F_2-180F_4-4G_2$	43475	43806
$^3F=F_0-13F_2-180F_4$		50151
$z^3F=2F_0-34F_2-180F_4-6G_2$		96406
$z^1F=2F_0-34F_2-180F_4-2G_2$		102751
$^3D=F_0-18F_2-225F_4-4G_2$	32828	32909
$^1D=F_0-18F_2-225F_4$		39254
$z^3D=3F_0-10F_2-300F_4-9G_2$		197459
$z^1D=3F_0-10F_2-300F_4-3G_2$		206977
$^3P=F_0-28F_2-105F_4-4G_2$	29912	30329
$^3P=F_0-28F_2-105F_4$		36674
$^3P=F_0+20F_2-240F_4-3G_2$		84650
$^1P=F_0+20F_2-240F_4-G_2$		87822
$^7S=F_0-35F_2-315F_4-5G_2$	0.00	−37
$^5S=F_0-35F_2-315F_4+G_2$	9472.86	9555
$^3S=F_0-3F_2-195F_4-3G_2$		57580
$^1S=F_0-3F_2-195F_4-G_2$		60752

$F_0=10F_0(nd, nd)+5F_0(n's, nd)=84173.83$
$F_2=F_2(nd, nd)=1355.969$
$F_4=F_4(nd, nd)=91.49416$, $G_2=G_2(n's, nd)=1586.311$

represent the interaction of the s electron with the d^5 electrons must be omitted. If G_2 is omitted, pairs of equivalent terms are obtained, each pair representing a term of d^5 with the same value of L and a multiplicity, $2S+1$, midway between the multiplicities of the two terms of d^5s from which the pair arose. For example, $d^5\,{}^2I=F_0-24F_2-90F_4$, where now $F_0=10F_0(nd, nd)$. Laporte and Mack[8] have carried out similar calculations for d^5s in connection with their work on tungsten.

The results for the term values of d^3s in terms of the Slater-Condon[9] Fs and Gs together with the observed and calculated values for V II are given in Table I. Table II gives the separations for d^3s. The agreement is fair except for the upper separation of the ^3Ds and the lower separation of the ^3Ps which were not used to calculate ζ_{nd}. The assignments of the ^3Fs on this basis seem satisfactory. The observed and calcu-

[8] Otto Laporte and J. E. Mack, Phys. Rev. **58**, 188A (1940).
[9] For a definition of these radial integrals and a complete account of the theory cf. Condon and Shortley, *The Theory of Atomic Spectra* (Cambridge University Press, 1935) Chapters VI and VII.

lated terms for V II $3d^4$ from Ostrofsky's formulas are given in Table III. The parameters were found from ^3H, ^3G, ^3D, ^1I, and ^1F as these terms were considered the most reliable. Finally Table IV gives the formulas for the term values of d^5s and the observed and calculated values from Mn II.

Although the agreement of the observed and calculated term values is rough in terms of the accuracy with which spectra may be observed, some idea of the relative positions of the terms is a help in analysis as Meggers and Moore[1] have pointed out. As a further aid in the analysis of Mn II, it would be advisable to separate the different terms of the same kind in d^5 by the methods[6] used for d^3. I am grateful to Professor C. W. Ufford for suggesting this problem and for his assistance in solving it.

FEBRUARY 15, 1941 PHYSICAL REVIEW VOLUME 59

Magnetization Near Saturation in Polycrystalline Ferromagnets

T. HOLSTEIN, *New York University, New York, New York*

AND

H. PRIMAKOFF, *Queens College, Flushing, New York*

(Received December 16, 1940)

An important mechanism involved in the variation of the magnetization of ferromagnets near saturation is the rotation of the magnetization vector under the combined influence of the magnetic field and crystalline anisotropy torques. The effect of this mechanism in polycrystalline specimens has been calculated by Akulov and Gans; their result is $M_{Av}=M_0[1-(c/M_0^2)H^{-2}]$, where H is the sum of the external and demagnetizing fields, M_0 the saturation magnetization, and c a constant proportional to the square of the crystalline anisotropy constant. The Akulov-Gans derivation, however, is subject to a serious error; namely, neglect of the internal magnetic field arising from the magnetization itself. In the present paper, this internal field is taken into account; then, with the dual assumption, of randomness of orientation of crystallographic axes, and irregularity of shapes of the individual crystal grains, one obtains the formula, $M_{Av}=M_0[1-(c'/M_0^2)H^{-2}]$. Here, c' is a slowly varying function of H; for $H\gg 4\pi M_0$, $c'=c$; $H\ll 4\pi M_0$, $c'=\frac{1}{2}c$. Applications of the last formula to the analysis of the experimental data are discussed.

I. INTRODUCTION

ACCORDING to present day theories[1] of the magnetization curve of a polycrystalline ferromagnetic in high fields, an important contribution to the deviation of the observed magnetization, $|\mathbf{M}|_{Av}$, from its saturation value $|\mathbf{M}_0|$, arises from the crystalline anisotropy torques. These torques, acting on the magnetization vector of each crystal grain, tend to rotate this vector away from the direction of the external magnetic field, and toward the direction of the nearest easy axis of magnetization within the grain in question. Thus, in the equilibrium position, the direction of the magnetization vector in any crystal grain is determined by the balance of the crystalline and magnetic torques acting on it, *viz.*:

$$\mathbf{T}=\mathbf{M}_0\times(\mathbf{H}+\mathbf{h}), \tag{1}$$

where $\mathbf{M}_0$ is the magnetization of the crystal grain under consideration; $\mathbf{H}$ the external magnetic field (the demagnetizing field due to the magnetization on the surface of the polycrystalline specimen is incorporated into $\mathbf{H}$); $\mathbf{h}$ the internal magnetic field, i.e., the magnetic field due to the magnetization vectors of the totality of crystal grains; $\mathbf{T}$ the torque due to the crystalline anisotropy forces within the crystal grain.[1]

$\mathbf{T}$ in any grain, depends on the direction of $\mathbf{M}_0$ with respect to the crystallographic axes of that grain, and is independent of position within any given single grain.[1] The magnitude of $\mathbf{T}$ is proportional to the "anisotropy constant" K.[1]

[1] N. S. Akulov, Zeits. f. Physik **69**, 822 (1931); R. Gans, Ann. d. Physik **15**, 28 (1932). Cf. also, E. C. Stoner, *Magnetism and Matter* (Methuen, London, 1934), p. 405; F. Bitter, *Introduction to Ferromagnetism* (McGraw-Hill, New York, 1937), p. 222; R. Becker and W. Döring, *Ferromagnetismus* (Springer, Berlin, 1939), p. 167.

It is obvious that $\mathbf{h}$ and $\mathbf{M}_0$ cannot be assumed constant even within a single crystal grain and must hence be considered as functions of position within the polycrystalline specimen. However, only the direction of $\mathbf{M}_0$ varies with position, since the magnitude of $\mathbf{M}_0$ is the intrinsic domain magnetization and is therefore constant.

The problem of calculating the deviation of $|\mathbf{M}|_{Av}$ from $|\mathbf{M}_0|$ as a function of $\mathbf{H}$ was first considered by Akulov and by Gans[1] on the basis of the general mechanism outlined above. These authors obtained the result:

$$|\mathbf{M}|_{Av}=|\mathbf{M}_0|\left(1-\left(\frac{\beta K^2}{|\mathbf{M}_0|^2}\right)H^{-2}\right), \tag{2}$$

with $\beta=0.0872$ for Fe; 0.0762 for Ni.

However, Akulov and Gans, in their derivation of (2), neglected completely the internal magnetic field $\mathbf{h}$, and thus the torque term $\mathbf{M}_0\times\mathbf{h}$ in Eq. (1). The neglect of this torque term cannot be considered satisfactory since it is of the same order of magnitude as the term $\mathbf{M}_0\times\mathbf{H}$, for the range of external fields $\mathbf{H}$ used in the experiments.[2] It is not possible to dismiss the term $\mathbf{M}_0\times\mathbf{h}$ with the observation that $|\mathbf{h}|\ll|\mathbf{H}|$, since $\mathbf{H}$ and $\mathbf{M}_0$ are almost parallel, while $\mathbf{h}$ has a direction which in general, is quite different from that of $\mathbf{M}_0$ and $\mathbf{H}$.

In this paper, the deviation of $|\mathbf{M}|_{Av}$ from $|\mathbf{M}_0|$, considered as a function of $\mathbf{H}$, will be obtained taking the internal magnetic field $\mathbf{h}$ into account.

II. Derivation of Expression for the Deviation of $|\mathbf{M}|_{Av}$ from $|\mathbf{M}_0|$

It is convenient to resolve $\mathbf{M}_0$ into components $\mathbf{M}$ and $\mathbf{m}$, parallel and perpendicular, respectively, to $\mathbf{H}$. Thus,

$$\mathbf{M}_0=\mathbf{M}+\mathbf{m} \tag{3}$$

and Eq. (1) becomes

$$\mathbf{T}=\mathbf{m}\times\mathbf{H}+\mathbf{M}\times\mathbf{h}+\mathbf{m}\times\mathbf{h}, \tag{4}$$

while the observed magnetization $|\mathbf{M}|_{Av}$ is given by the integral of $|\mathbf{M}|$ over the volume of the polycrystalline specimen, i.e.,

$$|\mathbf{M}|_{Av}\equiv\frac{1}{V}\int_V|\mathbf{M}|d\mathbf{r}=\frac{|\mathbf{M}_0|}{V}\int_V\left(1-\frac{|\mathbf{m}|^2}{|\mathbf{M}_0|^2}\right)^{\frac{1}{2}}d\mathbf{r}. \tag{5}$$

Since only the magnetization observed at high external fields[3] is under consideration, the deviation of $|\mathbf{M}|_{Av}$ from $|\mathbf{M}_0|$ is small, and the following approximations may be considered as holding at each point within the specimen:

$$|\mathbf{m}|/|\mathbf{M}_0|\ll1, \tag{6}$$

$$\frac{|\mathbf{M}|-|\mathbf{M}_0|}{|\mathbf{M}_0|}=\frac{|\mathbf{M}_0-\mathbf{m}|-|\mathbf{M}_0|}{|\mathbf{M}_0|}\leqq\frac{|\mathbf{m}|^2}{|\mathbf{M}_0|^2}. \tag{7}$$

From (6), (7), it follows that with neglect of terms $\leqq|\mathbf{m}|^2/|\mathbf{M}_0|^2$ or higher, $\mathbf{M}$ is constant in *magnitude*, as well as in direction.

Further,

$$\mathbf{m}\times\mathbf{h}\leqq0+O(|\mathbf{m}|^2). \tag{8}$$

since

$$\mathbf{h}=-\operatorname{grad}\int\frac{-\operatorname{div}\mathbf{M}_0}{|\mathbf{r}-\mathbf{r}'|}d\mathbf{r}'$$

$$\leqq-\operatorname{grad}\int\frac{-\operatorname{div}\mathbf{m}}{|\mathbf{r}-\mathbf{r}'|}d\mathbf{r}',$$

and hence $\mathbf{h}\leqq\mathbf{m}$.

The approximations (6)–(8) applied to Eqs. (5), (4) yield:

$$|\mathbf{M}|_{Av}=|\mathbf{M}_0|\left(1-\frac{1}{2|\mathbf{M}_0|^2V}\int_V|\mathbf{m}|^2d\mathbf{r}\right), \tag{9}$$

$$\mathbf{T}=\mathbf{m}\times\mathbf{H}+\mathbf{M}\times\mathbf{h}. \tag{10}$$

Further, in view of (6)–(8), $\mathbf{T}$ in any crystal grain can be taken as dependent only on the direction of the vector $\mathbf{M}$ or $\mathbf{H}$ with respect to the crystallographic axes of that grain, since $\mathbf{M}_0$ may be taken parallel to $\mathbf{M}$ to the first order in $|\mathbf{m}|/|\mathbf{M}_0|$. $\mathbf{T}$ is hence independent of $\mathbf{m}$.

Thus to find $|\mathbf{M}|_{Av}$, it remains to calculate from Eq. (10) $\mathbf{m}$ as a function of position within the specimen, and then to evaluate the integral in (9). This procedure will now be carried out.

First, taking the vector product of both sides

[2] These experiments are discussed in Section IV; the magnitude of the fields used is ~2000—4000 gauss. Cf. reference 5.

[3] These fields are such that $|\mathbf{M}|_{Av}$ is well above the "knee" of the magnetization curve; e.g., $H>1000$ gauss for Fe.

of Eq. (10) with $\mathbf{H}$, and solving for $\mathbf{m}$, one obtains,

$$\mathbf{m}=\mathbf{F}+(4\pi)^{-1}\alpha[\mathbf{h}-(\mathbf{h}\cdot\mathbf{H})(\mathbf{H}/|\mathbf{H}|^2)] \quad (11)$$

with the abbreviations

$$\mathbf{F}\equiv(\mathbf{H}\times\mathbf{T})/|\mathbf{H}|^2, \quad (12)$$

$$\alpha\equiv 4\pi|\mathbf{M}|/|\mathbf{H}|\leqq 4\pi|\mathbf{M}_0|/|\mathbf{H}|. \quad (13)$$

One also has the general field equations relating $\mathbf{h}$ and $\mathbf{m}$,

$$\text{div } \mathbf{h}=-4\pi \text{ div } \mathbf{M}_0\leqq -4\pi \text{ div } \mathbf{m}, \quad (14)$$

$$\text{curl } \mathbf{h}=0. \quad (15)$$

Introducing the Fourier resolution[4] of $\mathbf{m}$,

$$\mathbf{m}=\int \mathbf{m}_k \exp(2\pi i\mathbf{k}\cdot\mathbf{r})d\mathbf{k}, \quad (16)$$

one obtains from (9)

$$|\mathbf{M}|_{Av}=|\mathbf{M}_0|\left(1-\frac{1}{2|\mathbf{M}_0|^2V}\int|\mathbf{m}_k|^2d\mathbf{k}\right), \quad (17)$$

while from (11), (14), (15) the x, y, z components of $\mathbf{m}_k$ satisfy the relations:

$$\mathrm{m}_{kx}=F_{kx}+(4\pi)^{-1}\alpha\mathrm{h}_{kx}, \quad (18a)$$

$$\mathrm{m}_{ky}=F_{ky}+(4\pi)^{-1}\alpha\mathrm{h}_{ky}, \quad (18b)$$

$$\mathrm{m}_{kz}=0, \quad (18c)$$

$$\mathbf{k}\cdot\mathbf{h}_k=-4\pi\mathbf{k}\cdot\mathbf{m}_k, \quad (19)$$

$$\mathbf{k}\times\mathbf{h}_k=0. \quad (20)$$

In Eqs. (18), (19), (20), $\mathbf{F}_k$, $\mathbf{h}_k$ are the vector Fourier components of $\mathbf{F}$ and $\mathbf{h}$, similar to $\mathbf{m}_k$ being the vector Fourier component of $\mathbf{m}$ in (16); F_{kx}, h_{kx} are the x components of $\mathbf{F}_k$, $\mathbf{h}_k$; the z axis has been chosen parallel to $\mathbf{H}$.

To proceed further one eliminates $\mathbf{h}_k$ from (18), (19), (20), finding $\mathbf{m}_k$ as a function of $\mathbf{k}$. One has as the solution of (19), (20) for $\mathbf{h}_k$,

$$\mathbf{h}_k=-4\pi\mathbf{n}\mathbf{n}\cdot\mathbf{m}_k, \quad (21)$$

with $\mathbf{n}\equiv\mathbf{k}/|\mathbf{k}|$,

whence, substituting (21) into (18), and solving for m_{kx}, m_{ky}, one obtains

$$\mathrm{m}_{kx}=\frac{F_{kx}(1+\alpha n_y^2)+F_{ky}\alpha n_x n_y}{1+\alpha(n_x^2+n_y^2)}, \quad (22)$$

$$\mathrm{m}_{ky}=\frac{F_{kx}\alpha n_x n_y+F_{ky}(1+\alpha n_x^2)}{1+\alpha(n_x^2+n_y^2)},$$

$$\mathrm{m}_{kz}=0.$$

Finally, substituting (22) into (17), one obtains

$$|\mathbf{M}|_{Av}=|\mathbf{M}_0|\left(1-\frac{1}{2|\mathbf{M}_0|^2V}\left[\int\frac{(1+\alpha n_y^2)^2+\alpha^2n_x^2n_y^2}{(1+\alpha(n_x^2+n_y^2))^2}|F_{kx}|^2d\mathbf{k}\right.\right.$$

$$\left.\left.+\int\frac{(1+\alpha n_x^2)^2+\alpha^2n_x^2n_y^2}{(1+\alpha(n_x^2+n_y^2))^2}|F_{ky}|^2d\mathbf{k}+2\int\frac{(2+\alpha n_x^2+\alpha n_y^2)\alpha n_x n_y}{(1+\alpha(n_x^2+n_y^2))^2}|F_{kx}F_{ky}|d\mathbf{k}\right]\right). \quad (23)$$

Now it will be shown in Section III below, that as far as the integrations over $\mathbf{k}$ in Eq. (23) are concerned, one may effectively take

$$|F_{kx}|^2=|F_{ky}|^2=\tfrac{1}{2}|F_k|^2, \quad (24a)$$

$$|F_{kx}F_{ky}|=0, \quad (24b)$$

and take $|F_k|^2$ to depend only on the magnitude of $\mathbf{k}$, i.e.,

$$|F_k|^2=\Phi(|\mathbf{k}|). \quad (24c)$$

[4] The Fourier analysis method has been used by W. F. Brown, Jr., in a related problem, cf. Phys. Rev. **58**, 736 (1940).

Thus,

$$|\mathbf{M}|_{Av}=|\mathbf{M}_0|\left(1-\frac{(4\pi)^{-1}}{4|\mathbf{M}_0|^2V}\int\Phi(|\mathbf{k}|)|\mathbf{k}|^2d|\mathbf{k}|4\pi\int\int\left(1+\frac{1}{(1+\alpha(n_x^2+n_y^2))^2}\right)\sin\theta_k d\theta_k d\phi_k\right)$$

$$=|\mathbf{M}_0|\left(1-\frac{1}{8|\mathbf{M}_0|^2V}\int_V|\mathbf{F}|^2d\mathbf{r}\int_0^\pi\left(1+\frac{1}{(1+\alpha\sin^2\theta_k)^2}\right)\sin\theta_k d\theta_k\right)$$

$$=|\mathbf{M}_0|\left(1-\frac{\{|\mathbf{T}\sin(\mathbf{T},\mathbf{H})|^2\}_{Av}}{4|\mathbf{M}_0|^2}H^{-2}\left[1+\tfrac{1}{2}(1+\alpha)^{-1}+\tfrac{1}{4}(1+\alpha)^{-\frac{1}{2}}\alpha^{-\frac{1}{2}}\log\left(\frac{(1+\alpha)^{\frac{1}{2}}+\alpha^{\frac{1}{2}}}{(1+\alpha)^{\frac{1}{2}}-\alpha^{\frac{1}{2}}}\right)\right]\right). \quad (25)$$

Equation (25) is the desired expression for the functional dependence of $|\mathbf{M}|_{Av}-|\mathbf{M}_0|$ on $\mathbf{H}$. In the limiting cases of $\alpha\ll1$ and $\gg1$, Eq. (25) reduces to the following simple forms:

$$|\mathbf{M}|_{Av}=|\mathbf{M}_0|\left(1-\frac{\{|\mathbf{T}\sin(\mathbf{T},\mathbf{H})|^2\}_{Av}}{2|\mathbf{M}_0|^2}H^{-2}\right), \quad \text{when } \alpha\ll1, \text{ i.e., } 4\pi M_0\ll H, \quad (26)$$

$$|\mathbf{M}|_{Av}=|\mathbf{M}_0|\left(1-\frac{\{|\mathbf{T}\sin(\mathbf{T},\mathbf{H})|^2\}_{Av}}{4|\mathbf{M}_0|^2}H^{-2}\right), \quad \text{when } \alpha\gg1, \text{ i.e., } 4\pi M_0\gg H. \quad (27)$$

Equation (26) may be derived by neglecting the term proportional to α in Eq. (11), or equivalently, by neglecting $\mathbf{M}\times\mathbf{h}$ in Eq. (10), or $\mathbf{M}_0\times\mathbf{h}$ in Eq. (1). Equation (26) is thus identical with Eq. (2) derived by Akulov and Gans. Thus it is seen that the Eq. (2) or (26), of Akulov and Gans is only applicable, if $H\gg4\pi M_0=21{,}800$ gauss in Fe, 6400 gauss in Ni. It should further be emphasized that only in the limiting cases $4\pi M_0\gg H$, $4\pi M_0\ll H$, does $|\mathbf{M}|_{Av}-|\mathbf{M}_0|$ vary, as const. H^{-2} (with different constants for the two limits). For intermediate field strengths, the dependence of $|\mathbf{M}|_{Av}$ on $\mathbf{H}$ is much more involved, being given by Eq. (25).

III. Justification of Equations (24)

It now remains to justify Eqs. (24). One must consider the evaluation of the integrals in Eq. (23). These integrals are of the type:

$$\int\Psi_x(\mathbf{n})F_{kx}^2d\mathbf{k}, \quad \int\Psi_y(\mathbf{n})F_{ky}^2d\mathbf{k},$$

$$\int\Psi_{xy}(\mathbf{n})F_{kx}F_{ky}d\mathbf{k}. \quad (28)$$

Now

$$\mathbf{F}_k=\int_V\mathbf{F}(\mathbf{r})\exp(2\pi i\mathbf{k}\cdot\mathbf{r})d\mathbf{r}$$

$$=\sum_j\int_{V_j}\mathbf{F}(\mathbf{r})\exp(2\pi i\mathbf{k}\cdot\mathbf{r})d\mathbf{r}, \quad (29)$$

where the volume integrals in the sum over j extend over V_j, the volume of the jth crystal grain. In V_j, $\mathbf{T}$ and hence $\mathbf{F}$, are constant both in magnitude and direction; one writes the constant value of $\mathbf{F}$ in V_j as $\mathbf{F}_j$. Thus,

$$\mathbf{F}_k=\sum_j\mathbf{F}_j\int_{V_j}\exp(2\pi i\mathbf{k}\cdot\mathbf{r})d\mathbf{r}$$

$$=\sum_j\mathbf{F}_j\exp(2\pi i\mathbf{k}\cdot\mathbf{R}_j)\int_{V_j}\exp[2\pi i\mathbf{k}\cdot(\mathbf{r}-\mathbf{R}_j)]d\mathbf{r}$$

$$\equiv\sum_j\mathbf{F}_j\exp(2\pi i\mathbf{k}\cdot\mathbf{R}_j)V_jW_j(\mathbf{k}), \quad (30)$$

where $\mathbf{R}_j$ is a vector from the center of the polycrystalline specimen to the center of the jth crystal grain, and $W_j(\mathbf{k})$ is the spatial average of $\exp[2\pi i\mathbf{k}\cdot(\mathbf{r}-\mathbf{R}_j)]$ over V_j.

The perfect randomness of the distribution of the orientations of the crystallographic axes of the various crystal grains within the polycrystalline specimen leads to the following "randomness properties" of the vectors $\mathbf{F}_j$:

(A) There is no correlation between the magnitudes and directions of the vectors $\mathbf{F}_j$ and

$\mathbf{F}_l$. $(l \neq j)$, i.e.,

$$|\sum_j \mathbf{F}_j| \sim (\sum_j |\mathbf{F}_j|^2)^{\frac{1}{2}} \equiv [(V/\langle V_j\rangle_{\mathrm{Av}})\langle |\mathbf{F}_j|^2\rangle_{\mathrm{Av}}]^{\frac{1}{2}}, \quad (31)$$

where $V/\langle V\rangle_{\mathrm{Av}}$ is the number of terms in the sum over j.

(B) There is no correlation between the magnitude and direction of $\mathbf{F}_j$ and the position of the jth crystal grain within the specimen, i.e.,

$$\sum_j f(\mathbf{F}_j) g(\mathbf{R}_j) \sim \langle |g(\mathbf{R}_j)| \rangle_{\mathrm{Av}} \sum_j f(\mathbf{F}_j), \quad (32)$$

where $f(\mathbf{F}_j)$ is any function of $\mathbf{F}_j$, $g(\mathbf{R}_j)$ is any function of $\mathbf{R}_j$, and

$$\langle |g(\mathbf{R}_j)| \rangle_{\mathrm{Av}} = (V/\langle V_j\rangle_{\mathrm{Av}})^{-1} \sum_j |g(\mathbf{R}_j)|.$$

(C) There is no correlation between the direction of $\mathbf{F}_j$ and any fixed direction within the specimen, i.e.,

$$\sum_j F_{jx}^2 = \sum_j F_{jy}^2 = \tfrac{1}{2}|\mathbf{F}_j|^2;$$

or

$$\langle F_{jx}^2\rangle_{\mathrm{Av}} = \langle F_{jy}^2\rangle_{\mathrm{Av}} = \langle \tfrac{1}{2}|\mathbf{F}_j|^2\rangle_{\mathrm{Av}}. \quad (33)$$

From Eq. (30) one sees that $\mathbf{F}_\mathbf{k}$ oscillates rapidly when $\mathbf{k}$ varies over a region V^{-1}, since $\mathbf{R}_j$ in $\exp(2\pi i \mathbf{k}\cdot\mathbf{R}_j)$ is $\sim V^{\frac{1}{3}}$. On the other hand, from Eqs. (30), (32), (31),

$$|\mathbf{F}_\mathbf{k}| \sim \langle |\exp(2\pi i \mathbf{k}\cdot\mathbf{R}_j) V_j W_j(\mathbf{k})| \rangle_{\mathrm{Av}} \times [(V/\langle V_j\rangle_{\mathrm{Av}})\langle |\mathbf{F}_j|^2\rangle_{\mathrm{Av}}]^{\frac{1}{2}}$$

$$\sim (V^{\frac{1}{3}}/\langle V_j\rangle_{\mathrm{Av}}^{\frac{1}{3}})\langle |V_j W_j(\mathbf{k})|\rangle_{\mathrm{Av}} \langle |\mathbf{F}_j|^2\rangle_{\mathrm{Av}}^{\frac{1}{2}} \quad (34)$$

and thus the variation with $\mathbf{k}$ of the order of magnitude of $\mathbf{F}_\mathbf{k}$ is independent of the rapid oscillations due to $\exp(2\pi i \mathbf{k}\cdot\mathbf{R}_j)$ and is determined only by the $W_j(\mathbf{k})$. Also, from their definition, the $W_j(\mathbf{k})$ vary appreciably with $\mathbf{k}$ only when $\mathbf{k}$ ranges over a region $\sim V_j^{-1}$; in particular, $W_j(\mathbf{k}) \leqq 1$ if $|\mathbf{k}| \lesssim V_j^{-\frac{1}{3}}$, and $W_j(\mathbf{k})$ decreases if $|\mathbf{k}|$ exceeds $V_j^{-\frac{1}{3}}$.

Thus, turning back to the integrals of Eq. (28), one sees that the effective region of integration in $\mathbf{k}$ space is defined by the condition $|\mathbf{k}| \lesssim V_j^{-\frac{1}{3}}$. Now Ψ depends only on $\mathbf{n} = \mathbf{k}/|\mathbf{k}|$; one calculates the variation in $\mathbf{n}$, $\Delta\mathbf{n}$, corresponding to a variation in $\mathbf{k}$, $\Delta\mathbf{k}$, and finds

$$\Delta\mathbf{n} \leqq [\mathbf{k}\times(\Delta\mathbf{k}\times\mathbf{k})]/|\mathbf{k}|^3$$

over most of the effective region of integration. Therefore, Ψ varies appreciably only when $\mathbf{k}$ varies over a region V_j^{-1}.

Thus, it is possible to divide the $\mathbf{k}$ space into cells of size Ω, which, if $V^{-1} \ll \Omega \ll V_j^{-1}$ possess the following properties: (1) Many oscillations of $\mathbf{F}_\mathbf{k}$, $|\mathbf{F}_\mathbf{k}|^2$, etc., take place in Ω. (2) The order of magnitude of $|\mathbf{F}_\mathbf{k}|^2$ and of the value of Ψ, remain effectively constant over Ω.

It therefore follows that the integrals (28) can be written as

$$\int \Psi_x F_{\mathbf{k}x}^2 d\mathbf{k} \leqq \sum_\rho \Psi_x(\mathbf{k}_\rho/|\mathbf{k}_\rho|) \int_{\Omega_\rho} F_{\mathbf{k}x}^2 d\mathbf{k}$$

$$\leqq \int \Psi_x(\mathbf{k}/|\mathbf{k}|) \left\{ \Omega^{-1} \int_\Omega F_{\mathbf{k}'x}^2 d\mathbf{k}' \right\} d\mathbf{k} \quad (35)$$

and hence the $F_{\mathbf{k}x}^2$ in (28) are effectively replaced by their "smoothed over" values:

$$\Omega^{-1} \int_\Omega F_{\mathbf{k}'x}^2 d\mathbf{k}'.$$

Now the "smoothed over" values of $F_{\mathbf{k}x}^2$, $F_{\mathbf{k}y}^2$, $F_{\mathbf{k}x}F_{\mathbf{k}y}$ satisfy, as is shown immediately below the following relations:

$$\Omega^{-1} \int_\Omega F_{\mathbf{k}x}^2 d\mathbf{k} = \Omega^{-1} \int_\Omega F_{\mathbf{k}y}^2 d\mathbf{k} = \tfrac{1}{2}\Omega^{-1} \int_\Omega |\mathbf{F}_\mathbf{k}|^2 d\mathbf{k}, \quad (36a)$$

$$\Omega^{-1} \int_\Omega F_{\mathbf{k}x} F_{\mathbf{k}y} d\mathbf{k} = 0, \quad (36b)$$

and thus, by use of Eqs. (35), (36a), (36b), the validity of Eqs. (24a), (24b), is established.

To prove Eq. (36a), for example, one has:

$$\Omega^{-1} \int_\Omega F_{\mathbf{k}x}^2 d\mathbf{k} = \Omega^{-1} \sum_j F_{jx}^2 V_j^2 \int_\Omega [W_j(\mathbf{k})]^2 d\mathbf{k} + \Omega^{-1} \sum_{j\neq l} F_{jx}F_{lx}V_jV_l \int_\Omega \exp(2\pi i \mathbf{k}\cdot\mathbf{R}_{jl}) W_j(\mathbf{k}) W_l(\mathbf{k}) d\mathbf{k}$$

$$\leqq \sum_j F_{jx}^2 V_j^2 [W_j(\mathbf{k}_0)]^2 + \sum_{j\neq l} F_{jx}F_{lx}V_jV_l W_j(\mathbf{k}_0) W_l(\mathbf{k}_0) \exp(2\pi i \mathbf{k}_0\cdot\mathbf{R}_{jl}) \times (\Omega X_{jl} Y_{jl} Z_{jl})^{-1} \sin(\pi\Delta k_x X_{jl}) \sin(\pi\Delta k_y Y_{jl}) \sin(\pi\Delta k_z Z_{jl}) \quad (37)$$

where $\mathbf{k}_0$ is a vector from the origin of $\mathbf{k}$ space to the center of Ω and $\Delta k_x \Delta k_y \Delta k_z = \Omega$. The last (approximate) equality in Eq. (37) is valid, since in Ω each $W_j(\mathbf{k})$ is approximately constant.

From Eq. (32), the order of magnitude of the single sum is:

$$\sim \langle V_j^2 [W_j(\mathbf{k}_0)]^2 \rangle_{Av} \sum_j F_{jx}^2$$

$$\equiv \langle V_j^2 W_j^2 \rangle_{Av} (V/\langle V_j \rangle_{Av}) \langle F_{jx}^2 \rangle_{Av}, \quad (38)$$

while the order of magnitude of the double sum,

$$\sim (\Omega V)^{-1} \langle | V_j V_l W_j(\mathbf{k}_0) W_l(\mathbf{k}_0) \times \exp(2\pi i \mathbf{k}_0 \cdot \mathbf{R}_{jl}) | \rangle_{Av} \sum_{j \neq l} F_{jx} F_{lx},$$

$$\sim (\Omega V)^{-1} \langle | V_j V_l W_j(\mathbf{k}_0) W_l(\mathbf{k}_0) \times \exp(2\pi i \mathbf{k}_0 \cdot \mathbf{R}_{jl}) | \rangle_{Av} (\sum_j F_{jx})^2,$$

$$\sim (\Omega V)^{-1} \langle | V_j^2 W_j^2 | \rangle_{Av} (V/\langle V_j \rangle_{Av}) \langle F_{jx}^2 \rangle_{Av}, \quad (39)$$

the last (order of magnitude) equality being a consequence of Eq. (31).

Thus, from (38) and (39) the ratio of the orders of magnitude of the double sum and the single sum is $(V\Omega)^{-1} \ll 1$. Hence,

$$\Omega^{-1} \int_\Omega F_{kx}^2 = \Omega^{-1} \sum_j F_{jx}^2 V_j^2 [W_j(\mathbf{k}_0)]^2, \quad (40)$$

and similarly

$$\Omega^{-1} \int_\Omega F_{ky}^2 d\mathbf{k} = \Omega^{-1} \sum_j F_{jy}^2 V_j^2 [W_j(\mathbf{k}_0)]^2. \quad (41)$$

"Randomness properties" (B) and (C) now insure the equality of the right-hand sides of Eqs. (40) and (41), and Eq. (36a) follows immediately.

To prove Eq. (36b), one observes that $\Omega^{-1} \int_\Omega F_{kx} F_{ky} d\mathbf{k}$ can be expressed as $\sum_j + \sum_{j \neq l}$, and that from Eq. (32),

$$\sum_j \sim \langle V_j^2 W_j^2 \rangle_{Av} \sum_j F_{jx} F_{jy}$$

$$\sim \langle V_j^2 W_j^2 \rangle_{Av} [(V/\langle V_j \rangle_{Av}) \langle F_{jx}^2 \rangle_{Av} \langle F_{jy}^2 \rangle_{Av}]^{\frac{1}{2}}, \quad (42)$$

the last (order of magnitude) equality being a consequence of "randomness properties" (A) and (C).

Thus the ratio of the orders of magnitude of the single sum in $\Omega^{-1} \int_\Omega F_{kx} F_{ky} d\mathbf{k}$, and of the single sum in $\Omega^{-1} \int_\Omega F_{kx}^2 d\mathbf{k}$, is (cf. Eqs. (38) and (42)), $\sim \langle V_j \rangle_{Av}^{\frac{1}{2}} / V^{\frac{1}{2}} \ll 1$. Further, by an argument similar to that given in connection with Eq. (39), it can be shown that the double sum in $\Omega^{-1} \int_\Omega F_{kx} F_{ky} d\mathbf{k}$ is negligible compared with the single sum. Therefore, in comparison to the integral $\Omega^{-1} \int_\Omega F_{kx}^2 d\mathbf{k}$ the integral $\Omega^{-1} \int_\Omega F_{kx} F_{ky} d\mathbf{k}$ can be taken to be equal to zero (to within terms $\sim \langle V_j \rangle_{Av}^{\frac{1}{2}} / V^{\frac{1}{2}} \ll 1$, and $(V\Omega)^{-1} \ll 1$).

It now remains to justify Eq. (24c). For this purpose it is necessary to make use of another "randomness property"; *viz.:* The shapes of the individual crystal grains are not correlated in any way with a fixed set of directions in the crystal. Then, apart from the rapid oscillations of $|\mathbf{F}_\mathbf{k}|^2$ with $\mathbf{k}$ which are smoothed out by the integrations over Ω in Eq. (35) or (36) or (23),

$$|\mathbf{F}_\mathbf{k}|^2 = \left| \sum_j \mathbf{F}_j \int_{V_j} \exp(2\pi i \mathbf{k} \cdot \mathbf{r}) d\mathbf{r} \right|^2,$$

can only depend on $|\mathbf{k}|$. Hence the validity of Eq. (24c).

IV. Discussion of Experiments

The experimentally observed variation[5] of the magnetization of polycrystalline ferromagnetics with external magnetic field at high fields is customarily described by an empirical relation of the form:[5]

$$\frac{d|\mathbf{M}|_{obs}}{dH} = AH^{-2} + BH^{-3} + CH, \quad (43)$$

where A, B, C, are assumed to be independent of H.

It has further been observed that C is independent of the metallurgical history of the specimen;[5] it therefore must arise from the variation of the intrinsic domain magnetization with the field. The magnitude, temperature dependence, and actual slow variation with field,

[5] A. R. Kaufmann, Phys. Rev. **55**, 1142 (1939); **57**, 1089 (1939). H. Polley, Ann. d. Physik **36**, 625 (1939). Only Ni and Fe but not Co, were investigated.

of C, have been treated in a recent paper by the present authors.[6]

A and B depend on the metallurgical history of the polycrystalline specimen;[5] A is conditioned by the plastic deformation of the material,[5] (small for well-annealed specimens) and is temperature independent,[5] whereas, B is determined by the crystalline properties and the elastic state,[5] and is furthermore strongly temperature dependent.[5] The theoretical interpretation of the term AH^{-2} is still in doubt; however, a recent paper by W. F. Brown, Jr.,[4] ascribes this term to the existence of anisotropy torques which are *concentrated* along lines of dislocation produced by plastic deformation.

Finally, the term BH^{-3} arises from the mechanism discussed in this paper, i.e., from the rotation of the magnetization vector away from the direction of H and toward the various directions of easy magnetization (in the various individual crystal grains) by crystalline anisotropy torques constant within any one single grain. Comparing the identical Eqs. (2) and (26), one sees that

$$K=[\{|\mathbf{T}\sin(\mathbf{T},\mathbf{H})|^2\}_{Av}/2\beta]^{\frac{1}{2}}, \qquad (44)$$

whence from Eqs. (26), (27), $d|\mathbf{M}|_{Av}/dH$ may be written in the form BH^{-3} in the two limiting cases, i.e.,

$$d|\mathbf{M}|_{Av}/dH=(2\beta K^2/|\mathbf{M}_0|^2)H^{-3},$$

$$\text{when } 4\pi M_0 \ll H; \qquad (45)$$

$$d|\mathbf{M}|_{Av}/dH=(\beta K^2/|\mathbf{M}_0|^2)H^{-3},$$

$$\text{when } 4\pi M_0 \gg H. \qquad (46)$$

For intermediate values of H, $d|\mathbf{M}|_{Av}/dH$ is obtained by a differentiation in Eq. (25), and can be written in the form BH^{-3} only if B itself is considered as a (slowly varying) function of H.

Now in all the experiments so far performed, H was considerably less than $4\pi M_0$, so that, in evaluating K from the experiments, one should use the relation:[7]

$$K=[\beta^{-1}|\mathbf{M}_0|^2 \times(\text{observed coefficient of } H)]^{\frac{1}{2}}. \qquad (47)$$

On the other hand, these experiments have previously been interpreted in terms of the Akulov-Gans equation (2) or (26) or (45); thus the values of K, previously deduced from the existing experimental data, are smaller than they should be by a factor equal to $2^{\frac{1}{2}}$. If these previously deduced values of K be all multiplied by $2^{\frac{1}{2}}$, they agree somewhat better than before with the values of K obtained directly from the magnetization curves of single crystal grains; cf. especially the experimental data given in Polley.[8]

The analysis of the present paper can be tested by experiments on the magnetization curves of polycrystalline specimens, in which, both the limiting cases, $4\pi M_0 \gg H$, $4\pi M_0 \ll H$, and also the case of intermediate H (described by the complete Eq. (25)) are studied. Now, both for iron and nickel, K is so small, that unless H is considerably less than $4\pi M_0$, the whole term BH^{-3} is negligible. For cobalt, however, the crystalline anisotropy energy and hence K, are so large, that the portion of $d|\mathbf{M}|_{obs}/dH$ arising from the mechanism under discussion, could easily be observed as a function of H for values of H less than, of the order of, and considerably greater than, $4\pi M_0$.[9] In this way, a complete experimental test of the Eqs. (25), (26), (27) can be obtained.

[6] T. Holstein and H. Primakoff, Phys. Rev. **58**, 1098 (1940).

[7] This formula, as well as the rest of the analysis in the present paper and in the derivation of the Akulov-Gans equation (2), is based on the assumption that the crystalline anisotropy torques are just those present in a *strain-free* material. The existence of strains creates additional anisotropy torques, which, if constant over regions comparable in size to a single crystal grain (if not, cf. W. F. Brown, Jr., reference 4) can be easily incorporated into the present treatment. The only resulting difference in the final formulae is that K in Eq. (44) and hence in Eqs. (45), (46), (47) has to be amplified to include the "strain anisotropy" constant, and that the numerical value of β must be changed somewhat.

[8] Reference 5, p. 643, Fig. 12.

[9] Since cobalt has a hexagonal lattice, the numerical value of β for Co will differ from the values quoted in Eq. (2), which are only valid for the cubic lattices of Ni and Fe.

Phase Series

E. J. HELLUND*

(Received October 18, 1940)

An expansion theorem for the calculation of the parameters occurring in the scattering cross sections has been developed. The series converges exponentially and is expressible in terms of known functions, provided the interactions are expressed as a power series in r and $1/r$.

INTRODUCTION

THE solution of problems involving the scattering of one particle by another is attended by extreme difficulties. In general, evaluation of cross sections can be obtained only in infinite series, each term of such a series containing a parameter (phase), which must be determined from a linear differential equation of the second order. The evaluation of this parameter must proceed, usually, by numerical integration of this equation. Such calculations are excessively laborious and are, furthermore, subject to numerous errors. It has seemed desirable, therefore, to derive an expansion for the phases, in series form, the convergence of which could be accurately determined. Such an expansion possesses a particular advantage which lies in the latitude permissible in the choice of function to represent the interaction between particles. This is of special importance in the evaluation of integrals involving the interaction potential and other known functions. Such integrals invariably arise, as the distortion of the wave function of one particle by another involves the values of the interaction for all distances of separation. Apart from the points mentioned, however, a series solution holds little practical superiority over the numerical integration of the differential equation.

1. First approximations

The problem to be solved is, then, the determination of $I(\theta)d\omega$, the number of particles scattered into a given solid angle $d\omega$ per unit time, when the incident beam is such that one particle crosses unit area per unit time. The series expansion for $I(\theta)$ then has the form:[1,2]

$$I(\theta)=|f(\theta)|^2, \tag{1a}$$

where

$$f(\theta)=(1/2ik)\sum(2l+1)\times[\exp(2i\delta_l)-1]P_l(\cos(\theta)), \tag{1b}$$

$$k^2=4\pi^2m^2v^2/h^2=8\pi^2mE/h^2, \tag{1c}$$

and δ_l is a constant to be determined from the equation,

$$\frac{d^2(r\psi)}{dr^2}+\left(k^2-\frac{8\pi^2mV(r)}{h^2}-\frac{(l)(l+1)}{r^2}\right)(r\psi)=0. \tag{2}$$

One selects that solution finite at the origin (or that solution of lower order singularity at the origin,[3] and determines δ_l from its behavior at infinity. δ_l is then defined by the asymptotic solution,

$$\psi\sim(1/r)\sin(kr-\tfrac{1}{2}l\pi+\delta_l). \tag{3}$$

The determination of δ_l is then the immediate point of attack. Various formulae have been given for δ_l which are due, in order, to Born,[4] Jeffreys,[5] and Massey and Mohr.[6]

$$\delta_l=-\frac{4\pi^3m}{h^2}\int_0^\infty V(r)J_{l+\frac{1}{2}}^2(kr)rdr, \tag{4}$$

$$\delta_l=\tfrac{1}{4}\pi+\tfrac{1}{2}l\pi-kr_0+\int_{r_0}^\infty(F^{\frac{1}{2}}-k)dr, \tag{5}$$

$$\delta_l=\int_{r_0'}^\infty\left[F+\frac{8\pi^2m}{h^2}V(r)\right]^{\frac{1}{2}}dr-\int_{r_0}^\infty F^{\frac{1}{2}}dr \tag{6},$$

* Now with the Battelle Memorial Institute, Columbus, Ohio.

[1] H. Faxén and J. Holtsmark, Zeits. f. Physik **45**, 307 (1927).

[2] N. F. Mott and H. S. W. Massey, *Theory of Atomic Collisions* (Clarendon Press, Oxford, 1933), first edition, p. 24.

[3] Reference 2, p. 30.

[4] Reference 2, p. 28.

[5] Jeffreys, Proc. London Math. Soc., Series 2, **23**, Part 6; or reference 2, p. 92.

[6] H. S. W. Massey and C. B. O. Mohr, Proc. Roy. Soc. **A144**, 202 (1934).

where

$$F(r)=(8\pi^2m/h^2)(E-V(r))-l(l+1)/r^2.$$

Formula (4) is valid for small phases, that of (5) for large phases and for (6) Massey and Mohr claim accuracy for both large and small phases. Actually, all three expressions must be regarded as first approximations, not valid generally for large phases. An exact solution of (2) in finite terms has never been given, except for special choice of $V(r)$. Moreover, any expression of the solution of (2) by a simple integral of some function of $V(r)$, may be seen by actual substitution to solve this equation for $V(r)$ replaced by a function of $V(r)$ and $dV(r)/dr$. The accuracy of (5) and (6) for large phases is then dependent on the choice of $V(r)$, and unless one has some independent criterion for their accuracy, their use in calculations is somewhat hazardous. It is possible, however, to give a series for δ_l, the first term of which is the expression (4).

2. Derivation of the first-order equations

Let us suppose, considering one dimension only, that it be required to determine the conditions necessary that a function f of variables r, ξ, η satisfy Eq. (2). ξ and η are functions of ψ so chosen that

$$f(r,\xi,\eta)=r\psi; \tag{7}$$

$$\partial f(r,\xi,\eta)/\partial r=\partial(r\psi)/\partial r \tag{8}$$

for $r=r_1$ and $r=r_1+\Delta r_1$. ξ, η must then possess first derivatives defined by the following system:[7]

$$\frac{\partial f}{\partial\xi}\frac{d\xi}{dr}+\frac{\partial f}{\partial\eta}\frac{d\eta}{dr}=0, \tag{9}$$

$$\frac{\partial^2 f}{\partial\xi\partial r}\frac{d\xi}{dr}+\frac{\partial^2 f}{\partial\eta\partial r}\frac{d\eta}{dr}=-\left(\frac{\partial^2 f}{\partial r^2}+H_\psi f\right), \tag{10}$$

where $H_\psi(r)$ has been set for the coefficient of $(r\psi)$ in (2). In particular, if one takes f as a linear function of ξ and η,

$$f=\xi\varphi_1+\eta\varphi_2, \tag{11}$$

where φ_1 and φ_2 both satisfy the condition

$$\partial^2\varphi/\partial r^2=-(H_\varphi)(\varphi), \tag{12}$$

one has the system

$$d\xi/dr-(\varphi_1\varphi_2\xi+\varphi_2^2\eta)(H_\psi-H_\varphi)/W(\varphi)=0, \tag{13}$$

$$d\eta/dr+(\varphi_1^2\xi+\varphi_1\varphi_2\eta)(H_\psi-H_\varphi)/W(\varphi)=0, \tag{14}$$

where $W(\varphi)$ indicates the Wronskian of φ_1, φ_2,

$$W(\varphi)=\varphi_1(\partial\varphi_2/\partial r)-\varphi_2(\partial\varphi_1/\partial r). \tag{15}$$

The Wronskian, under the condition (12), is a constant for all values of r[8].

It is a simple matter to confirm that (11) does actually satisfy (2) provided that also (12) and (13) are satisfied.

Equations (13) and (14) may, for convenience, be written in matrix form.

$$\begin{pmatrix}\xi\\ \eta\end{pmatrix}-\int_c^r\begin{pmatrix}\varphi_1\varphi_2, & \varphi_2^2\\ -\varphi_1^2, & -\varphi_1\varphi_2\end{pmatrix}\times\left(\frac{H_\psi-H_\varphi}{W(\varphi)}\right)\begin{pmatrix}\xi\\ \eta\end{pmatrix}dr=\begin{pmatrix}\xi_c\\ \eta_c\end{pmatrix}, \tag{16}$$

where ξ_c and η_c are arbitrary values assigned to ξ and η for $r=c$.

3. Solution of the integral equation

Equation (16) is a Volterra integral equation, of the second kind, for the unknowns ξ and η. If one denotes the unknown matrix by y, the constant matrix by $g(c)$, the solution is given by the series:[9]

$$y=g(c)+\sum_1^\infty K_jg(c), \tag{17}$$

where K is so defined that

$$K_j=\int_c^r K(r_j)dr_j\int_c^{r_j}K(r_{j-1})dr_{j-1}\cdots\times\int_c^{r_2}K(r_1)dr_1 \tag{18}$$

and K denotes the four-component matrix of (16).

[7] This procedure has some resemblance to that of A. Schuchowitzky and M. Olewsky, Physik. Zeits. Sowjetunion, 11.5 pp. 498–512 (1937). They however, use finite intervals, and after determining some parameters so as to assure continuity of the wave function, the remainder are evaluated by use of the variational principle.

[8] The derivative vanishes identically.

[9] Gerhard Kowalewski, *Integral Gleichungen* (Walter de Gruyter and Co., Berlin, 1930), first edition, pp. 49–90. See also E. G. C. Poole, *Theory of Linear Differential Equations* (Oxford Clarendon Press, 1936), Chapter I, for discussions on the convergence and uniqueness of the expansion.

One may easily demonstrate the convergence of (17) as follows: If φ_1 and φ_2 are finite in the interval r to c, let us replace each element of the matrix by M^2 where M exceeds both φ_1 and φ_2 over the entire interval. Also, let us take the absolute value of $H_\psi - H_\varphi$ at every point in the interval. One then obtains a series, term by term larger than (17), of the form,

$$\binom{\xi_c}{\eta_c}+\sum_{j=1}^{\infty}\frac{1}{j!}\left[\int_c^r\left|\frac{H_\psi-H_\varphi}{W(\varphi)}\right|\right.$$

$$\times 2M^2\binom{1}{1}\left(\frac{\xi_c+\eta_c}{2}\right). \quad (19)$$

The series (17) thus is absolutely convergent and summable in any order,[10] provided $|(H_\psi)-(H_\varphi)|$ is integrable in the interval c, r. The series likewise will still converge as r approaches infinite values, provided the integral converges.

4. Differential equation for δ_l

In order to evaluate the series (17) it is convenient to use a vector representation instead of a matrix representation. One then considers the pair as a two-component vector and the matrix of four elements as a product (dyadic) of two two-component vectors, which are

$$\varphi \equiv (\varphi_1, \varphi_2); \quad \bar{\varphi} \equiv (\varphi_2, -\varphi_1). \quad (20), (21)$$

φ and $\bar{\varphi}$ are thus mutually perpendicular.

If one denotes the vector ξ, η by P, then corresponding to (13) and (14), one has,

$$dP/dr - \bar{\varphi}(\varphi\cdot P)(H_\psi - H_\varphi)/W(\varphi) = 0, \quad (22)$$

where $\varphi\cdot P$ denotes the scalar product $\varphi_1\xi+\varphi_2\eta$.

One may set P equal to the product of a scalar and a unit vector of components $\cos\gamma$ and $\sin\gamma$. The resulting equation for γ is,

$$\frac{d\gamma}{dr}+\frac{(\varphi_1^2+\varphi_2^2)(H_\psi-H_\varphi)}{W(\varphi)}\sin^2(\gamma+\alpha)=0, \quad (23)$$

where $\tan\alpha \equiv \varphi_1/\varphi_2$.

γ may be identified with the phase angle δ_l, depending on asymptotic behavior of φ_1 and φ_2 at infinity. As a particular example, if $\varphi_1 = \sin(kr)$, $\varphi_2 = \cos(kr)$, then $\gamma_{r\to\infty} = \delta_l + l\pi/2$.

From (23), one may derive the perturbation formula

$$\gamma = \gamma_0 - \exp\{-G_1\}\int \exp\{+G_1\}G_2(H_\psi - H_\psi^0)dr, \quad (24)$$

where

$$G_1 = \int\left(\frac{\varphi_1^2+\varphi_2^2}{W(\varphi)}\right)(H_\psi^0 - H_\varphi)\sin 2(\gamma_0+\alpha)dr;$$

$$G_2 = \left(\frac{\varphi_1^2+\varphi_2^2}{W(\varphi)}\right)\sin^2(\gamma_0+\alpha)$$

by setting γ equal to $\gamma_0+(\gamma-\gamma_0)$, where γ_0 satisfies (23) for the potential $V(r^0)$. The Born formula (4) is a less accurate expression, obtained by equating γ_0 to zero, and retaining only term linear in V. Another perturbation formula could be obtained by using the Picard second approximation[11] on (23).

One may also formulate the eigenvalue problem from (23), for δ_l by requiring the solution of the following equation to approach zero as r approaches infinity:

$$\frac{d\gamma}{dr}+\frac{1}{k}\left(\frac{8\pi^2 m}{h^2}V(r)+\frac{l(l+1)}{r^2}\right)$$

$$\times\sin^2\left\{\gamma+kr-\frac{l\pi}{2}+\delta_l\right\}=0. \quad (25)$$

It is not the only solution as the addition of any multiple of π to the solution of (25) is also an acceptable solution.

5. Explicit series for δ_l

Using (22), one may write (17) in the following manner,

$$\xi=\xi_c+\sum_{j=1}^{\infty}\int_c^r dr_j\cdots dr_2\int_c^{r_2}\varphi_2(r_j)\{\varphi_1\xi_c+\varphi_2\eta_c\}\prod^{j\to 1}\Gamma(s)\cdot\prod^{j\to 2}\{\varphi_1(r_s)\varphi_2(r_{s-1})-\varphi_2(r_s)\varphi_1(r_{s-1})\}dr_1, \quad (26)$$

$$\eta=\eta_c-\sum_{j=1}^{\infty}\int_c^r dr_j\cdots dr_2\int_c^{r_2}\{\varphi_1\xi_c+\varphi_2\eta_c\}\varphi_1(r_j)\prod^{j\to 1}\Gamma(s)\cdot\prod^{j\to 2}\{\varphi_1(r_s)\varphi_2(r_{s-1})-\varphi_2(r_s)\varphi_1(r_{s-1})\}dr_1, \quad (27)$$

[10] E. T. Whittaker and G. N. Watson, *Modern Analysis* (Cambridge University Press, 1935), fourth edition, pp. 18–28.
[11] E. G. C. Poole, reference 9.

where $\Gamma(s)=[H_\psi(r_s)-H_\varphi(r_s)]/W(\varphi)$ and the following inequalities hold,

$$r_j>r_{j-1}>r_{j-2}\cdots>r_2>r_1. \tag{27a}$$

The ratio of ξ to η then determines the phase δ_l. In the event ξ_c and η_c are not specified, and φ_1 is bounded at the origin, ξ_c and η_c are replaced by 1 and 0, and c is taken to be zero. This procedure is permissible, however, only when the series still converges. In general this will hold provided $H_\psi-H_\varphi$ is everywhere finite, and decreases faster than $1/r$ as r approaches infinity.[12]

If one employs the functions $r^{\frac{1}{2}}J_{l+\frac{1}{2}}(kr)$ and $r^{\frac{1}{2}}J_{-l-\frac{1}{2}}(kr)$ for φ_1 and φ_2 in (26) and (27), the Wronskian of φ becomes $(-1)^{l+1}(2/\pi)$, and $H_\psi-H_\varphi$ becomes $-8\pi^2mV(r)/h^2$. To terms of the second order, then, one has for δ_l, with $c=0$, $\xi_0=1$, $\eta_0=0$,

$$\delta_l=-\frac{4\pi^3m}{h^2}\int_0^\infty J^2_{l+\frac{1}{2}}(kr)rV(r)dr+(-1)^l\frac{16\pi^2m^2}{h^4}\int_0^\infty J^2_{l+\frac{1}{2}}(kr)rV(r)dr\int_0^\infty J_{-l-\frac{1}{2}}(kr)J_{l+\frac{1}{2}}(kr)rV(r)dr$$

$$+(-1)^{l+1}\frac{16\pi^2m^2}{h^2}\int^\infty dr_2\int_0^{r_2}\{J_{l+\frac{1}{2}}(kr_2)J_{-l-\frac{1}{2}}(kr_1)-J_{-l-\frac{1}{2}}(kr_2)J_{l+\frac{1}{2}}(kr_1)\}\cdot J_{l+\frac{1}{2}}(kr_2)J_{-l-\frac{1}{2}}(kr_1)\{r_2r_1V(r_2)V(r_1)dr_1\}. \tag{28}$$

In general, for the choice of functions given above, one may write for $\tan\delta_l$, the following quotient,

$$\tan\delta_l=(-1)^l\frac{(-1)^{l+1}\frac{4\pi^3m}{h^2}\int_0^\infty J^2_{l+\frac{1}{2}}(kr)drrV(r)+\sum_{j=2}^\infty a_j}{1+(-1)^l\frac{4\pi^3m}{h^2}\int_0^\infty J_{-l-\frac{1}{2}}(kr)J_{l+\frac{1}{2}}(kr)rV(r)dr+\sum_{j=2}^\infty b_j}, \tag{29}$$

where

$$a_j=-\left[(-1)^l\frac{4\pi^3m}{h^2}\right]^j\int_0^\infty dr_j\cdots dr_2\int_0^{r_2}\prod^{j\to2}\{J_{l+\frac{1}{2}}(kr_s)J_{-l-\frac{1}{2}}(kr_{s-1})-J_{-l-\frac{1}{2}}(kr_s)J_{l+\frac{1}{2}}(kr_{s-1})\}$$

$$\cdot\prod^{j\to1}\{r_sV(r_s)\}J_{l+\frac{1}{2}}(kr_j)J_{l+\frac{1}{2}}(kr_1)dr_1 \tag{30}$$

and

$$b_j=\left[(-1)^l\frac{4\pi^3m}{h^2}\right]^j\int_0^\infty dr_j\cdots dr_2\int_0^{r_2}\prod^{j\to2}\{J_{l+\frac{1}{2}}(kr_s)J_{-l-\frac{1}{2}}(kr_{s-1})-J_{-l-\frac{1}{2}}(kr_s)J_{l+\frac{1}{2}}(kr_{s-1})\}$$

$$\cdot\prod^{j\to1}\{r_sV(r_s)\}J_{-l-\frac{1}{2}}(kr_j)J_{l+\frac{1}{2}}(kr_1)dr_1. \tag{31}$$

If the range of the potential $V(r)$ is not too great, one may use an approximation for $\varphi_1(r_s)\varphi_2(r_{s-1})-\varphi_2(r_s)\varphi_1(r_{s-1})$, obtained by expanding the functions φ_1 and φ_2 of r_{s-1}, about the point $r=r_s$. Retaining only the first term, one has,

$$\varphi_1(r_s)\varphi_2(r_{s-1})-\varphi_2(r_s)\varphi_1(r_{s-1})=-(r_s-r_{s-1})W(\varphi), \tag{32}$$

where the Wronskian $W(\varphi)$ is a constant.

Three factors limit the magnitude of (30) and (31): the inequalities (27a), the range of $V(r)$, and the form of the integrand, (32). The range is a constant, and one may easily see that the approximation (32) is less serious the higher the order of a_j or b_j.

[12] The asymptotic form of the wave function is periodic with respect to $(kr-\text{const.}\times\log r)$. Reference 2, Chapter III; reference 10, Chapter XVI, for $V\sim1/r$.

6. Application to various models

When the interaction potential is such that ξ_c and η_c of (26) and (27) can be determined ($c>0$), it is possible to use simpler functions than those employed in (29). A more convenient set is r^{l+1} and r^{-l}. With this choice one finds that $H_\psi - H_\varphi = k^2 - 8\pi^2 m V/h^2$. Now if $V(r)=\infty$, $0<r<c$. $V(r)=\sum \mu_j r^{-\nu_j}$, $c<r<d$ then one may set $\xi_c = c^{-l-1}$, $\eta_c = -c^l$ and calculate $\xi\cdot\eta$, $\partial\xi/\partial r$, and $\partial\eta/\partial r$, in known functions for $r=d$. At this point the solution may be joined to that given by the functions $r^{\frac{1}{2}}J_{l+\frac{1}{2}}(kr)$ and $r^{\frac{1}{2}}J_{-l-\frac{1}{2}}(kr)$ and again one may determine from the asymptotic behavior at infinity, the phase δ_l.

Instead of taking $V(r)$ to be infinite for $0<r<c$, one may also assume $V(r)=\sum G_j r^j$, $0<r<c$. Again the functions r^{l+1}, r^{-l} may be employed to determine ξ_c and η_c, repeating the previous analysis.

It is possible to show that the series (26) and (27), with the above choice of functions, is absolutely convergent, being less than the corresponding series, near the origin

$$\sum 2^j \frac{\left[\int_0^r \left| k^2 - \frac{8\pi^2 m}{h^2} V(r) \right| r dr\right]^j}{j!(2l+1)^j}. \tag{33}$$

One may, therefore, treat potentials, with these functions, which are singular at the origin, provided such singularities are of an order less than the inverse square.

Letters to the Editor

PROMPT publication of brief reports of important discoveries in physics may be secured by addressing them to this department. Closing dates for this department are, for the first issue of the month, the eighteenth of the preceding month, for the second issue, the third of the month. Because of the late closing dates for the section no proof can be shown to authors. The Board of Editors does not hold itself responsible for the opinions expressed by the correspondents.

Communications should not in general exceed 600 words in length.

Radioactive Isotopes of Osmium

G. T. SEABORG AND G. FRIEDLANDER
Department of Chemistry, Radiation Laboratory, Department of Physics, University of California, Berkeley, California
January 31, 1941.

OSMIUM has the following stable isotopes:[1]

Mass	184	186	187	188	189	190	192
Abundance in %	0.018	1.59	1.64	13.3	16.1	26.4	41.0

Slow neutron bombardment of osmium should, therefore, be expected to yield at least two radioactive osmium isotopes, Os^{191} and Os^{193}. When the present work was started, only one osmium activity had been reported,[2] its half-life being given as 40 hours. Meanwhile Zingg[3] has reported two periods obtained by slow neutron bombardment of osmium, one of 29.8 ± 1 hours and one of about 10 days.

We bombarded osmium metal, surrounded by paraffin, with neutrons from the 60-inch cyclotron for several days. The chemically separated osmium fraction showed two periods, one of 32 ± 2 hours and one of 17 ± 1 days. From absorption measurements, the upper energy limits of the beta-particles from these two activities were found to be about 1.5 Mev and 0.35 Mev, respectively. Both activities have gamma-rays associated with them.

How these two periods are to be distributed between Os^{191} and Os^{193} cannot be decided by bombardment of neighboring elements with neutrons, protons, deuterons, or alpha-particles, assuming the ordinary nuclear reactions. A clue to the assignment might be expected from fast neutron bombardment of osmium. This should produce Os^{191} by the reaction $Os^{192}(n,2n)Os^{191}$, while Os^{193} cannot be formed by a similar reaction. In addition, n,γ reactions leading to both isotopes will occur, even with moderately fast neutrons.

We surrounded one sample of osmium with boron carbide and cadmium, another one with paraffin, and bombarded them with beryllium+16-Mev deuteron neutrons under otherwise identical conditions. Both the 32-hour and the 17-day periods were stronger in the slow neutron sample and the ratio of 32-hour to 17-day activity was twice as large with the fast as with the slow neutrons. The latter result may indicate that the 17-day period is due to Os^{193} and the 32-hour period to Os^{191}, although this is not the only possible interpretation and the possibility of isomerism cannot be excluded.

It is a pleasure to thank Professor E. O. Lawrence for his continued interest and to express our gratitude to the Rockefeller Foundation and the Research Corporation whose financial support made this work possible.

[1] A. O. Nier, Phys. Rev. **52**, 885 (1937).
[2] I. V. Kurtchatow, C. D. Latyschew, L. M. Nemenow and I. P. Selinow, Physik. Zeits. Sowjetunion **8**, 589 (1935).
[3] E. Zingg, Helv. Phys. Acta **13**, 219 (1940).

Coulomb Exchange Energy in Light Nuclei

M. PHILLIPS
Brooklyn College, Brooklyn, New York
AND
E. FEENBERG
New York University, New York, New York
January 22, 1941

A NUMBER of isobaric mass differences of the type $(Z+1,Z)-(Z,Z+1)$ are known with considerable accuracy. The recent determinations of Haxby, Shoupp, Stephens and Wells[1] yield

$$(7)\ Be^7-Li^7 = 9.4\pm0.3 \text{ in } 10^{-4}\text{mu},$$
$$(9)\ B^9-Be^9 = 11.6\pm0.2 \text{ " " ,}$$
$$(11)\ C^{11}-B^{11} = 21.3\pm0.2 \text{ " " ,}$$
$$(13)\ N^{13}-C^{13} = 23.8\pm0.4 \text{ " " .}$$

In addition[2]

$$(15)\ O^{15}-N^{15} = 30.8\pm2.0 \text{ " " .}$$

The large differences (11)−(9) and (15)−(13) and the small differences (9)−(7) and (13)−(11) find a simple qualitative explanation in the periodic variation of the Coulomb exchange energy as calculated in the Hartree approximation.[3,4] In the notation of references 3 and 4 the theoretical results are

$$\{Be^7-Li^7\}-\{Li^5-He^5\} = L_e+2K_e/3,$$
$$\{B^9-Be^9\}-\{Be^7-Li^7\} = L_e-6K_e,$$
$$\{C^{11}-B^{11}\}-\{B^9-Be^9\} = L_e+2K_e/3,$$
$$\{N^{13}-C^{13}\}-\{C^{11}-B^{11}\} = L_e-6K_e,$$
$$\{O^{15}-N^{15}\}-\{N^{13}-C^{13}\} = L_e+2K_e/3.$$

Here L_e and K_e are the direct and exchange Coulomb integrals, respectively, for protons in the p shell. With the exception of (1) and (2) these equations are listed in reference 4. The theory yields numerical values $L_e\sim4.9\times10^{-4}$ mu, $K_e\sim0.30\times10^{-4}$ mu, but no quantitative significance is claimed for these numbers. The experimental mass differences are fitted reasonably well by $L_e=7.0\times10^{-4}$ mu and $K_e=0.7\times10^{-4}$ mu. In view of the crudeness of the Hartree approximation we prefer not to stress the possibility of numerical agreement, especially since supplementary effects, such as the one studied by Bethe,[5] may account for part of the observed periodicity.

[1] Haxby, Shoupp, Stephens and Wells, Phys. Rev. **58**, 1035 (1940).
[2] Fowler, Delsasso and Lauritsen, Phys. Rev. **49**, 561 (1936). The upper limit of the position spectrum from O^{15} is 1.7 Mev by inspection and 2.0 Mev by the K-U plot. We use the value 1.85 ± 0.20 Mev to compute the mass difference (15).
[3] E. Feenberg and E. Wigner, Phys. Rev. **51**, 95 (1937).
[4] E. Feenberg and M. Phillips, Phys. Rev. **51**, 597 (1937).
[5] H. A. Bethe, Phys. Rev. **54**, 436 (1938).

Cosmic Rays at a Depth Equivalent to 1400 Meters of Water

Y. NISHINA, Y. SEKIDO, Y. MIYAZAKI AND T. MASUDA
Institute of Physical and Chemical Research, Komagome, Hongo, Tokyo, Japan
December 31, 1940.

VARIOUS authors[1] have studied the nature of cosmic rays under very thick layers of matter. For the same purpose we have been performing experiments in Simidu tunnel (600 m above sea level, geographic $\varphi = 36.8°$N, $\lambda = 138.9°$E, geomagnetic $\varphi = 26.6°$N) of the government railways. An observation hut was built in one of the manholes of the tunnel under a vertical thickness of about 500 m of rocks, which consists mainly of diorite, the average density being probably 2.8, thus making the depth equivalent to about 1400 m of water.

The experimental arrangements are shown in Fig. 1. We shall denote the coincidence discharge of any one Geiger-Müller counter in each of the trays *A*, *B* and *C*, respectively, as being caused by a "single ray" and that of any one counter in each of the trays *A* and *B* and any two counters in the tray *C*, respectively, as being caused by a "shower." It is thus possible that "single rays" are sometimes showers in reality. These two types of coincidences are recorded simultaneously through two separate sets of amplifiers on the same paper tape, which is moved continuously by means of a clockwork. Lead absorbers of various thickness were placed either at the position I or II on a wood support 8 cm in thickness. Measurements were carried out for 4600 hours of observation between September, 1939, and July, 1940.

The results of the experiments are shown in Fig. 2, from which we can draw the following conclusions.

(1) There exist both "single rays" and "showers" which are hard and absorbed only gradually by 30 cm Pb. The relative abundance of "showers" to "singles" is higher than that at sea level, as was observed by various authors.[1] From this abundance, geometrical conditions and the above meaning of the word "singles" as well as from the similarity in the form of the absorption curves I for "singles" and "showers" in Fig. 2, we think that a greater part of "singles" are fragments of hard showers. We come thus to the conclusion that there exists a very high proportion of hard showers at a depth of about 1400 m water equivalent. Barnóthy and Forró observed a sharp minimum of the absorption curve at 10 cm Pb, while our minimum lies within the range of statistical fluctuations.

(2) As seen from Fig. 2, the position of lead either at I or at II makes no statistically significant difference in the number of coincidences. This fact seems to show the absence of non-ionizing primary rays for the hard ionizing showers which we observe, as mentioned above, in our apparatus. It is, however, also probable that the non-ionizing rays, even if they exist, do not produce the hard secondaries within such a thin layer of matter as 20 cm Pb, because the hard showers mentioned have an average range much larger than 30 cm Pb, and these must therefore have mostly been produced within a very thick layer of rock. It is thus difficult to decide from our results whether the primaries

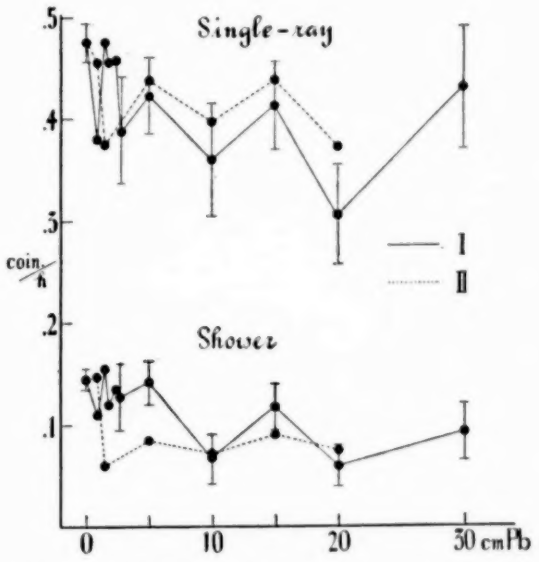

FIG. 2. Number of single rays and showers as a function of thickness of lead.

for the hard showers observed are ionizing particles such as mesons or protons,[2] or non-ionizing particles—say neutrinos—as was proposed by Barnóthy and Forró.[3]

This work was carried out as a part of the program of the Cosmic-Ray Sub-Committee of the Japan Society for the Promotion of Scientific Research. Our measurements were made possible by the kind assistance rendered by the Department of Railways and its various offices at Ueno, Minakami and Yusawa stations and we wish to express our cordial thanks to all officials concerned. We acknowledge the kind help given by our colleagues Messrs. M. Iio and T. Kameta for the preparations as well as for the observations throughout this work.

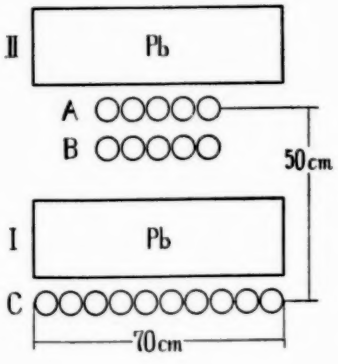

FIG. 1. Arrangement of counters.

[1] J. Barnóthy and M. Forró, Phys Rev. **55**, 870 (1939); **58**, 844 (1940); V. C. Wilson, Phys. Rev. **55**, 6 (1939); J. Clay, Rev. Mod. Phys. **11**, 128 (1939).
[2] J. Clay, reference 1.
[3] J. Barnóthy and M. Forró, Nature **138**, 325 (1936); Zeits. f. Physik **104**, 744 (1937).

Change in Height of a Mesotron-Producing Layer of Air

NIEL F. BEARDSLEY
University of Chicago, Chicago, Illinois
January 30, 1941

IN connection with the correlation studies on the effect of air conditions aloft on cosmic-ray intensity at the surface[1] it was convenient to apply the theory of Blackett[2] to a particular set of observations. Blackett assumed a mesotron-producing layer of air at about 16 km which had a mean change of height between summer and winter of 500 m and a mean temperature change of 10°C. From our data the mean density at this height is 0.1773×10^{-3} g·cm^{-3}. By linear interpolation of density and pressure between 15–16 km and 16–17 km we computed the height Z_ρ of this density for each of the 123 days in 1939 for which the radiosonde flight at the Anacostia Naval Air Station reached the necessary height and also the Compton-Bennett shielded ionization meters were in operation at both Cheltenham and at Huancayo, Peru.

We made a least-squares determination of the constants in an equation connecting the variation of cosmic-ray intensity with (a) the mass of air above this mesotron-producing layer represented by P_s, (b) the height of the layer Z_ρ and (c) the mass, $(P_0=P_s)$, of air below this layer. We found

$$\delta I'/I' = -0.93\delta(P_0-P_s) - 33.58\delta Z_\rho - 1.15\delta P_s$$

(pressures in mb)

$\delta I'/I'$ is the variation from balance in units of 0.1 percent of the intensity at Cheltenham corrected for world-wide changes as measured by the meter at Huancayo. Let $\delta I''/I'$ be the variation in intensity because of the change in height of the mesotron-producing layer only. Then from $\delta I''/I' = -\delta Z/L$ we get the mean path before disintegration of the mesotrons as $L_\rho=29.8$ km. Blackett assumed 32 km.

A two-constant equation for these same data gives

$$\delta I'/I' = -0.92\delta P_0 - 32.35\delta Z_\rho$$

with $L_\rho=30.9$ km. In both these cases approximately 60 percent of the variance of I' is associated with the variables chosen.

From our present knowledge of cosmic rays, it seems probable that the mean mesotron-producing layer ought to be associated with a given pressure rather than with a given density. However, using a constant pressure of 107 mb we find

$$\delta I'/I' = -0.94\delta P_0 - 40.79\delta Z_p$$

with $L_p=24.52$ km and only 50 percent of the variance of I' associated with P_0 and Z_p.

These results indicate that Blackett's assumption of a decaying mesotron formed at a height which changes from day to day is a possible explanation for some of the variations observed in cosmic-ray intensity at the surface. Some method for using the probable fact that mesotrons are produced at varying rates at different levels will be needed to make this correlation more exact.

[1] N. F. Beardsley, Phys. Rev. **59**, 233 (1941).
[2] P. M. S. Blackett, Phys. Rev. **54**, 973 (1938).

Capture Cross Sections for Slow Neutrons

K. SINMA AND F. YAMASAKI
Nuclear Research Laboratory, Institute of Physical and Chemical Research, Tokyo, Japan
January 8, 1941

RECENTLY Rasetti[1] and Goldhaber and O'Neal[2] have determined the capture cross sections of various isotopes for C neutrons by comparing the intensities of β-rays from radioactive isotopes produced by capture with that of an isotope Mn^{56}, whose absolute cross section of formation was measured by Lapointe and Rasetti[3] and was found to be $\sigma=9.4\times10^{-24}$ cm^2.

Since the summer of 1939, we have been measuring the capture cross sections for slow neutrons with a similar method by using a strong neutron source (Be+D) obtained with our cyclotron. We shall also give here our results. A paraffin cylinder 14 cm in diameter and 14 cm in height was placed about 30 cm away from the source, and substances to be measured were placed at its center, together with a standard sample. The activity of the substance in question was then compared with that of the standard and thus the relative capture cross sections were determined for about fifty isotopes. The measurements of activity were made with a Geiger-Müller tube counter or a Lauritsen electroscope, both with a window of aluminum foil 0.013 mm thick.

Absolute capture cross sections were then calculated in the following manner. Dunning, Pegram, Fink and Mitchell[4] obtained large absorption cross sections for slow neutrons in the elements Rh, Ag, Re and Au. From the table of isotopes, we can conclude that these absorption processes are almost entirely due to the capture of slow neutrons. By comparing our results for these elements with the absolute cross sections of the above-mentioned authors, we can thus convert our relative cross sections into the absolute values. The results are given in Table I.

From this we can see that Rasetti's values are systematically larger than ours. The origin of the discrepancies

TABLE I. *Conversion of our relative capture cross sections into absolute values.*

Isotope	Decay Period	σ in 10^{-24} cm^2	Isotope	Decay Period	σ in 10^{-24} cm^2
Na^{23}	14.8 hr.	0.38	Ru^{104}	20 hr.	0.48
Mg^{26}	10.2 min.	0.028	Rh^{103}	4.2 min.	8.8
Al^{27}	2.4 min.	0.15	Rh^{103}	44 sec.	140
Si^{30}	170 min.	0.063	Pd^{108}	13 hr.	20
P^{31}	14.3 days	0.15	Pd^{110}	17 min.	0.55
Cl^{37}	37 min.	0.38	Ag^{107}	2.3 min.	26.7
K^{41}	12.4 hr.	0.7	Ag^{109}	22 sec.	70
Sc^{45}	85 days	2.8	In^{113}	48 days	24
V^{51}	3.9 min.	3.5	In^{115}	54 min.	125
Mn^{55}	2.59 hr.	6.0	Sb^{121}	2.8 days	8.0
Co^{57}	11 min.	48	Sb^{123}	60 days	1.6
Co^{59}	7 yr.	3.8	I^{127}	25 min.	6.5
Ni^{62}	2.6 hr.	0.35	Ba^{138}	86 min.	3.0
Cu^{63}	12.8 hr.	1.3	La^{139}	31 hr.	5.5
Cu^{65}	5 min.	1.5	Eu^{151}	9.2 hr.	530
Zn^{68}	57 min.	0.48	Dy^{164}	2.5 hr.	1600
Ga^{69}	20 min.	0.68	Ta^{181}	97 days	4.5
Ga^{71}	14 hr.	1.3	W^{186}	24 hr.	33
As^{75}	26.8 hr.	1.5	Re^{185}	90 hr.	85
Br^{79}	4.4 hr.	1.4	Re^{187}	16 hr.	63
Br^{79}	18 min.	4.3	Ir^{191}	60 days	190
Br^{81}	34 hr.	1.1	Ir^{193}	19 hr.	63
Y^{89}	60 hr.	0.73	Pt^{198}	31 min.	9.5
Nb^{93}	6.6 min.	0.005	Au^{197}	2.7 days	130
Ru^{102}	4 hr.	0.19	Tl^{203}	4 min.	0.19

probably lies in the difference in the absolute values taken for reference in converting the relative cross sections into absolute ones.

A more detailed report is now in press and will soon appear in the *Scientific Papers of the Institute of Physical and Chemical Research* (Tokyo).

We wish to express our best thanks to Dr. Y. Nishina for his valuable help and encouragement.

[1] F. Rasetti, Phys. Rev. **58**, 869 (1940).
[2] M. Goldhaber and R. D. O'Neal, Phys. Rev. **59**, 109A (1941).
[3] C. Lapointe and F. Rasetti, Phys. Rev. **58**, 554 (1940).
[4] J. R. Dunning, G. B. Pegram, G. A. Fink and D. P. Mitchell, Phys. Rev. **48**, 265 (1935).

Radioactive $_{21}Sc^{41}$, $_{18}A^{35}$ and $_{16}S^{31}$

D. R. Elliott and L. D. P. King
Purdue University, West Lafayette, Indiana
January 31, 1941

THE production of these Wigner-type nuclei has already been reported.[1] Energy measurements of the emitted positrons have now been completed by means of a cloud chamber with air and alcohol vapor at atmospheric pressure.

Targets were held in the beam and then placed in a holder which could be swung up to a thin window on the side of the cloud chamber. A picture was taken within two seconds after the sample was removed from the beam. The cyclotron was on only during the actual bombardments which varied from 0.5 to 5 seconds, depending on the sample used. Only one photograph was made for each bombardment, and four bombardments were made per minute. To eliminate the influence of longer periods induced in the samples, six samples were used successively.

The half-life for $_{21}Sc^{41}$ was reported as 0.87 ± 0.03 second.[1] Figure 1 shows the spectrum for the positrons observed from the reaction $_{20}Ca^{40}(d,n)_{21}Sc^{41}$. The magnetic field used was 1276 oersteds; the observed ρ maximum was 142 mm. The upper energy limit obtained for the $_{21}Sc^{41}$ positrons is 4.94 ± 0.07 Mev.

The maximum energy of the positrons and the half-life of A^{35} and S^{31} have been recently also reported by the Princeton group.[2] Their value of 3.2 ± 0.02 seconds for the half-life and 3.85 ± 0.07 Mev for the upper limit of the positrons for S^{31} are in good agreement with our values, 3.18 ± 0.04 seconds[1, 3] and 3.87 ± 0.15 Mev, respectively.

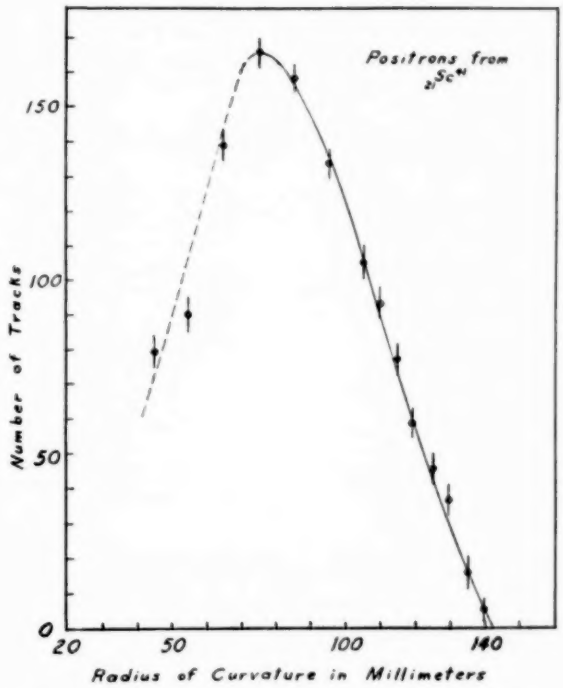

FIG. 1. Positrons from Sc^{41}. Maximum energy 4.94 ± 0.07 Mev, half-life 0.87 ± 0.03 second.

For A^{35} the value of 2.2 ± 0.2 seconds for the half-life and 4.38 ± 0.07 Mev for the maximum positron energy, obtained at Princeton are to be compared with our values of 1.91 seconds and 4.41 ± 0.09 Mev.[1, 2] Since the half-life for A^{35} did not agree with the Princeton results, this period was remeasured with greater accuracy giving 1.88 ± 0.04 seconds. Because of the high energy of the positrons from all of these isotopes, it has been possible to place suitable filters between the samples and the counter so that practically pure periods were obtained.

All of these results are in good agreement with calculated values.[2]

[1] L. D. P. King and D. R. Elliott, Phys. Rev. **59**, 108A (1941).
[2] White, Cruetz, Delsasso and Wilson, Phys. Rev. **59**, 63 (1941).
[3] L. D. P. King and D. R. Elliott, Phys. Rev. **58**, 846 (1940).